Stony Brook University

Chromatin Protein HMGB2 In Neural Progenitor Cells & Adult Neurogenesis

A Dissertation Presented

by

Ariel Benjamin Abraham

To

The Graduate School
In Partial Fulfillment of the
Requirements
For the Degree of
Doctor of Philosophy
in
Molecular and Cellular Pharmacology
Stony Brook University

December 2010

Stony Brook University

The Graduate School

Ariel Benjamin Abraham

We, the dissertation committee of the above candidate for the
Doctor of Philosophy degree, hereby recommend
acceptance of this dissertation.

Styliani-Anna E. Tsirka, Ph.D. – Dissertation Advisor
Professor, Department of Pharmacological Sciences

Joav Prives, Ph.D. – Chairperson of Defense
Professor, Department of Pharmacological Sciences

Holly Colognato, Ph.D.
Professor, Department of Pharmacological Sciences

Shaoyu Ge, Ph.D.
Assistant Professor, Department of Neurobiology & Behavior

This dissertation is accepted by the Graduate School

Lawrence Martin
Dean of the Graduate School

Abstract of the Dissertation

Chromatin Protein HMGB2 in Neural Progenitor Cells & Adult Neurogenesis

by

Ariel Benjamin Abraham

Doctor of Philosophy

in

Molecular and Cellular Pharmacology

Stony Brook University

2010

Neural stem cells (NSCs) and neural progenitor cells (NPCs) are distinct groups of cells present in the embryonic and adult mammalian central nervous system (CNS). Proliferation of NSCs and NPCs is regulated by several molecular factors including the cyclin dependant kinase inhibitors (CDKI), such as $p16^{Ink4a}$, and negative regulators of cell cycle, such as $p19^{Arf}$. Chromatin proteins, including chromatin protein high mobility group A2 (HMGA2), regulate the expression of $p16^{Ink4a}$ and $p19^{Arf}$ in NSCs and NPCs, demonstrating the critical regulatory role that chromatin proteins play in NSC and NPC proliferation. In addition to HMGA2, it is likely that other chromatin proteins expressed in NSCs

can and mediate NSC proliferation. The purpose of this project was to: 1) study and characterize the expression of HMG-B family members in NSCs, 2) test the hypothesis that HMGB2 regulates proper maintenance of adult subventricular zone (SVZ) NSCs and NPCs, and 3) test the hypothesis that changes in HMGB2-dependant progenitor maintenance in vivo is mechanistically related to changes in expression of different CDKIs in adult SVZ progenitor cells.

Using neurosphere assays, I have determined the differential expression of HMGB mRNAs in proliferating and differentiating embryonic NSCs. HMG-B chromatin proteins, and predominantly HMGB2, were dynamically expressed in embryonic NSCs suggesting a possible regulatory role in NSC proliferation and neurogenesis. I performed in vivo proliferation and differentiation assays using HMGB2-/- mice to determine the role of HMGB2 in SVZ NSC proliferation and olfactory bulb (OB) neurogenesis. Young adult HMGB2-/- mice had altered SVZ proliferation, and different numbers of SVZ NSCs and NPCs. These cellular changes in the SVZ were associated with changes in expression in several cyclin dependant kinase inhibitors. Young adult HMGB2-/- mice displayed aberrant changes in the rates of newly born neurons in the olfactory bulb. Finally, a subset (50%) of young adult HMGB2-/- mice exhibited ventriculomegaly. These results demonstrate that HMGB2 is a mediator of proper NSC cell cycle and OB neurogenesis.

Dedicated to my parents, Susan and Isaac Abraham, whose unconditional love and support made this dissertation possible.

Table of Contents

List of Tables

List of Figures

List of Abbreviations

CNS:	Central nervous system
NSC(s):	Neural Stem Cell(s)
NPC(s):	Neural Progenitor Cell(s)
HMGA2:	High mobility group A2
HMGB2:	High mobility group B2
SVZ:	Subventricular zone
RMS:	Rostral migratory stream
DG:	Dentate Gyrus
SGZ:	Subgranule zone
OB:	Olfactory bulb
GL:	Glomerular Layer of Olfactory Bulb
GCL:	Granule Cell Layer of Olfactory Bulb
BrdU:	Bromodeoxyuridine
CDKI(s):	cyclin dependant kinase inhibitor(s)
CIP/KIP:	CDK-inhibitory protein/Kinase-inhibitor protein
$p16^{Ink4a}$:	cyclin dependant kinase inhibitor $p16^{INK4a}$
$p21^{Cip1/Waf1}$:	cyclin dependant kinase inhibitor $p21^{Cip1/Waf1}$
$p27^{Kip1}$:	cyclin dependant kinase inhibitor $p27^{Kip1}$
$p19^{Arf}$:	$p19^{ARF}$ protein
GFAP:	Glial Fibrillary Acid Protein
DCX:	Doublecortin
NestinGFP:	GFP expression under the nestin promoter

Acknowledgements

I would like to thank my family for their support. I believe that my parents, Susan and Isaac Abraham, made this work possible by raising me with unconditional love and support. My parents provided positive encouragement from an early age in all my academic pursuits, including my love for math and science, which I believe played an integral role in all my future academic accomplishments. I would like to thank my sister, Tamar, and my brother-in-law, Aaron, and my niece Liea for all their love and support.

I would like to thank my advisor Dr. Stella Tsirka. Dr. Tsirka is a terrific advisor and as I reflect on my time during graduate school I realize that the time spent in her lab was both the most intellectually rewarding, fulfilling and challenging time during graduate school. Dr. Tsirka's continued support for my project, as well as a side project on p73 which we worked on in collaboration with Dr. Ute Moll's lab, were both fruitful and productive. Additionally, as a graduate student I was never afraid to make a mistake, either at the bench or in lab meeting, and that was because Dr. Tsirka fosters an open and inclusive intellectual environment in which people can comment and contribute freely. It was precisely because of this positive environment that so many students succeed in Dr. Tsirka's lab.

I would like to thank the members of my committee, Dr. Joav Prives, Dr. Holly Colognato, and Dr. Shaoyu Ge. I really enjoyed Drs. Prives', Colognato's and Ge's questions during and after my committee meetings, which helped me think critically about my project and helped focused my experiments to answer specific scientific questions. Specifically, I would also like to thank Dr. Colognato for reviewing the manuscript containing the data from my project and providing questions and critical comments that helped address specific remaining unanswered questions that were subsequently addressed. Additionally, I would like to thank Dr. Adan Aguirre who is not an official member of my committee but who we have collaborated with in recent months and has functioned as an informal member of my committee, providing critical help with experiments as well as insight, feedback, and support on my project.

I would to thank several additional faculty members and post-docs who helped me during graduate school. . I would like to thank Dr. Mirjana Savatic for her guidance early in graduate school. I would like to thank Dr. Emily Chen and Dr. Toni Koller for our proteomics collaboration. I would like to thank Dr. Grisha Enikolopov (Cold Spring Harbor Labs) who was a rotation advisor and allowed me to continue working with the NestinGFP transgenic mice that he created in his laboratory. I would like to thank Dr. Lou Manganas and Dr. Juan Encinas who were both post-docs whom I met during graduate school, and who taught me how to culture neurospheres/neural progenitor cells and conduct high quality immunofluorescence and confocal imaging techniques to visualize the neural stem cells in vivo. These techniques would later become the cornerstone of my dissertation work. I would like to thank Dr. Eli Hatchwell, who took the time to personally teach me how to design primers to conduct qRT-PCR analysis, and who personally reviewed qRT-PCR data generated from my experiments. Lastly, I would like to thank Dr. Marco Bianchi (San Raffaele) for generating and sharing the HMGB2 transgenic mice.

I would also like to thank and acknowledge the contributions that Dr. Mike Frohman has made as director of the MSTP at Stony Brook University, as well as Howard Crawford, the deputy director of MSTP. The program has evolved tremendously over the years, due in large part to Dr. Frohman's and Dr. Crawford's dedication and hard work. Also, I would like to thank Dr. Frohman for his personal support during graduate school, he made himself available to talk on numerous occasions and his insight and guidance are greatly appreciated.

Finally, I would like to thank my girlfriend Christine Ardito. Christine has been a tremendous, positive and wonderful part of my life during these last few years. She is warm, funny, loving, and generous. There were many times in graduate school when lab experiments, grant/manuscript writing, graduate school requirements and MSTP requirements all coincided with each other and made for an extremely stressful time, but Christine's love and support made everything better. I thank her for everything she has done, for her tireless support, and for her love and generosity.

Chapter I:
Introduction

Neural Stem Cells & Neurogenesis

Neural stem cells (NSCs) are a distinct group of cells that reside in the developing embryonic and mature adult mammalian central nervous system (Gage, 2000; Kriegstein and Alvarez-Buylla, 2009). NSCs proliferate and give rise to neural progenitor cells (NPCs) which differentiate into three principal cells in the CNS, neurons, astrocytes and oligodendrocytes (Gage, 2000; Ming and Song, 2005).

Neurogenesis, the process by which new neurons are created, occurs during development and continues in select regions of adult CNS (Ming and Song, 2005). Neurogenesis in the adult CNS occurs in two locations; the dentate gyrus (DG) within the hippocampal formation, and the olfactory bulb (OB). Evidence of adult neurogenesis was first described in the DG in rodents (Altman and Das, 1965a, b, 1966; Caviness, 1973), and later confirmed in adult primates (Kornack and Rakic, 1999) and humans (Eriksson et al., 1998). Evidence of postnatal OB neurogenesis in rodents emerged shortly thereafter (Altman, 1969), with subsequent confirmation that OB neurogenesis arises from the forebrain subventricular zone (SVZ) in mice (Lois et al., 1996; Wichterle et al., 1997; Kirschenbaum et al., 1999) and humans (Curtis et al., 2007). Neurogenesis in the DG occurs when NSCs in the subgranular zone (SGZ) proliferate and give rise to

progenitor cells which migrate and differentiate into the new granular neurons in the granule cell layer of the DG (Seki and Arai, 1991, 1993; Eriksson et al., 1998; Kornack and Rakic, 1999; Seri et al., 2001; Seri et al., 2004). Neurogenesis in the OB occurs when NSCs in the SVZ proliferate and give rise to progenitor cells which migrate through a rostral migratory stream (RMS) to the OB and differentiate into newborn neurons in the OB (Lois and Alvarez-Buylla, 1994; Lois et al., 1996; Doetsch et al., 1997; Wichterle et al., 1997; Doetsch et al., 1999; Kirschenbaum et al., 1999; Curtis et al., 2007). The current hypothesis regarding cell lineage in the adult SVZ-OB neurogenic cascade is that NSCs (type B cells) proliferate and give rise to amplifying NPCs (type C cells), and NPCs proliferate and give rise to neuroblasts (type A cells), which migrate through the RMS and differentiate into neurons in the OB (Doetsch et al., 1997; Doetsch et al., 1999). The image of the SVZ stem cell niche containing type B, C, and A cells can be found in Figure 1A.

Molecular Mechanisms of Neural Stem Cell Maintenance

Studies of the embryonic and adult NSCs and NPCs have defined the location and the function of several mitogens which regulate NSC proliferation, including epidermal growth factor (EGF) and fibroblast growth factor (FGF) (Reynolds et al., 1992; Reynolds and Weiss, 1992, 1996; Gritti et al., 1999; Doetsch et al., 2002a). Other studies have specifically addressed the molecular control of NSC maintenance, demonstrating the critical regulatory roles of different signaling pathways involved in NSC maintenance, including Notch

(Hitoshi et al., 2002; Alexson et al., 2006; Mizutani et al., 2007) and Bone Morphogenic Protein (BMP)(Lim et al., 2000). Despite these studies, the precise molecular mechanisms of NSC maintenance in the post-natal mouse brain remain unclear. The use of aging mice as a model to study NSC maintenance has provided greater insight into NSC maintenance. NSC maintenance decreases with increasing age; the total numbers of NSCs and proliferating NSCs in the SVZ stem cell niche decline with age (Maslov et al., 2004). The cellular consequence of this decrease in NSC maintenance is a decrease in OB neurogenesis in aged mice (Enwere et al., 2004). A molecular contributor to the decrease in NSC maintenance in the SVZ during aging is the increase in $p16^{Ink4a}$ expression (Molofsky et al., 2006). $p16^{Ink4a}$ is a well-known cyclin-dependant kinase inhibitor (CDKI) that suppresses G1-Cdk complex activity in the G1 phase of the cell cycle (Lowe and Sherr, 2003; Alberts, 2008). Transcriptional control of $p16^{Ink4a}$ expression is mediated by the chromatin protein bmi-1 (Jacobs et al., 1999) which regulates $p16^{Ink4a}$ expression in NSCs (Molofsky et al., 2003; Molofsky et al., 2005). A recent study demonstrated that an additional chromatin protein, non-histone nuclear protein high mobility group A2 (HMGA2), regulated $p16^{Ink4a}$ expression in NSCs (Nishino et al., 2008). HMGA2 expression is spatially and temporally specified in CNS tissue; expression remains high in the neuroepithelium of the developing embryonic telencephalon (E11-E14.5) and the lateral ventricle of the CNS during the early post-natal period (P0), decreases throughout post-natal development and adulthood, and expression ceases in old age (P600) (Nishino et al., 2008). HMGA2 represses $p16^{Ink4a}$ expression.

Consequently, NSC proliferation and self-renewal are robust during embryonic development when HMGA2 expression is high and $p16^{Ink4a}$ expression is low, and as developmental time and aging progress HMGA2 expression decreases and $p16^{Ink4a}$ expression increases, resulting in a decrease in NSC proliferation and self-renewal. In NSCs HMGA2 expression is negatively regulated by microRNA Let7b (Lee and Dutta, 2007), a microRNA with temporally specified expression in NSCs (Nishino et al., 2008). This temporally specified Let7b-HMGA2 axis regulates in concert $p16^{Ink4a}$ expression, which in turn controls NSC proliferation and self-renewal (Levi and Morrison, 2008), demonstrating the critical role chromatin protein HMGA2 plays in proper NSC maintenance. A diagram depicting the HMGA2-$p16^{Ink4a}$ molecular mechanism of NSC proliferation can be found in Figure 1B.

In addition to $p16^{Ink4a}$, several additional CDKIs regulate proliferation of NSCs and NPCs in the SVZ and play a role in NSC maintenance and OB neurogenesis. These CDKIs include members of the CIP/KIP family of CDKIs. One CIP/KIP family protein, $p21^{Cip1/Waf1}$, is a CDKI which has previously been shown to mediate NSC maintenance (Kippin et al., 2005). Young adult $p21^{Cip1/Waf1-/-}$ mice (1-4 months old) have increased *in vivo* SVZ proliferation (as assessed by BrdU incorporation), but neurospheres isolated from these young $p21^{Cip1/Waf1-/-}$ mice have impaired self-renewal compared to age-matched WT mice. Aged $p21^{Cip1/Waf1-/-}$ mice (16 months old) have decreased *in vivo* SVZ proliferation, and neurospheres cultured from these aged $p21^{Cip1/Waf1-/-}$ mice have impaired self-renewal compared to aged-match WT mice (Kippin et al., 2005),

demonstrating that $p21^{Cip1/Waf1}$ plays a role in proper NSC maintenance in the SVZ in aging mice. A second CIP/KIP family member protein, $p27^{Kip1}$, mediates NPC proliferation in vivo (Doetsch et al., 2002b). Young adult $p27^{Kip1-/-}$ mice (9 weeks old) have increased numbers of amplifying NPCs (type C cells), decreased numbers of neuroblasts (type A cells) in the SVZ compared to age-matched WT mice (Doetsch et al., 2002b). It remains unclear whether these changes in SVZ NPC and neuroblast cell numbers persist in aged $p27^{Kip1-/-}$ mice, or whether aged $p27^{Kip1-/-}$ mice experience any form of impaired NSC maintenance compared to aged WT mice. Finally, p53, a tumor suppressor protein and known mediator of CDKI $p21^{Cip1/Waf1}$ and $p27^{Kip1}$ expression, also regulates NSC maintenance; neurospheres grown from the SVZ of young adult $p53^{-/-}$ mice (2-3 months old) have increased proliferation and self-renewal (Meletis et al., 2006). Young $p53^{-/-}$ mice also exhibit increases in SVZ proliferation in vivo compared to WT mice. $p53^{-/-}$ neurospheres have greatly reduced expression of $p21^{Cip1/Waf1}$ mRNA expression and a two-fold decrease in $p27^{Kip1}$ mRNA expression compared to WT neurospheres from the SVZ of age-matched mice. A diagram depicting the integrated molecular mechanism of NSC proliferation, including $p21^{Cip1/Waf1}$, $p27^{Kip1}$, and p53, can be found in Figure 1C. These results demonstrate that $p21^{Cip1/Waf1}$, $p27^{Kip1}$, and p53 expression are involved in proper NSC maintenance in young adult mice.

HMG-B Proteins and Function

High mobility group (HMG) proteins are members of the HMG superfamily, a family of non-histone proteins found in the nuclei of mammalian cells, that bind to nucleosomes and the minor groove of DNA in a sequence independent manner (Bustin, 1999; Thomas, 2001; Hock et al., 2007). The HMG superfamily is composed of three subfamilies, the HMG-A, HMG-B, and HMG-N (Bustin, 1999, 2001; Bianchi and Agresti, 2005). The members of each subfamily have a distinct functional motif that mediates nucleosome or DNA binding (Bustin, 1999, 2001). The HMG-A subfamily functional motif is the AT hook (ATH) and the HMG-B subfamily functional motif is the HMG-box, which both bind to the minor groove of DNA(Bustin, 1999). The HMG-N subfamily functional motif is the nucleosome binding domain (NBD), which binds to nucleosomes (Bustin, 1999). The HMG-B subfamily includes proteins HMGB1, 2, 3, and 4. All HMGB proteins contain two HMG-box domains followed by an acidic amino acid domain at the C terminus of the protein (Thomas, 2001). The HMG-boxes are 80 amino acids in length and composed of three alpha helices, which twist and fold to create an L shape (Read et al., 1993; Weir et al., 1993). The HMG-boxes bind to the minor groove of DNA and loosen the DNA by inserting hydrophobic R group(s) from the first alpha helix of the HMG-box into the minor groove of DNA (Weir et al., 1993; Love et al., 1995; Werner et al., 1995; Bustin, 1999). It is through these domains that HMG-B proteins act as modulators of transcription, replication, recombination, and DNA repair (Bianchi and Agresti, 2005).

HMG-B Proteins and Neural Stem Cells

The association between members of the HMG-B subfamily of chromatin proteins and NSCs is not fully understood. Transcriptional profiling of SVZ NSCs indicated that NSCs express HMGB1 and HMGB2 mRNA (Ramalho-Santos et al., 2002). A subsequent study of SVZ NSCs reported HMGB1, HMGB2, and HMGB3 mRNA expression in NSCs (Fortunel et al., 2003). Analysis of gene expression overlap between NSCs, embryonic stem cells (ESCs) and retinal progenitor cells (RPCs) identified HMGB2 gene expression in all three populations (Fortunel et al., 2003). HMGB2 mRNA expression was also identified in peri-natal NSCs, was upregulated in undifferentiated neurospheres (Karsten et al., 2003) and decreased in differentiating neurospheres (Gurok et al., 2004). Consistent with these findings, an *in vivo* transcriptional profiling study of SVZ and OB gene expression found that HMGB2 mRNA expression was 17 fold higher in the SVZ than the OB, a finding confirmed by northern blot analysis (Lim et al., 2006). These findings suggest a possible role for HMGB2 in NSC proliferation in the SVZ stem cell niche. Despite these previous studies and the newly found regulatory role for HMGA2 in NSC proliferation, no comprehensive study to characterize the expression of HMG-Bs in NSCs has been conducted, nor has any study specifically addressed the role of individual HMGBs, such as HMGB2, in NSC maintenance and neurogenesis. Therefore, the purpose of this project is to: 1) study and characterize the expression of HMG-B family members in NSCs, 2) test the hypothesis that HMGB2 regulates proper maintenance of adult SVZ NSCs and NPCs, and 3) test the hypothesis that changes in HMGB2-

dependant progenitor maintenance *in vivo* is mechanistically related to changes in expression of different CDKIs in the adult SVZ progenitor cells (Figure 1D).

To characterize the expression of HMG-Bs in NSCs the proteome of embryonic NSCs was analyzed using shotgun proteomics. This lead to the identification of 384 proteins expressed in proliferating embryonic NSCs, including members of the HMG-B family, which were validated by western blot analysis. Using neurosphere assays, the expression of all HMG-B mRNAs in proliferating and differentiating embryonic NSCs were studied and the differential expression of HMG-B mRNA in proliferating and differentiating embryonic NCS were characterized. The differential expression of HMG-B chromatin proteins was also characterized in proliferating and differentiating NSCs. All HMG-B proteins (B1-4) were identified in proliferating embryonic NSCs at varying time points during neural development. HMGB1 and HMGB2 proteins are differentially expressed in differentiating embryonic NSCs. The possible regulatory role for HMGB2 in NSC maintenance and neurogenesis was examined using in vivo and in vitro assays. In vivo proliferation assays using HMGB2-/- mice demonstrate that young adult HMGB2-/- mice have SVZ hyperproliferation and increased numbers of SVZ NSCs and neuroblasts, but decreased numbers of NPCs in vivo. In vivo staining to examine changes in CDKI expression in young compound transgenic NestinGFP+HMGB2-/- mice were associated with changes in SVZ expression of different negative regulators of cell cycle, including $p21^{Cip1/Waf1}$, $p27^{Kip1}$, and p53. *In vivo* differentiation assays using HMGB2-/- mice to determine the role of HMGB2 in OB neurogenesis

demonstrate that young adult HMGB2-/- mice displayed aberrant increases in newly born neurons in the OB granule cell layer, but not the OB glomerular layer. Finally, a subset (50%) of young adult HMGB2-/- mice exhibits ventriculomegaly. These results demonstrate that HMGB2 is a mediator of proper proliferation of SVZ neural progenitors and OB neurogenesis in vivo.

Figure 1: (A) The SVZ neural stem cell niche, containing type B NSCs, type C NPCs, and type A neuroblasts, modified from (Lim et al., 2006). (B) HMGA2-p16^{Ink4a} mechanism of NSC proliferation during aging in vivo, modified (in color) from (Levi and Morrison, 2008). (C) Integrated mechanism of NSC proliferation. (D) Relationship of HMGB2 to proper NSC proliferation and CDKI expression.

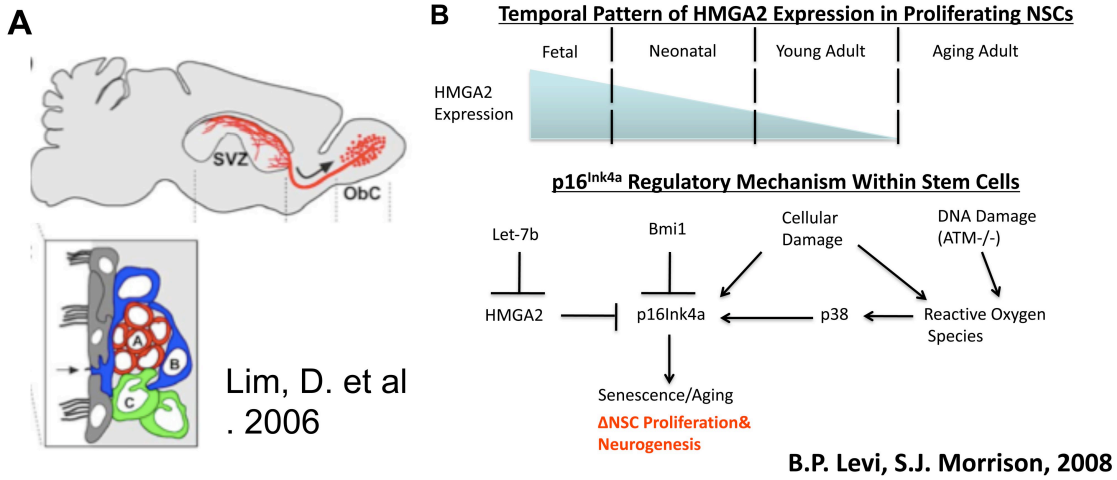

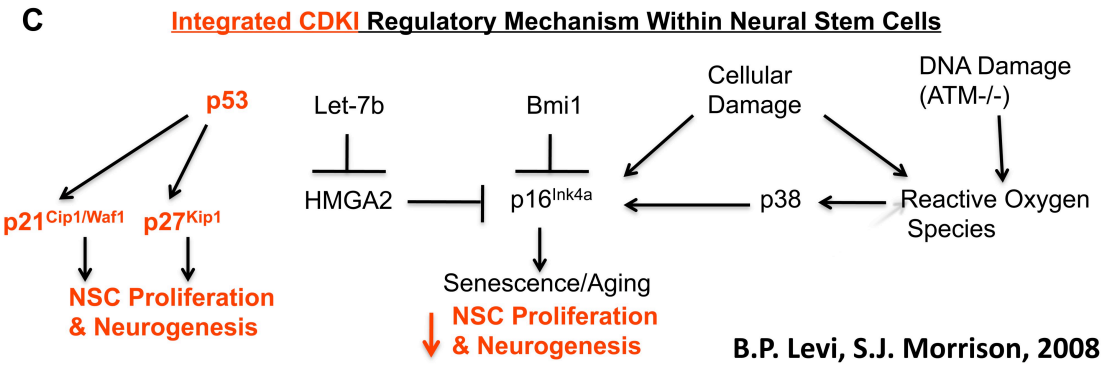

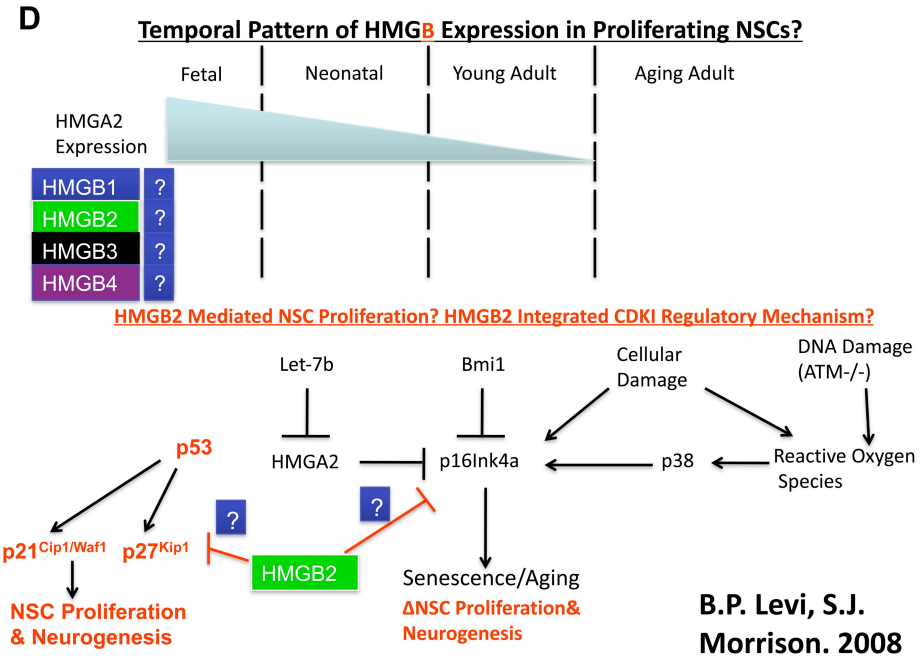

Chapter II
General Methods

Genotyping

HMGB2-/- mice were generated and characterized previously (Ronfani et al., 2001); NestinGFP transgenic mice were also generated previously (Mignone et al., 2004). Mouse genotyping was conducted by digesting mice tails in DNA digestion buffer containing (final) 100mM NaCl, 10mM Tris-HCl (pH8), 25mM EDTA, 0.5% (w/v) SDS, and 0.1 mg/ml proteinase K dissolved in milliQ water overnight (or for six hours) at 55°C. DNA digestion buffer was mixed with one equivalent volume of phenol/chloroform/isoamyl alcohol (25:24:1), centrifuged, and the aqueous phase collected. The aqueous phase was mixed with chloroform, centrifuged, and re-collected, and was slowly mixed with one equivalent volume of isopropanol to precipitate DNA. After gentle mixing, precipitated DNA was centrifuged for 15 min, and DNA was washed with 500μL of 70% ethanol. DNA pellets were centrifuged a final time for 10 minutes and the ethanol supernatant was discarded. DNA cell pellets were dried briefly and resuspended in 100μL of Tris EDTA (TE) solution, pH 7.5

NestinGFP mouse tail DNA was genotyped using the following primers:

Oligo 1 (5' CGY-FP): 5' ATC ACA TGG TCC TGC TGG AGT TC 3'

Oligo 2 (3' 2nd Intron): 5' GGA GCT GCA CAC AAC CCA TTG CC 3'

Primers were mixed with genomic DNA and PCR reaction buffer, $MgCl_2$, dNTPs, and Taq polymerase (Sigma). Cycling conditions were as follows; 3 minutes at 94°C, melting for 30 seconds at 94°C, annealing for 1 minute at 64°C, extension for 1 minute at 72°C, with repeat of 35 cycles, followed by 5 minutes at 72°C and 4°C hold until the end. PCR reactions were run on a 1.5% agarose gel run in 1x TAE solution. The presence of a 700 base pair band indicated that mice were NestinGFP positive mice.

HMGB2 mouse tail DNA was genotyped using the following primers:

HMGB2 Oligo 1 (Forward): 5' CGG ACA GCT AGG AGC TTT GAA GTC 3'

HMGB2 Oligo 2 (reverse): 5' GCG ATG GGT TCG TTA GTT CTC AG 3'

LacZ Oligo 1 (Forward): 5' GCT GGC GTA ATA GCG AAG AGG 3'

LacZ Oligo 2 (Reverse): 5' ATG CGC TCA GGT CAA ATT CAG AC 3'

Primers were mixed with genomic DNA and PCR reaction buffer, $MgCl_2$, dNTPs, and Taq polymerase (Sigma). Cycling conditions were as follows; 5 minutes at 95°C, melting for 45 seconds at 95°C, annealing for 30 seconds at 60°C, extension for 30 seconds at 72°C, with repeat of 35 cycles, followed by 5 minutes at 72°C and 4°C hold until the end. PCR reactions were run on a 1.5% agarose gel run in 1x TAE solution. The presence of a 236 base pair band in the HMGB2 PCR reaction indicated the presence of WT HMGB2 mouse allele, while the presence of a 413 base pair band in the LacZ PCR reaction indicated the presence of the LacZ HMGB2 knockout allele. Mice with both HMGB2 WT and LacZ alleles are HMGB2+/- heterozygotes.

PCR reactions of all alleles from of all mice (NestinGFP transgenic, HMGB2 transgenic, and compound NestinGFP-HMGB2 transgenic mice) was performed separately to prevent generating non-specific amplification products that would yield false positive genotypes. All PCR reactions were run using previously known positive controls for the NestinGFP, WT HMGB2 allele, and LacZ HMGB2 knockout allele, as well as a negative PCR control. In all PCR reactions positive controls were positive and negative PCR controls were negative, and PCR reactions were repeated if any controls failed.

Immunofluorescence

For immunofluorescence (IF) staining, brain serial sections from each mouse were transferred to a new six well plate, washed with PBS, and antigen retrieval was performed using 2N HCl treatment for 1 hour at 37°C, followed by two washes in 0.1M Borate Buffer (pH 8) and two washes in 1x PBS. In immunofluorescence experiments in which antigen retrieval was not required sections were not treated with HCL and washed twice with 1x PBS. Sections were blocked with 10% goat serum/0.3%BSA/0.2%TritonX/PBS solution for 2 hours at room temperature (Sigma). Sections were stained with primary antibody/antibodies (for multi-fluorophore labeling) in 0.3%BSA/0.2%TritonX/PBS solution overnight at 4°C. Primary antibody/antibodies were removed and all sections were washed extensively with PBS and stained with species-specific highly cross absorbed secondary antibodies used for duel/multi-fluorophore staining. All secondary antibody stains were performed in 0.3%BSA/0.2%TritonX

/PBS solution at room temperature for 1 hour. Secondary antibodies were removed and all sections were wash extensively with PBS, were mounted on Superfrost plus micro slides (VWR), covered with Fluormount G mounting media (Southern Biotech) and covered with a cover glass (Fisher).

Western Blot Analysis

NSC cell lysates were generated from neurospheres (for compatibility with proteomics parameters see Chapter III and IV for specific conditions and reagents used for NSC lysis). Protein was determined using the DC protein assay (Biorad). Equal amounts of proteins were prepared by mixing protein lysates with 6x SDS sample (loading) buffer containing 350μM Tris pH 6.8, 30% glycerol, 10% SDS and 0.01% Bromophenol Blue. Beta-mercaptoethanol was added to samples at a dilution of 1:20, and all samples were heated at 95°C for 10 minutes, followed by centrifugation. Samples were loaded into Tris glycine SDS-polyacrylamide gels, containing a 5% stacking gel (pH6.8) and a 12% or 15% resolving gel (pH 8.8). All gels were loaded with Precision Plus protein ladder (Bio-Rad). Gel electrophoresis was done using 1x running buffer containing (final) 25mM Tris base, 192mM glycine, and 0.1% SDS for 20 minutes at 80 volts (stacking), followed by electrophoresis for 1 hour at 120 volts (resolving). For protein transfer, transfer buffer solution was composed of 25mM Tris base, 192mM glycine and 20% methanol, and proteins were transferred to PVDF membrane (previously activated by brief exposure to methanol) by running transfer apparatus at 120 volts for 1 hour at room temperature. Ice blocks were

used to prevent overheating of transfer apparatus. Following protein transfer to PVDF, the membrane was quickly rinsed with PBS and blocked with 4% BSA/ PBS for 2 hours at room temperature, and then incubated over night at 4ºC with primary antibody in 0.05% Tween20-PBS solution. All PVDF membranes were incubated with Mouse anti-alpha Tubulin (Sigma, 1:2000) as loading control. The following morning, the primary antibody was removed and the membrane was washed in 0.2% Tween20-PBS solution. PVDF membranes with then incubated with either Alexa goat anti-Mouse 680 (Invitrogen) and/or IR DYE Donkey anti-Rabbit 800 (Jackson) antibodies at 1:10,000 in 0.05%Tween20-PBS solution for 1 hour at room temperature. Secondary antibodies were then removed and the membrane was washed extensively with 0.2%Tween20-PBS solution. The membranes were scanned using the LICOR Odyssey Scanner with 700 and 800 nm laser excitation to visualize the reacting protein bands.

RT-PCR Analysis

RNA was isolated from neurospheres using the Rneasy RNA Isolation Kit (Qiagen) and total RNA levels were quantified using Nanodrop (Thermo Scientific). Prior to reverse transcription all RNA samples were treated with DNAse (Invitrogen) to degrade genomic DNA. 750 ng of DNAse-treated total RNA was reverse transcribed using the Superscript III First-Strand Synthesis System for RT-PCR (Invitrogen) according to manufacturer protocol. All cDNA samples were treated with RNAse (Invitrogen) following completion of RT-PCR reaction according to manufacturer protocol. PCR reactions were run using gene

specific primers for HMGB1, HMGB2, HMGB3, and HMGB4 and β-Actin primers were used as an endogenous control. PCR reactions for samples treated without the reverse transcriptase enzyme (–RT reactions) were run with all four gene specific HMG-B primers, and all –RT reactions were negative. HMG-B primer sequences are listed below:

HMGB1(L) 5'ACAGAGCGGAGAGAGTGAGG 3' and

HMGB1(R) 5'TTTGCCTCTCGGCTTTTTAG 3';

HMGB2(L) 5' TGTCCTCGTACGCCTTCTTC 3' and

HMGB2(R) 5' CCTCCTCATCTTCTGGTTCG 3';

HMGB3(L) 5'GCGAACAATACAGGTACGACTC 3' and

HMGB3(R) 5' CTTGGCACCATCAAACTTCC 3';

HMGB4(L) 5' CGGGACCACTATGCTATGCT 3' and

HMGB4(R) 5' CTTCCTGCCTTGACATTGG 3'.

Cycling conditions for HMGB1 were as follows: 95ºC for 15 min, 94ºC for 15 seconds (melting), 53.2ºC for 30 seconds (annealing), 72ºC for 30 seconds (extension), repeat for 35 cycles, 4º hold until end. Annealing temperatures were modified to 58.1ºC for HMGB2 and HMGB3, and 50.3ºC for HMGB4. PCR reactions were run on a 1.5% agarose/TAE gel containing ethidium bromide (1:20,000) in 1x TAE solution and visualized by ultraviolet (UV) light.

Chapter III:

Shotgun Proteomics Analysis of Embryonic Neurospheres And the Identification of HMG-B Chromatin Proteins In Embryonic Neural Stem/Progenitor Cells

The first experiment of this project was to study and characterize the expression of HMG-B family members in NSCs. A neurosphere formation assay was employed to isolate and grow NSCs from the brains of embryonic E12.5 C57Bl6/wild type mice as previously described in the literature (Reynolds et al., 1992; Reynolds and Weiss, 1992, 1996). To gain further molecular insight into these proliferating NSCs the proteome of the NSCs was analyzed using quantitative shotgun proteomics analysis (Liao et al., 2009). Shotgun proteomics analysis is a powerful tool in which complex mixtures of proteins are cleaved using proteolysis, such as enzymatic proteolysis, and the peptide products of the proteolysis are identified using mass spectrometry and comparison against known mass spectrometry/peptide databases. This technique can also be used to identify proteins expressed in cells, and to quantify the abundance of each protein present in different cells. Despite the ability to use this powerful technique to identify and quantify protein abundance, there are technical

limitations associated with the approach. One limitation is that cell lysis and protein solubilization usually involves the use of detergents, such as sodium dodecyl sulfate (SDS), which are not compatible with mass spectrometry. In light of this incompatibility, protein lysates not generated with detergents are less likely to dissolve lipophilic proteins. Therefore, the ability to detect these more lipophilic proteins by mass spectrometry is diminished, creating, theoretically, a bias in favor of detection of soluble hydrophilic proteins, but not insoluble lipophilic proteins. Previous studies have examined the use of special surfactants, including acid labile surfactants, to solubilize lipophilic proteins in cell lysates and that are compatible with mass spectrometry (Chen et al., 2007). The use of surfactants like Rapigest^{SF} (Waters) increases the detection of different proteins by shotgun proteomics analysis (Chen et al., 2007). Using mass spectrometry compatible surfactants, such as Rapigest^{SF} (Waters), and protein solubilizers, such as Invitrosol (Invitrogen), shotgun proteomics analysis was conducted using neurosphere lysates. This allowed us to study the proteome of proliferating embryonic NSCs. Additionally, neurosphere lysates were fractionated into membrane and soluble fractions using commercially available fractionation kits (Native membrane protein extraction kit, Calbiochem), including the use of acid-labile surfactants such as Rapigest to solubilize proteins, and was analyzed by quantitative shotgun proteomics to help further identify proteins that were not initially identified in whole cell neurosphere lysates. Using this approach, three technical replicates of neurosphere lysates were analyzed by shotgun proteomics analysis and led to the identification of several hundred

proteins expressed in proliferating NSCs, including numerous uncharacterized proteins in NSCs.

Material and Methods

Neurosphere Formation Assay, Passaging, and Differentiation

All experiments conform to the University guidelines on the ethical use of animals and were approved by the Institutional Animal Care and Use Committee. Pregnant C57 wild type mice were euthanized under deep anesthesia at E12.5. Embryos were placed in ice-cold NSC Proliferation media composed of Neurobasal media containing Neurocult proliferation supplement (Stem Cell Technologies) and antibiotic/ antimycotic (Gibco). Embryonic mouse brains were dissected out and mechanically dissociated by trituration. Cells were centrifuged at 800 rpm for 5 minutes, supernatant was removed and the cell pellet was resuspended in 10mL of NSC proliferation media. Viable cells were counted by trypan blue staining. Primary neurospheres were grown in a 5% CO2 chamber at 37º C by seeding $8x10^6$ viable cells at a cell concentration of $2x10^5$/mL in NSC proliferation media containing 20ng/mL of recombinant human epidermal growth factor (rhEGF)(Sigma).

Primary neurospheres were passaged after 7 days in vitro using the Neurocult Chemical Dissociation Kit (Stem Cell Technologies), according to manufacturer protocol. Dissociated NSCs were filtered through a 40μm filter (BD Falcon) to remove any remaining debris, and trypan blue was used to determine viable NSC number. $2x10^6$ NSCs were replated in vented T-75 flasks (BD

Falcon) at a cell concentration of $5x10^4$ cells/mL in NSC proliferation media containing 20ng/mL rhEGF. NSCs from each passage were replated at the same cell ($5x10^4$ cells/mL) and EGF (20ng/mL) concentrations in NSC proliferation media.

Neurosphere differentiation assay was performed by cleaning glass coverslips with 2N NaOH, extensive washing and UV sterilization for 30 minutes, followed by coating coverslips with 100ug/mL poly-D-Lysine (Sigma) for one hour at room temperature and 20ug/mL Laminin (Sigma) in PBS for 3-4 hours at 37º C. After laminin coating, neurospheres were plated on glass coated coverslips and differentiated in Neurocult differentiation media (Stem Cell Technologies) without EGF supplementation. Differentiation media changes were done once per day per well, until cells were fixed with 4% paraformaldehyde(PFA)/PBS solution and prepared for immunofluorescence.

Immunofluorescence

For immunofluorescence (IF) staining, proliferating and differentiated neurospheres were fixed with 4%PFA/PBS and washed three times with PBS. Immunofluorescence was performed as described in Chapter II – General Methods, except that spheres, not brain sections, were stained using this protocol. Specifically, proliferating spheres were stained with primary antibodies Rat anti-CD133 (Prominin1, Clone 13A4, 1:500, Ebioscience) and Rabbit anti-GFAP (1:1000, Millipore) in 0.3%BSA/0.2%TritonX/PBS solution overnight at 4°C. Differentiating spheres were stained with primary antibodies anti-GFAP and

anti-Beta3 tubulin (1:500, Millipore), and anti-CNP (1:100, Sigma) in 0.3%BSA/ 0.2%TritonX/PBS solution over night at 4°C. Primary antibodies were removed and all spheres were washed extensively with PBS and stained with species-specific highly cross absorbed secondary antibodies conjugated to Alexa488 (Invitrogen) or Rhodamine RedX or Cy3 (Jackson). All secondary antibody stains were performed in 0.3%BSA/0.2%TritonX/PBS solution at room temperature for 1 hour. Secondary antibodies were removed and spheres were wash with PBS, and glass coverslips with spheres were placed onto Superfrost plus micro slide (VWR) containing Fluormount G mounting media (Southern Biotech).

Quantitative Shotgun Proteomic Analysis

NSC Lysis

NSC lysis buffer was made using 8M Urea (Sigma) in 50mM Ammonium bicarbonate (pH7.5) (Sigma) using HPLC-grade water (Thermo Scientific). 1mg of RapiGest^{SF} Powder (Waters) was reconstituted with 50mM ammonium bicarbonate to make 2% RapiGest (w/v). 5x Invitrosol LC/MS protein solubilizer (Invitrogen MS10007) and complete Mini, EDTA-free protease inhibitor cocktail were purchased separately (Roche 11836170001). To make mass-spectrometry compatible NSC lysis buffer, protease inhibitor (1x), Invitrosol (1x), Urea (4M final) and RapiGest^{SF} (0.1% w/v final) were added to ammonium bicarbonate solution (50mM final). NSCs were lysed with 100µL of cold lysis buffer on ice, and a 25 gauge needle attached to a 1mL syringe (BD) was used to lyse cells

and shear DNA. A different needle and syringe was used for each biological NSC sample and all technical replicates. Lysates were incubated in a foam pad attached to a vortex for 30 minutes at 4º to facilitate the solubilization of proteins, centrifuged at 13200 rpm at 4º for 30 minutes, and supernatants were transferred to new ice-cooled non-stick microcentrifuge tubes and left on ice. Insoluble proteins remaining in the NSC debris pellet were solubilized by adding 100µL of NSC lysis buffer containing 6M Urea ([final]) to the remaining NSC pellet. Tubes containing insoluble protein pellets and additional lysis buffer were vortexed at 4º for 30 minutes, centrifuged at 13200 rpm at 4º for 30 minutes, and supernatants were pooled with their respective soluble protein supernatants on ice. For fractionated NSC lysates, NSCs were lysed and fractionated according to manufacturer protocol using the ProteoExtract native membrane protein extraction kit (Calbiochem). Protein determination was preformed using the EZQ Protein Quantitation Kit (Invitrogen).

Digestion and Preparation of *Whole* NSC and *Soluble Fraction* NSC Protein Lysates

10µg of protein from each sample was precipitated using methanol-chloroform precipitation. Protein pellets were resuspended in 1x Invitrosol, heated to 60º for 5 minutes, cooled to room temperature, dissolved in acetonitrile (Sigma) and sonicated for 2 hours in a 37º water bath. Protein was digested with Trypsin (Sigma, 1:100) at 37º over night, and quenched the following day with 90% Formic acid (10% final). Peptide pellets were dried down by speed vacuum

to almost dry and resuspended in buffer A (5% acetonitrile/ 95%water/ 0.1%Formic Acid).

Digestion and Preparation of *Membrane* NSC Protein Lysates

10 μg of membrane protein was methanol-chloroform precipitated, resuspended in Rapigest, reduced using TCEP (2-Carboxylethyl-Phosphine), alkylated with iodoacetamide (IAM), and digested with trypsin (1:50) over night. RapiGest was hydrolyzed by adding 90% Formic Acid (10% final), and incubated in a shaking 37º water bath for 4 hours. Samples were dried down by speed vacuum and resuspended in buffer A.

1D LC MS/MS and Database Analysis

NSC peptides were analyzed using the LTQ XL linear ion trap mass spectrometer (Finnigan, Thermo Scientific). MS/MS spectra were extracted from the RAW file with ReAdW.exe (http://sourceforge.net/projects/sashimi). The resulting mzXML file contains all the data for all MS/MS spectra and can be read by the subsequent analysis software. The MS/MS data were searched with Inspect (Tanner et al., 2005) against a database containing a mouse database (IPI ver. 3.43 containing 54,215 entries) with added *E.coli* and common contaminant proteins (in total 4,605 proteins) in addition to a shuffled database of the aforementioned proteins. Only peptides with at least a p value of 0.01 were analyzed further.

Western Blot Analysis & Confirmation of Proteomics Data

Cell lysates from proliferating E12.5 neurospheres were generated according to the Methods section entitled “NSC Lysis” in this chapter, and the general western blot protocol described in Chapter II – General Methods was followed for protein detection. Specifically, several different western blots were preformed to detect and confirm expression of proteins identified by shotgun proteomics, including intermediate filament vimentin, nuclear matrix protein matrin3, chromatin proteins HMGB1 and HMGB2, protein kinase C substrate myristoylated alanine rich C kinase substrate (MARCKS), RNA binding protein TARDBP, and heterochromatin protein 1 gamma.

RT-PCR Analysis

Cell lysates from proliferating E12.5 neurospheres were generated and mRNA isolated and analyzed by RT-PCR according to the methods sections entitled “RT-PCR Analysis” in the general methods sections in Chapter II – General Methods.

Results

HMG-B mRNAs and Proteins Are Expressed in Proliferating NSCs

E12.5 neurospheres were immunoreactive for NSC markers CD133 and glial fibrillary acid protein (GFAP) (Figure2A-D), were highly proliferative and capable of extensive self-renewal. NSCs were multipotent, and differentiated into GFAP+

astrocytes, BetaIII Tubulin+ neurons and CNP+ oligodendrocytes, when plated on laminin and poly-D-lysine (Figure2E, F). Using mass spectrometry compatible components (RapiGest^{SF} and Invitrosol) as described above (Chen et al., 2007), the shotgun proteomics analysis identified 384 proteins expressed in soluble, membrane, and whole cell lysates of proliferating E12.5 neurospheres. The full list of proteins can be found in Table 1, including a heat map of the differential expression of proteins in proliferating E12.5 neurospheres according to cell compartment (soluble vs. membrane vs. whole cell lysate), as well as differential expression according to neurosphere passage (passage 2 vs. 8). The distribution of proteins in different subcellular compartments can be seen in Figure 3. This shotgun proteomics analyses identified several protein markers of NSCs, including GFAP, nestin, vimentin, and brain lipid binding protein (BLBP), as well as numerous proteins that have not been characterized in NSCs, such as the chromatin structural proteins HMGB1 and HMGB2.

The expression of some of the proteins identified in the proteomics analysis was confirmed by western blot analysis. The expression of vimentin was confirmed, as were several previously unreported proteins, including nuclear proteins such as matrin3 and chromatin structural proteins HMGB1 and HMGB2, myristoylated alanine rich C kinase substrate (marcks), heterochromatin protein 1-gamma (HP1-γ) and RNA binding protein TARDBP (Figure 4).

To further verify the expression of HMG-Bs in neurospheres, and explore whether the remaining members of the HMG-B family, HMGB3 and HMGB4, are also expressed in neurospheres, gene specific primers for all members of the

HMGB family were designed and used to conduct RT-PCR analysis for HMGB1, 2, 3, and 4 expression in proliferating neurospheres. Figure 5 is a diagram of the primer design used to generate specific HMGB primers to conduct RT-PCR analysis. RT-PCR analysis demonstrates that all HMBG mRNAs, HMGB1, 2, 3, and 4, were expressed in proliferating E12.5 neurospheres (Figure 6). All primers spanned exon-intron boundaries (except B4 which is an intron-less gene) and the size of all RT-PCR reaction amplification products were consistent with amplification of HMGB cDNA. Subsequent western blot analysis demonstrated that HMGB3 and HMGB4 proteins were expressed in proliferating neurospheres (Chapter IV, Figure 8), validating the RT-PCR data. In conclusion, three separate and independent methodologies, shotgun proteomic analysis, western blot analysis and RT-PCR analysis confirmed HMGB1 and HMGB2 mRNA and protein expression in proliferating E12.5 neurospheres, while two separate methodologies (western and RT-PCR analysis) confirm the expression of HMGB3 and HMGB4 in proliferating E12.5 neurospheres.

Figure 2: Immunofluorescence of (A) Dapi (B) CD133 (C) GFAP and (D) overlap in proliferating E12.5 neurospheres, and (E) GFAP, beta 3 tubulin and (F) CNP expression in differentiated neurospheres. White scale bars in (E) and (F) are 20 μm.

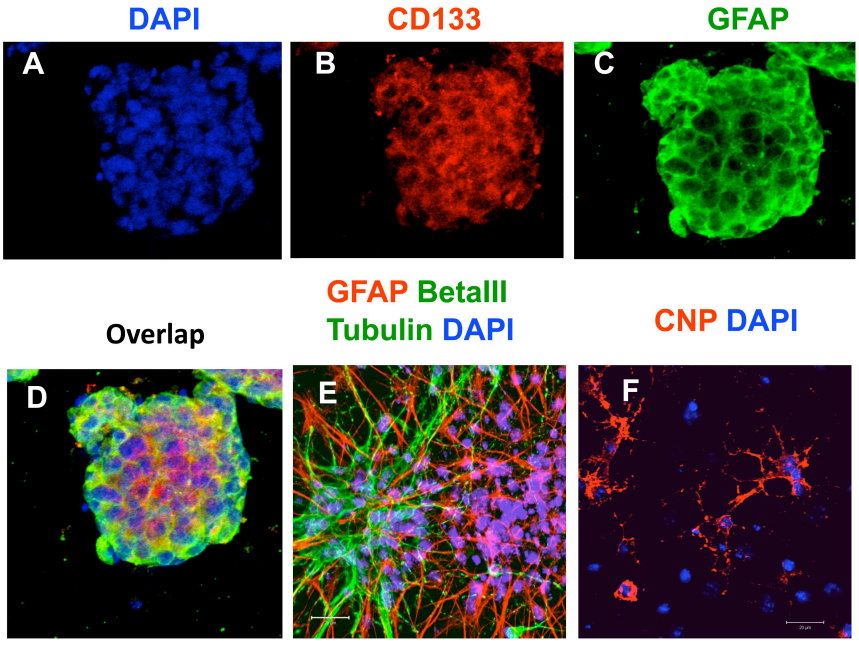

Figure 3: Subcellular distribution of proteins identified by shotgun proteomics analysis.

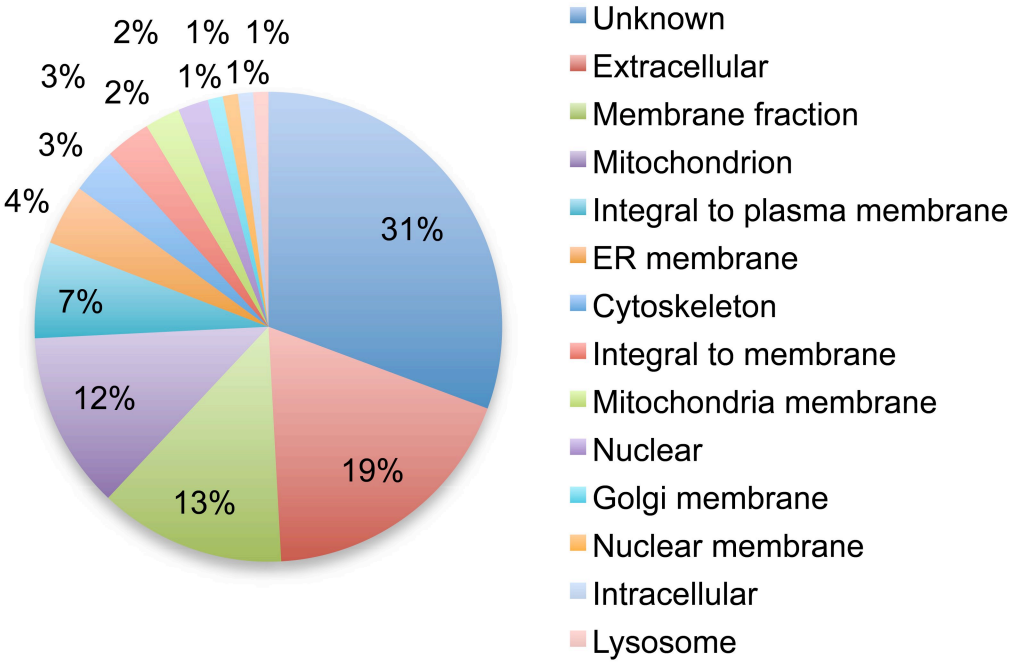

Figure 4: Western blot analysis of Vimentin, Matrin3, HMGB1, HMGB2, myristoylated alanine rich C kinase substrate (MARCKS), heterochromatin protein 1-gamma (HP1-γ) and TARDBP protein expression in cell lysates generated from E12.5 neurospheres. NSCs are labeled according to passage, e.g. p1, p2, p3 are with amount of loaded protein, e.g. 30 μg. Hela: Hela cell lysates, SKNSH; Neuroblastoma cell line SKNSH cell lysates.

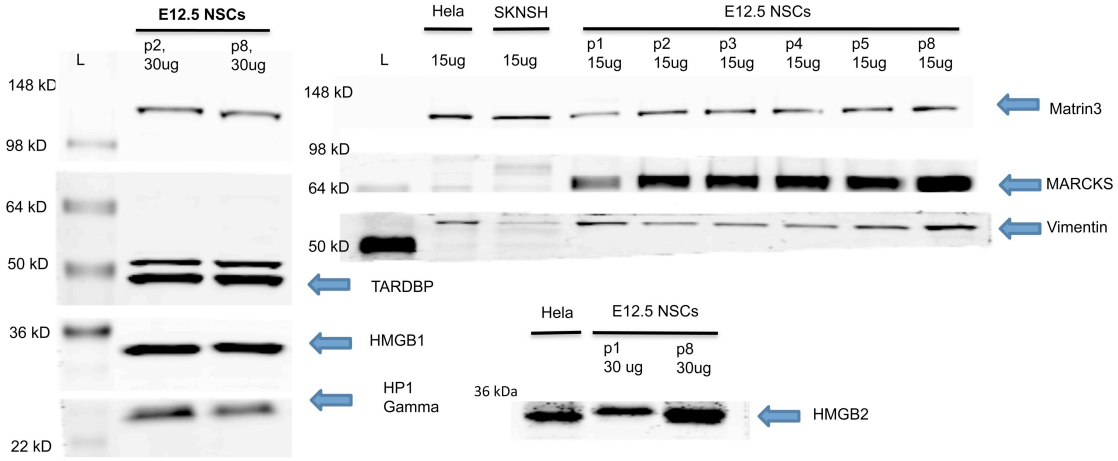

Figure 5: Diagram of primers designed to confirm HMGB1, 2, 3, and 4 expression by RT-PCR in proliferating E12.5 neurospheres.

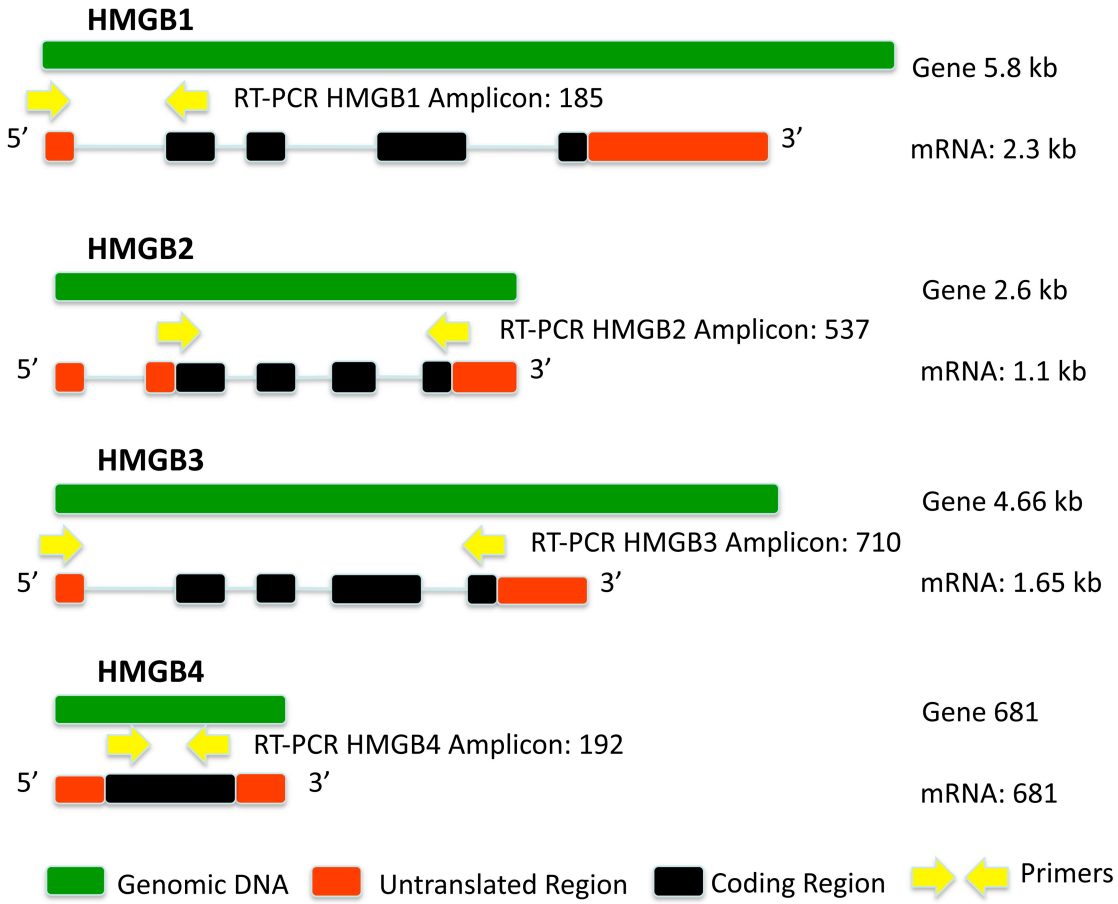

Figure 6: RT-PCR analysis of proliferating E12.5 neurospheres demonstrating expression of HMGB1, b2, b3, and b4 mRNA expression

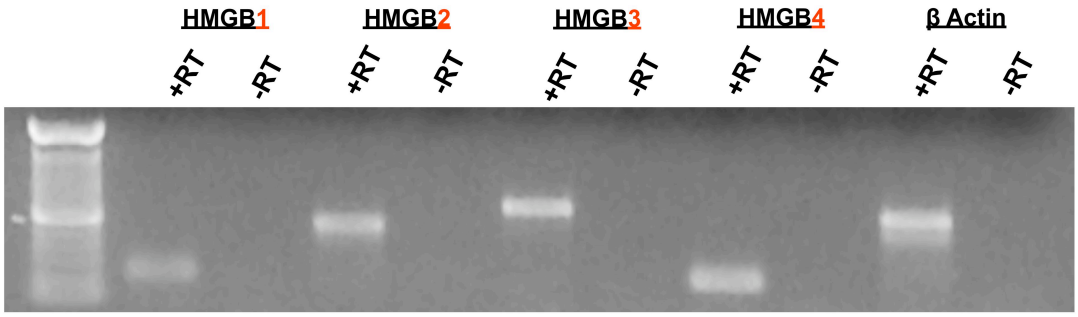

Table 1: Proteins in E12.5 neurospheres identified by shotgun proteomics.

IPI	Protein Description	peptides	coverage	Total Spectra	#1 (spectra)			#2 (spectra)			#1 (spectra)			#2 (spectra)		
					P2 (M)	P2 (T)	P2 (S)	P2 (M)	P2 (T)	P2 (S)	P8 (M)	P8 (T)	P8 (S)	P8 (M)	P8 (T)	P8 (S)
IPI00130280	SWISS-PROT:Q03265 Atp5a1 ATP synthase subunit	18	37.6%	131												
IPI00119618	SWISS-PROT:P35564 Canx Calnexin precursor	18	31.6%	107												
IPI00308885	SWISS-PROT:P63038-1 Hspd1 Isoform 1 of 60 kDa	16	33.5%	135												
IPI00323592	SWISS-PROT:P08249 Mdh2 Malate dehydrogenase,	11	34.9%	74												
IPI00468481	SWISS-PROT:P56480 Atp5b ATP synthase subunit b	19	35.3%	113												
IPI00229534	SWISS-PROT:P26645 Marcks Myristoylated alanine-r	27	77.7%	367												
IPI00880839	TREMBL:Q3TW93 Hspa9 heat shock protein 9	14	25.3%	78												
IPI00420569	SWISS-PROT:Q6PIE5 Atp1a2 Sodium/potassium-tra	13	14.0%	61												
IPI00319992	SWISS-PROT:P20029 Hspa5 78 kDa glucose-regulat	20	37.6%	131												
IPI00230108	SWISS-PROT:P27773 Pdia3 Protein disulfide-isomera	19	36.2%	98												
IPI00453826	SWISS-PROT:Q8K310 Matr3 Matrin-3	9	15.5%	58												
IPI00113869	SWISS-PROT:P18572-2 Bsg Isoform 2 of Basigin pre	5	18.7%	30												
IPI00222496	SWISS-PROT:Q922R8 Pdia6 CRL-1722 L5178Y-R cD	6	17.1%	29												
IPI00331628	SWISS-PROT:P51660 Hsd17b4 Peroxisomal multifun	7	11.7%	24												
IPI00408892	SWISS-PROT:P51150 Rab7 Ras-related protein Rab-	4	23.2%	21												
IPI00136703	SWISS-PROT:Q04447 Ckb Creatine kinase B-type	39	59.3%	418												
IPI00853914	REFSEQ:XP_001473875 LOC100045191 similar to	20	23.3%	123												
IPI00453692	SWISS-PROT:Q6P5H2-1 Nes Isoform 1 of Nestin	17	11.1%	54												
IPI00410819	TREMBL:Q3UC51 Ddost Bone marrow macrophage c	5	12.0%	26												
IPI00230351	SWISS-PROT:Q8K2B3 Sdha Succinate dehydrogenas	5	7.7%	23												
IPI00227299	SWISS-PROT:P20152 Vim Vimentin	23	48.9%	120												
IPI00553777	SWISS-PROT:P49312-2 Hnrnpa1 CRL-1722 L5178Y	9	26.3%	51												
IPI00874456	SWISS-PROT:O08749 Dld Dihydrolipoyl dehydrogena	5	12.0%	37												
IPI00119138	SWISS-PROT:Q9DB77 Uqcrc2 Cytochrome b-c1 com	6	15.7%	35												
IPI00129526	SWISS-PROT:P08113 Hsp90b1 Endoplasmin precurs	9	16.1%	33												
IPI00755916	TREMBL:Q8VC46 Ubb;Rps27a;Gm1821;Ubc ubiquiti	5	7.9%	62												
IPI00133522	SWISS-PROT:P09103 P4hb Protein disulfide-isomera	10	25.1%	39												
IPI00856379	TREMBL:A6ZI44 Aldoa Fructose-bisphosphate aldola	10	26.8%	70												
IPI00223443	SWISS-PROT:Q9Z204-2 Hnrnpc Isoform C1 of Heter	9	29.7%	44												
IPI00281011	SWISS-PROT:P28667 Marcksl1 MARCKS-related prot	7	53.0%	34												
IPI00759940	SWISS-PROT:P97807-2 Fh1 Isoform Cytoplasmic of	3	8.4%	13												
IPI00849786	REFSEQ:XP_001473871 LOC100045189 similar to	12	43.4%	164												
IPI00890005	SWISS-PROT:P61979-3 Hnrpk Isoform 3 of Heterog	14	36.7%	134												
IPI00129519	SWISS-PROT:Q91XV3 Basp1 Brain acid soluble prote	12	73.5%	109												
IPI00317794	SWISS-PROT:P09405 Ncl Nucleolin	10	16.3%	70												
IPI00407130	SWISS-PROT:P52480-1 Pkm2 Isoform M2 of Pyruva	13	28.1%	56												
IPI00123639	SWISS-PROT:P14211 Calr Calreticulin precursor	10	24.8%	41												
IPI00331597	SWISS-PROT:P43277 Hist1h1d Histone H1.3	7	29.0%	36												
IPI00113141	SWISS-PROT:Q9CZU6 Cs Citrate synthase, mitochon	7	17.5%	25												
IPI00132799	TREMBL:Q8R5L1 C1qbp complement component 1,	3	12.2%	24												
IPI00135686	SWISS-PROT:P24369 Ppib peptidylprolyl isomerase	4	24.1%	20												
IPI00154054	SWISS-PROT:Q8QZT1 Acat1 Acetyl-CoA acetyltrans	4	13.0%	19												
IPI00116753	SWISS-PROT:Q99LC5 Etfa Electron transfer flavopro	5	23.4%	18												
IPI00123704	SWISS-PROT:P14231 Atp1b2 Sodium/potassium-tra	2	4.8%	18												
IPI00137227	SWISS-PROT:P53994 Rab2a Ras-related protein Rab	2	14.2%	16												
IPI00869393	TREMBL:Q3TVZ1 Cat catalase	3	8.0%	16												
IPI00122547	SWISS-PROT:Q60930 Vdac2 Voltage-dependent ani	4	14.9%	14												
IPI00122549	SWISS-PROT:Q60932-1 Vdac1 Isoform Pl-VDAC1 of	4	15.2%	8												
IPI00116074	SWISS-PROT:Q99KI0 Aco2 Aconitate hydratase, mit	11	18.1%	50												
IPI00128973	SWISS-PROT:P06837 Gap43 Neuromodulin	4	28.2%	35												
IPI00133916	SWISS-PROT:O35737 Hnrph1 Heterogeneous nuclea	5	16.9%	33												
IPI00271951	SWISS-PROT:P08003 Pdia4 protein disulfide isomera	7	11.2%	31												
IPI00309035	SWISS-PROT:Q91YQ5 Rpn1 Dolichyl-diphosphooligos	7	16.0%	31												
IPI00648014	TREMBL:Q3UDA7 Npm1 Adult female placenta cDNA	6	24.5%	28												
IPI00318614	SWISS-PROT:P54071 Idh2 Isocitrate dehydrogenase	3	9.1%	27												
IPI00330958	SWISS-PROT:Q60668-1 Hnrpd Isoform 1 of Heterog	4	16.9%	26												
IPI00753028	ENSEMBL:ENSMUSP00000091727 LOC100041748	8	26.7%	25												
IPI00119114	SWISS-PROT:P51174 Acadl Long-chain specific acyl	3	8.1%	20												
IPI00321718	SWISS-PROT:O35129 Phb2 Prohibitin-2	4	22.1%	20												
IPI00623553	ENSEMBL:ENSMUSP00000087974 LOC100044492	7	31.3%	18												
IPI00111416	SWISS-PROT:Q9ER00 Stx12 Syntaxin-12	3	16.8%	17												
IPI00119203	SWISS-PROT:P50544 Acadvl Very long-chain specifi	7	15.4%	15												
IPI00153660	SWISS-PROT:Q8BMF4 Dlat Dihydrolipoyllysine-residu	3	6.5%	14												
IPI00121833	SWISS-PROT:Q921H8 Acaa1b;Acaa1a 3-ketoacyl-Co	4	13.7%	13												
IPI00230035	SWISS-PROT:Q62167 Ddx3x ATP-dependent RNA he	4	7.7%	12												
IPI00273164	SWISS-PROT:Q8BWF0 Aldh5a1 Succinate-semialdeh	4	10.1%	12												
IPI00133240	SWISS-PROT:Q9CR68 Uqcrfs1 Cytochrome b-c1 com	3	8.4%	10												
IPI00742278	TREMBL:Q3U2B2 Npc1 Niemann Pick type C1	2	1.9%	9												
IPI00137736	SWISS-PROT:P62858 Rps28;LOC100048156;LOC10	3	46.4%	29												
IPI00114209	SWISS-PROT:P26443 Glud1 Glutamate dehydrogena	5	11.1%	26												
IPI00889811	TREMBL:Q3U505 Rpn2 2 days neonate thymus thyr	4	10.4%	22												
IPI00121758	SWISS-PROT:Q921F2 Tardbp TAR DNA-binding prot	4	12.6%	21												
IPI00117352	SWISS-PROT:P99024 Tubb5 Tubulin beta-5 chain	3	9.9%	20												
IPI00115454	SWISS-PROT:Q99JR1 Sfxn1 Sideroflexin-1	3	11.2%	18												
IPI00109611	SWISS-PROT:Q9D6U8 2310056P07Rik E2-induced g	3	16.1%	12												
IPI00329953	TREMBL:Q8BH40 Stx7 Syntaxin-7	2	10.7%	12												
IPI00132762	SWISS-PROT:Q9CQN1 Trap1 Heat shock protein 75	2	4.0%	11												
IPI00223092	SWISS-PROT:Q8BMS1 Hadha Trifunctional enzyme s	6	9.8%	11												
IPI00653598	TREMBL:Q3THM1 Uqcrc1 ubiquinol-cytochrome c re	2	6.9%	10												
IPI00119219	SWISS-PROT:O70503-1 Hsd17b12 Isoform 1 of Est	2	9.3%	9												
IPI00120984	SWISS-PROT:Q9DCJ5 Ndufa8 NADH dehydrogenase	2	20.3%	8												
IPI00128441	TREMBL:Q3U8W9 Hnrnpr Bone marrow macrophage	5	9.8%	8												
IPI00330599	SWISS-PROT:Q80WJ7 Mtdh Protein LYRIC	3	7.1%	7												
IPI00110850	SWISS-PROT:P60710 Actb Actin, cytoplasmic 1	30	47.7%	272												
IPI00323357	SWISS-PROT:P63017 Hspa8 Heat shock cognate 71	20	33.3%	161												
IPI00110753	SWISS-PROT:P68369 Tuba1a Tubulin alpha-1A chai	12	40.1%	122												
IPI00462072	SWISS-PROT:P17182 Eno1;EG433182;LOC100044	14	46.5%	96												
IPI00648228	TREMBL:Q80XR6 Hnrpab Hnrpab protein	13	47.3%	86												
IPI00467833	SWISS-PROT:P17751 Tpi1 Triosephosphate isomera	6	33.3%	71												
IPI00830623	TREMBL:Q8CFQ9 Fus Fusion, derived from t(12;16)	9	29.6%	54												
IPI00129323	SWISS-PROT:P84104-1 Sfrs3 Isoform Long of Splici	3	21.3%	39												
IPI00556768	SWISS-PROT:Q569Z6 Thrap3 Thyroid hormone rece	7	8.6%	25												
IPI00134599	SWISS-PROT:P62908 Rps3 40S ribosomal protein S	3	15.6%	24												
IPI00230133	SWISS-PROT:P43276 Hist1h1b Histone H1.5	3	17.5%	23												
IPI00136883	TREMBL:Q3T984 Ptbp1 Activated spleen cDNA, RIK	4	11.3%	22												
IPI00849793	SWISS-PROT:P35979 Rpl12 60S ribosomal protein L	3	24.2%	22												
IPI00226073	SWISS-PROT:Q9Z2X1-1 Hnrpf Isoform 1 of Heterog	3	11.8%	21												
IPI00755120	TREMBL:A2AVJ7 Rrbp1 ribosome binding protein 1	7	5.9%	19												

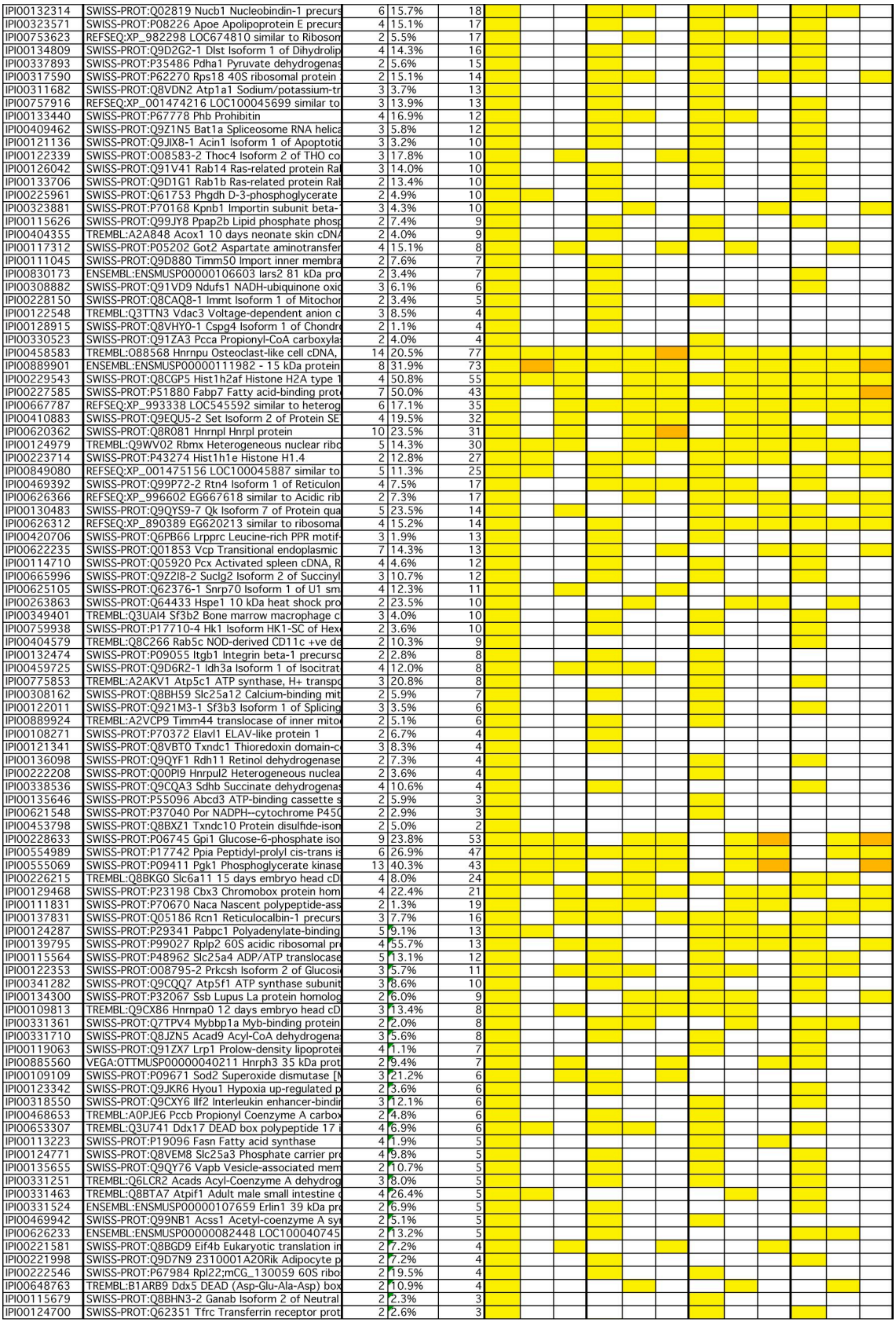

IPI00132314	SWISS-PROT:Q02819 Nucb1 Nucleobindin-1 precurs	6	15.7%	18													
IPI00323571	SWISS-PROT:P08226 Apoe Apolipoprotein E precurs	4	15.1%	17													
IPI00753623	REFSEQ:XP_982298 LOC674810 similar to Riboson	2	5.5%	17													
IPI00134809	SWISS-PROT:Q9D2G2-1 Dlst Isoform 1 of Dihydrolip	4	14.3%	16													
IPI00337893	SWISS-PROT:P35486 Pdha1 Pyruvate dehydrogenas	2	5.6%	15													
IPI00317590	SWISS-PROT:P62270 Rps18 40S ribosomal protein	2	15.1%	14													
IPI00311682	SWISS-PROT:Q8VDN2 Atp1a1 Sodium/potassium-tr	3	3.7%	13													
IPI00757916	REFSEQ:XP_001474216 LOC100045699 similar to	3	13.9%	13													
IPI00133440	SWISS-PROT:P67778 Phb Prohibitin	4	16.9%	12													
IPI00409462	SWISS-PROT:Q9Z1N5 Bat1a Spliceosome RNA helica	3	5.8%	12													
IPI00121136	SWISS-PROT:Q9JIX8-1 Acin1 Isoform 1 of Apoptotic	3	3.2%	10													
IPI00122339	SWISS-PROT:O08583-2 Thoc4 Isoform 2 of THO co	3	17.8%	10													
IPI00126042	SWISS-PROT:Q91V41 Rab14 Ras-related protein Rat	3	14.0%	10													
IPI00133706	SWISS-PROT:Q9D1G1 Rab1b Ras-related protein Rab	2	13.4%	10													
IPI00225961	SWISS-PROT:Q61753 Phgdh D-3-phosphoglycerate	2	4.9%	10													
IPI00323881	SWISS-PROT:P70168 Kpnb1 Importin subunit beta-1	3	4.3%	10													
IPI00115626	SWISS-PROT:Q99JY8 Ppap2b Lipid phosphate phosp	2	7.4%	9													
IPI00404355	TREMBL:A2A848 Acox1 10 days neonate skin cDNA	2	4.0%	9													
IPI00117312	SWISS-PROT:P05202 Got2 Aspartate aminotransfer	4	15.1%	8													
IPI00111045	SWISS-PROT:Q9D880 Timm50 Import inner membra	2	7.6%	7													
IPI00830173	ENSEMBL:ENSMUSP00000106603 Iars2 81 kDa pro	2	3.4%	7													
IPI00308882	SWISS-PROT:Q91VD9 Ndufs1 NADH-ubiquinone oxid	3	6.1%	6													
IPI00228150	SWISS-PROT:Q8CAQ8-1 Immt Isoform 1 of Mitochon	2	3.4%	5													
IPI00122548	TREMBL:Q3TTN3 Vdac3 Voltage-dependent anion c	3	8.5%	4													
IPI00128915	SWISS-PROT:Q8VHY0-1 Cspg4 Isoform 1 of Chondr	2	1.1%	4													
IPI00330523	SWISS-PROT:Q91ZA3 Pcca Propionyl-CoA carboxyla	2	4.0%	4													
IPI00458583	TREMBL:O88568 Hnrnpu Osteoclast-like cell cDNA,	14	20.5%	77													
IPI00889901	ENSEMBL:ENSMUSP00000111982 - 15 kDa protein	8	31.9%	73													
IPI00229543	SWISS-PROT:Q8CGP5 Hist1h2af Histone H2A type 1	4	50.8%	55													
IPI00227585	SWISS-PROT:P51880 Fabp7 Fatty acid-binding prot	7	50.0%	43													
IPI00667787	REFSEQ:XP_993338 LOC545592 similar to heterog	6	17.1%	35													
IPI00410883	SWISS-PROT:Q9EQU5-2 Set Isoform 2 of Protein SE	4	19.5%	32													
IPI00620362	SWISS-PROT:Q8R081 Hnrnpl Hnrpl protein	10	23.5%	31													
IPI00124979	TREMBL:Q9WV02 Rbmx Heterogeneous nuclear ribo	5	14.3%	30													
IPI00223714	SWISS-PROT:P43274 Hist1h1e Histone H1.4	2	12.8%	27													
IPI00849080	REFSEQ:XP_001475156 LOC100045887 similar to	5	11.3%	25													
IPI00469392	SWISS-PROT:Q99P72-2 Rtn4 Isoform 1 of Reticulon	4	7.5%	17													
IPI00626366	REFSEQ:XP_996602 EG667618 similar to Acidic rib	2	7.3%	17													
IPI00130483	SWISS-PROT:Q9QYS9-7 Qk Isoform 7 of Protein qua	5	23.5%	14													
IPI00626312	REFSEQ:XP_890389 EG620213 similar to ribosoma	4	15.2%	14													
IPI00420706	SWISS-PROT:Q6PB66 Lrpprc Leucine-rich PPR motif-	3	1.9%	13													
IPI00622235	SWISS-PROT:Q01853 Vcp Transitional endoplasmic	7	14.3%	13													
IPI00114710	SWISS-PROT:Q05920 Pcx Activated spleen cDNA, R	4	4.6%	12													
IPI00665996	SWISS-PROT:Q9Z2I8-2 Suclg2 Isoform 2 of Succinyl	3	10.7%	12													
IPI00625105	SWISS-PROT:Q62376-1 Snrp70 Isoform 1 of U1 sm	4	12.3%	11													
IPI00263863	SWISS-PROT:Q64433 Hspe1 10 kDa heat shock pro	2	23.5%	10													
IPI00349401	TREMBL:Q3UAI4 Sf3b2 Bone marrow macrophage c	3	4.0%	10													
IPI00759938	SWISS-PROT:P17710-4 Hk1 Isoform HK1-SC of Hex	2	3.6%	10													
IPI00404579	TREMBL:Q8C266 Rab5c NOD-derived CD11c +ve de	2	10.3%	9													
IPI00132474	SWISS-PROT:P09055 Itgb1 Integrin beta-1 precurso	2	2.8%	8													
IPI00459725	SWISS-PROT:Q9D6R2-1 Idh3a Isoform 1 of Isocitrat	4	12.0%	8													
IPI00775853	TREMBL:A2AKV1 Atp5c1 ATP synthase, H+ transpo	3	20.8%	8													
IPI00308162	SWISS-PROT:Q8BH59 Slc25a12 Calcium-binding mit	2	5.9%	7													
IPI00122011	SWISS-PROT:Q921M3-1 Sf3b3 Isoform 1 of Splicing	3	3.5%	6													
IPI00889924	TREMBL:A2VCP9 Timm44 translocase of inner mito	2	5.1%	6													
IPI00108271	SWISS-PROT:P70372 Elavl1 ELAV-like protein 1	2	6.7%	4													
IPI00121341	SWISS-PROT:Q8VBT0 Txndc1 Thioredoxin domain-c	3	8.3%	4													
IPI00136098	SWISS-PROT:Q9QYF1 Rdh11 Retinol dehydrogenase	2	7.3%	4													
IPI00222208	SWISS-PROT:Q00PI9 Hnrpul2 Heterogeneous nuclea	2	3.6%	4													
IPI00338536	SWISS-PROT:Q9CQA3 Sdhb Succinate dehydrogenas	4	10.6%	4													
IPI00135646	SWISS-PROT:P55096 Abcd3 ATP-binding cassette s	2	5.9%	3													
IPI00621548	SWISS-PROT:P37040 Por NADPH--cytochrome P450	2	2.9%	3													
IPI00453798	SWISS-PROT:Q8BXZ1 Txndc10 Protein disulfide-ison	2	5.0%	2													
IPI00228633	SWISS-PROT:P06745 Gpi1 Glucose-6-phosphate iso	9	23.8%	53													
IPI00554989	SWISS-PROT:P17742 Ppia Peptidyl-prolyl cis-trans is	6	26.9%	47													
IPI00555069	SWISS-PROT:P09411 Pgk1 Phosphoglycerate kinase	13	40.3%	43													
IPI00226215	TREMBL:Q8BKG0 Slc6a11 15 days embryo head cDI	4	8.0%	24													
IPI00129468	SWISS-PROT:P23198 Cbx3 Chromobox protein hom	4	22.4%	21													
IPI00111831	SWISS-PROT:P70670 Naca Nascent polypeptide-ass	2	1.3%	19													
IPI00137831	SWISS-PROT:Q05186 Rcn1 Reticulocalbin-1 precurs	3	7.7%	16													
IPI00124287	SWISS-PROT:P29341 Pabpc1 Polyadenylate-binding	5	9.1%	13													
IPI00139795	SWISS-PROT:P99027 Rplp2 60S acidic ribosomal pr	4	55.7%	13													
IPI00115564	SWISS-PROT:P48962 Slc25a4 ADP/ATP translocase	5	13.1%	12													
IPI00122353	SWISS-PROT:O08795-2 Prkcsh Isoform 2 of Glucosi	3	5.7%	11													
IPI00341282	SWISS-PROT:Q9CQQ7 Atp5f1 ATP synthase subunit	3	8.6%	10													
IPI00134300	SWISS-PROT:P32067 Ssb Lupus La protein homolog	2	6.0%	9													
IPI00109813	TREMBL:Q9CX86 Hnrnpa0 12 days embryo head cD	3	13.4%	8													
IPI00331361	SWISS-PROT:Q7TPV4 Mybbp1a Myb-binding protein	2	2.0%	8													
IPI00331710	SWISS-PROT:Q8JZN5 Acad9 Acyl-CoA dehydrogena	3	5.6%	8													
IPI00119063	SWISS-PROT:Q91ZX7 Lrp1 Prolow-density lipoprote	4	1.1%	7													
IPI00885560	VEGA:OTTMUSP00000040211 Hnrph3 35 kDa prot	2	9.4%	7													
IPI00109109	SWISS-PROT:P09671 Sod2 Superoxide dismutase [M	3	21.2%	6													
IPI00123342	SWISS-PROT:Q9JKR6 Hyou1 Hypoxia up-regulated p	2	3.6%	6													
IPI00318550	SWISS-PROT:Q9CXY6 Ilf2 Interleukin enhancer-bindir	3	12.1%	6													
IPI00468653	TREMBL:A0PJE6 Pccb Propionyl Coenzyme A carbox	2	4.8%	6													
IPI00653307	TREMBL:Q3U741 Ddx17 DEAD box polypeptide 17 i	4	6.9%	6													
IPI00113223	SWISS-PROT:P19096 Fasn Fatty acid synthase	4	1.9%	5													
IPI00124771	SWISS-PROT:Q8VEM8 Slc25a3 Phosphate carrier pro	4	9.8%	5													
IPI00135655	SWISS-PROT:Q9QY76 Vapb Vesicle-associated mem	2	10.7%	5													
IPI00331251	TREMBL:Q6LCR2 Acads Acyl-Coenzyme A dehydrog	3	8.0%	5													
IPI00331463	TREMBL:Q8BTA7 Atpif1 Adult male small intestine c	4	26.4%	5													
IPI00331524	ENSEMBL:ENSMUSP00000107659 Erlin1 39 kDa pro	2	6.9%	5													
IPI00469942	SWISS-PROT:Q99NB1 Acss1 Acetyl-coenzyme A syn	2	5.1%	5													
IPI00626233	ENSEMBL:ENSMUSP00000082448 LOC100040745	2	13.2%	5													
IPI00221581	SWISS-PROT:Q8BGD9 Eif4b Eukaryotic translation in	2	7.2%	4													
IPI00221998	SWISS-PROT:Q9D7N9 2310001A20Rik Adipocyte p	2	7.2%	4													
IPI00222546	SWISS-PROT:P67984 Rpl22;mCG_130059 60S ribo	2	19.5%	4													
IPI00648763	TREMBL:B1ARB9 Ddx5 DEAD (Asp-Glu-Ala-Asp) box	2	10.9%	4													
IPI00115679	SWISS-PROT:Q8BHN3-2 Ganab Isoform 2 of Neutral	2	2.3%	3													
IPI00124700	SWISS-PROT:Q62351 Tfrc Transferrin receptor prot	2	2.6%	3													

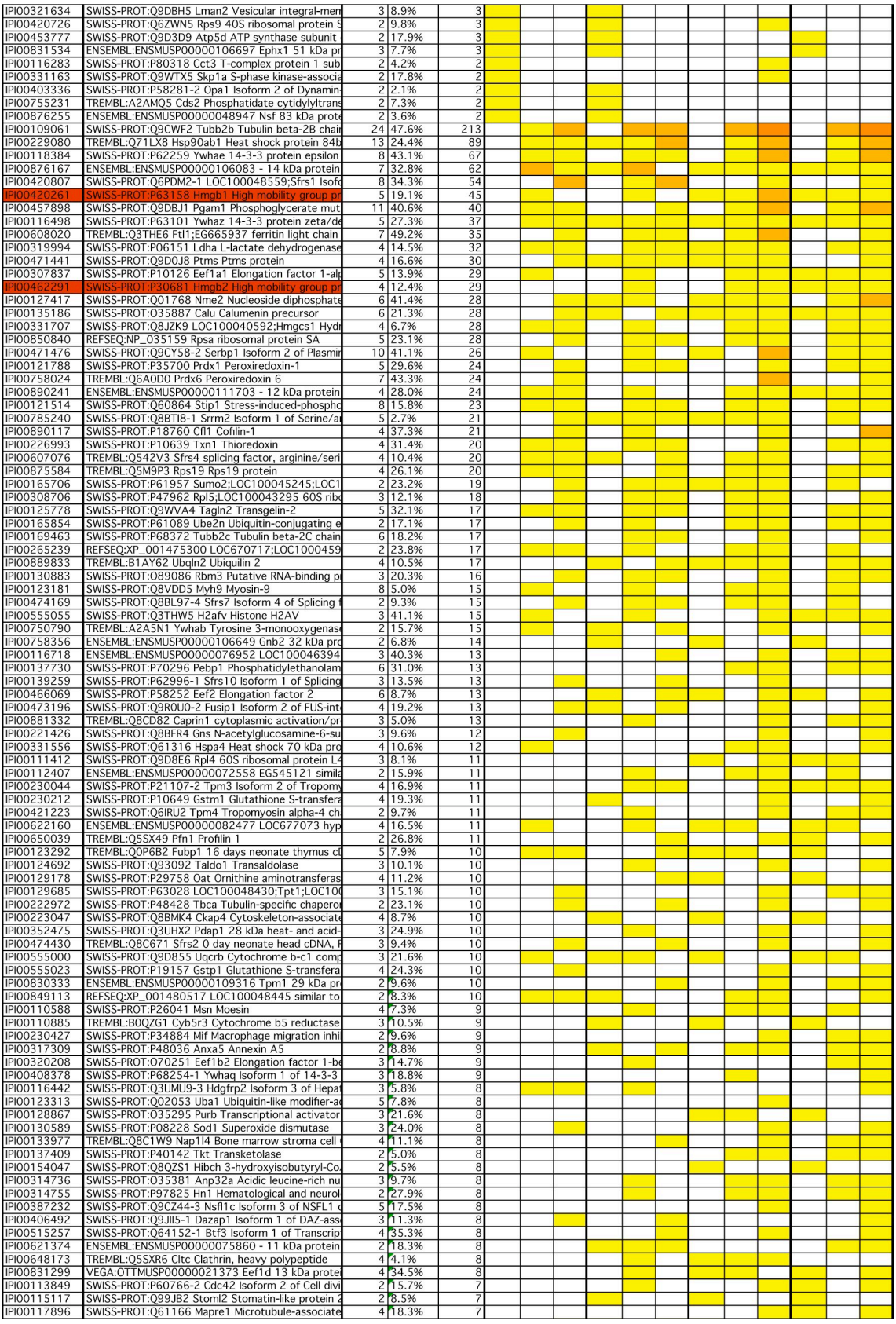

IPI00321634	SWISS-PROT:Q9DBH5 Lman2 Vesicular integral-mem	3	8.9%	3													
IPI00420726	SWISS-PROT:Q6ZWN5 Rps9 40S ribosomal protein S	2	9.8%	3													
IPI00453777	SWISS-PROT:Q9D3D9 Atp5d ATP synthase subunit	2	17.9%	3													
IPI00831534	ENSEMBL:ENSMUSP00000106697 Ephx1 51 kDa pr	3	7.7%	3													
IPI00116283	SWISS-PROT:P80318 Cct3 T-complex protein 1 sub	2	4.2%	2													
IPI00331163	SWISS-PROT:Q9WTX5 Skp1a S-phase kinase-associa	2	17.8%	2													
IPI00403336	SWISS-PROT:P58281-2 Opa1 Isoform 2 of Dynamin-	2	2.1%	2													
IPI00755231	TREMBL:A2AMQ5 Cds2 Phosphatidate cytidylyltrans	2	7.3%	2													
IPI00876255	ENSEMBL:ENSMUSP00000048947 Nsf 83 kDa prote	2	3.6%	2													
IPI00109061	SWISS-PROT:Q9CWF2 Tubb2b Tubulin beta-2B chair	24	47.6%	213													
IPI00229080	TREMBL:Q71LX8 Hsp90ab1 Heat shock protein 84b	13	24.4%	89													
IPI00118384	SWISS-PROT:P62259 Ywhae 14-3-3 protein epsilon	8	43.1%	67													
IPI00876167	ENSEMBL:ENSMUSP00000106083 - 14 kDa protein	7	32.8%	62													
IPI00420807	SWISS-PROT:Q6PDM2-1 LOC100048559;Sfrs1 Isofo	8	34.3%	54													
IPI00420261	SWISS-PROT:P63158 Hmgb1 High mobility group pr	5	19.1%	45													
IPI00457898	SWISS-PROT:Q9DBJ1 Pgam1 Phosphoglycerate mut	11	40.6%	40													
IPI00116498	SWISS-PROT:P63101 Ywhaz 14-3-3 protein zeta/de	5	27.3%	37													
IPI00608020	TREMBL:Q3THE6 Ftl1;EG665937 ferritin light chain	7	49.2%	35													
IPI00319994	SWISS-PROT:P06151 Ldha L-lactate dehydrogenase	4	14.5%	32													
IPI00471441	SWISS-PROT:Q9D0J8 Ptms Ptms protein	4	16.6%	30													
IPI00307837	SWISS-PROT:P10126 Eef1a1 Elongation factor 1-alp	5	13.9%	29													
IPI00462291	SWISS-PROT:P30681 Hmgb2 High mobility group pr	4	12.4%	29													
IPI00127417	SWISS-PROT:Q01768 Nme2 Nucleoside diphosphate	6	41.4%	28													
IPI00135186	SWISS-PROT:O35887 Calu Calumenin precursor	6	21.3%	28													
IPI00331707	SWISS-PROT:Q8JZK9 LOC100040592;Hmgcs1 Hydr	4	6.7%	28													
IPI00850840	REFSEQ:NP_035159 Rpsa ribosomal protein SA	5	23.1%	28													
IPI00471476	SWISS-PROT:Q9CY58-2 Serbp1 Isoform 2 of Plasmin	10	41.1%	26													
IPI00121788	SWISS-PROT:P35700 Prdx1 Peroxiredoxin-1	5	29.6%	24													
IPI00758024	TREMBL:Q6A0D0 Prdx6 Peroxiredoxin 6	7	43.3%	24													
IPI00890241	ENSEMBL:ENSMUSP00000111703 - 12 kDa protein	4	28.0%	24													
IPI00121514	SWISS-PROT:Q60864 Stip1 Stress-induced-phospho	8	15.8%	23													
IPI00785240	SWISS-PROT:Q8BTI8-1 Srrm2 Isoform 1 of Serine/a	5	2.7%	21													
IPI00890117	SWISS-PROT:P18760 Cfl1 Cofilin-1	4	37.3%	21													
IPI00226993	SWISS-PROT:P10639 Txn1 Thioredoxin	4	31.4%	20													
IPI00607076	TREMBL:Q542V3 Sfrs4 splicing factor, arginine/seri	4	10.4%	20													
IPI00875584	TREMBL:Q5M9P3 Rps19 Rps19 protein	4	26.1%	20													
IPI00165706	SWISS-PROT:P61957 Sumo2;LOC100045245;LOC1	2	23.2%	19													
IPI00308706	SWISS-PROT:P47962 Rpl5;LOC100043295 60S ribo	3	12.1%	18													
IPI00125778	SWISS-PROT:Q9WVA4 Tagln2 Transgelin-2	5	32.1%	17													
IPI00165854	SWISS-PROT:P61089 Ube2n Ubiquitin-conjugating e	2	17.1%	17													
IPI00169463	SWISS-PROT:P68372 Tubb2c Tubulin beta-2C chain	6	18.2%	17													
IPI00265239	REFSEQ:XP_001475300 LOC670717;LOC1000459	2	23.8%	17													
IPI00889833	TREMBL:B1AY62 Ubqln2 Ubiquilin 2	4	10.5%	17													
IPI00130883	SWISS-PROT:O89086 Rbm3 Putative RNA-binding p	3	20.3%	16													
IPI00123181	SWISS-PROT:Q8VDD5 Myh9 Myosin-9	8	5.0%	15													
IPI00474169	SWISS-PROT:Q8BL97-4 Sfrs7 Isoform 4 of Splicing f	2	9.3%	15													
IPI00555055	SWISS-PROT:Q3THW5 H2afv Histone H2AV	3	41.1%	15													
IPI00750790	TREMBL:A2A5N1 Ywhab Tyrosine 3-monooxygenase	2	15.7%	15													
IPI00758356	ENSEMBL:ENSMUSP00000106649 Gnb2 32 kDa pro	2	6.8%	14													
IPI00116718	ENSEMBL:ENSMUSP00000076952 LOC100046394	3	40.3%	13													
IPI00137730	SWISS-PROT:P70296 Pebp1 Phosphatidylethanolam	6	31.0%	13													
IPI00139259	SWISS-PROT:P62996-1 Sfrs10 Isoform 1 of Splicing	3	13.5%	13													
IPI00466069	SWISS-PROT:P58252 Eef2 Elongation factor 2	6	8.7%	13													
IPI00473196	SWISS-PROT:Q9R0U0-2 Fusip1 Isoform 2 of FUS-int	4	19.2%	13													
IPI00881332	TREMBL:Q8CD82 Caprin1 cytoplasmic activation/pr	3	5.0%	13													
IPI00221426	SWISS-PROT:Q8BFR4 Gns N-acetylglucosamine-6-su	3	9.6%	12													
IPI00331556	SWISS-PROT:Q61316 Hspa4 Heat shock 70 kDa pro	4	10.6%	12													
IPI00111412	SWISS-PROT:Q9D8E6 Rpl4 60S ribosomal protein L4	3	8.1%	11													
IPI00112407	ENSEMBL:ENSMUSP00000072558 EG545121 simila	2	15.9%	11													
IPI00230044	SWISS-PROT:P21107-2 Tpm3 Isoform 2 of Tropomy	4	16.9%	11													
IPI00230212	SWISS-PROT:P10649 Gstm1 Glutathione S-transfera	4	19.3%	11													
IPI00421223	SWISS-PROT:Q6IRU2 Tpm4 Tropomyosin alpha-4 ch	2	9.7%	11													
IPI00622160	ENSEMBL:ENSMUSP00000082477 LOC677073 hyp	4	16.5%	11													
IPI00650039	TREMBL:Q5SX49 Pfn1 Profilin 1	2	26.8%	11													
IPI00123292	TREMBL:Q0P6B2 Fubp1 16 days neonate thymus cD	5	7.9%	10													
IPI00124692	SWISS-PROT:Q93092 Taldo1 Transaldolase	3	10.1%	10													
IPI00129178	SWISS-PROT:P29758 Oat Ornithine aminotransferas	4	11.2%	10													
IPI00129685	SWISS-PROT:P63028 LOC100048430;Tpt1;LOC100	3	15.1%	10													
IPI00222972	SWISS-PROT:P48428 Tbca Tubulin-specific chaperon	2	23.1%	10													
IPI00223047	SWISS-PROT:Q8BMK4 Ckap4 Cytoskeleton-associate	4	8.7%	10													
IPI00352475	SWISS-PROT:Q3UHX2 Pdap1 28 kDa heat- and acid-	3	24.9%	10													
IPI00474430	TREMBL:Q8C671 Sfrs2 0 day neonate head cDNA, F	3	9.4%	10													
IPI00555000	SWISS-PROT:Q9D855 Uqcrb Cytochrome b-c1 comp	3	21.6%	10													
IPI00555023	SWISS-PROT:P19157 Gstp1 Glutathione S-transfera	4	24.3%	10													
IPI00830333	ENSEMBL:ENSMUSP00000109316 Tpm1 29 kDa pr	2	9.6%	10													
IPI00849113	REFSEQ:XP_001480517 LOC100048445 similar to	2	8.3%	10													
IPI00110588	SWISS-PROT:P26041 Msn Moesin	4	7.3%	9													
IPI00110885	TREMBL:B0QZG1 Cyb5r3 Cytochrome b5 reductase	3	10.5%	9													
IPI00230427	SWISS-PROT:P34884 Mif Macrophage migration inhi	2	9.6%	9													
IPI00317309	SWISS-PROT:P48036 Anxa5 Annexin A5	2	8.8%	9													
IPI00320208	SWISS-PROT:O70251 Eef1b2 Elongation factor 1-be	3	14.7%	9													
IPI00408378	SWISS-PROT:P68254-1 Ywhaq Isoform 1 of 14-3-3	3	18.8%	9													
IPI00116442	SWISS-PROT:Q3UMU9-3 Hdgfrp2 Isoform 3 of Hepat	3	5.8%	8													
IPI00123313	SWISS-PROT:Q02053 Uba1 Ubiquitin-like modifier-ac	5	7.8%	8													
IPI00128867	SWISS-PROT:O35295 Purb Transcriptional activator	3	21.6%	8													
IPI00130589	SWISS-PROT:P08228 Sod1 Superoxide dismutase	3	24.0%	8													
IPI00133977	TREMBL:Q8C1W9 Nap1l4 Bone marrow stroma cell	4	11.1%	8													
IPI00137409	SWISS-PROT:P40142 Tkt Transketolase	2	5.0%	8													
IPI00154047	SWISS-PROT:Q8QZS1 Hibch 3-hydroxyisobutyryl-Co	2	5.5%	8													
IPI00314736	SWISS-PROT:O35381 Anp32a Acidic leucine-rich nu	3	9.7%	8													
IPI00314755	SWISS-PROT:P97825 Hn1 Hematological and neurol	2	27.9%	8													
IPI00387232	SWISS-PROT:Q9CZ44-3 Nsfl1c Isoform 3 of NSFL1 c	5	17.5%	8													
IPI00406492	SWISS-PROT:Q9JII5-1 Dazap1 Isoform 1 of DAZ-ass	3	11.3%	8													
IPI00515257	SWISS-PROT:Q64152-1 Btf3 Isoform 1 of Transcrip	4	35.3%	8													
IPI00621374	ENSEMBL:ENSMUSP00000075860 - 11 kDa protein	2	18.3%	8													
IPI00648173	TREMBL:Q5SXR6 Cltc Clathrin, heavy polypeptide	4	4.1%	8													
IPI00831299	VEGA:OTTMUSP00000021373 Eef1d 13 kDa prote	4	34.5%	8													
IPI00113849	SWISS-PROT:P60766-2 Cdc42 Isoform 2 of Cell divi	2	15.7%	7													
IPI00115117	SWISS-PROT:Q99JB2 Stoml2 Stomatin-like protein 2	2	8.5%	7													
IPI00117896	SWISS-PROT:Q61166 Mapre1 Microtubule-associate	4	18.3%	7													

IPI00122174	ENSEMBL:ENSMUSP00000092849 Safb scaffold att	5	7.8%	7												
IPI00126000	SWISS-PROT:Q62446 Fkbp3 FK506-binding protein	3	17.9%	7												
IPI00132340	SWISS-PROT:Q9D0B0 Sfrs9 Splicing factor, arginine	2	9.5%	7												
IPI00230145	SWISS-PROT:P09528 Fth1 Ferritin heavy chain	2	13.7%	7												
IPI00313817	SWISS-PROT:P51859 Hdgf Hepatoma-derived growt	4	29.1%	7												
IPI00320399	SWISS-PROT:Q61029-1 Tmpo Isoform Beta of Lami	3	8.6%	7												
IPI00330804	SWISS-PROT:P07901 Hsp90aa1 Heat shock protein	2	4.1%	7												
IPI00607914	SWISS-PROT:O70133-3 Dhx9 Isoform 3 of ATP-dep	4	4.5%	7												
IPI00111960	SWISS-PROT:P70699 Gaa Lysosomal alpha-glucosid	2	2.8%	6												
IPI00115607	SWISS-PROT:Q99JY0 Hadhb Trifunctional enzyme su	2	4.2%	6												
IPI00117910	SWISS-PROT:Q61171 Prdx2 Peroxiredoxin-2	4	26.3%	6												
IPI00123199	SWISS-PROT:P28656 Nap1l1 Nucleosome assembly	2	9.0%	6												
IPI00137787	SWISS-PROT:P62918 Rpl8 60S ribosomal protein L8	2	7.4%	6												
IPI00223372	SWISS-PROT:Q8VH51-3 Rbm39 NOD-derived CD11c	3	9.4%	6												
IPI00225633	SWISS-PROT:P11031 Sub1 Activated RNA polymera	2	18.9%	6												
IPI00321978	SWISS-PROT:P34022 Ranbp1 Ran-specific GTPase-a	2	10.8%	6												
IPI00471443	SWISS-PROT:Q66JS6 LOC100042807;LOC100043	2	8.4%	6												
IPI00648352	TREMBL:A2AFK7 Eif4a3 DEAD (Asp-Glu-Ala-Asp) bo	2	5.9%	6												
IPI00830976	TREMBL:B1AU75 Nasp nuclear autoantigenic sperm	3	4.4%	6												
IPI00876559	TREMBL:Q9R1J3 Khsrp KH type splicing regulatory p	4	10.0%	6												
IPI00119458	SWISS-PROT:P05063 Aldoc Fructose-bisphosphate	3	11.0%	5												
IPI00123129	SWISS-PROT:Q78PY7 Snd1 Staphylococcal nuclease	2	2.9%	5												
IPI00123494	SWISS-PROT:Q8VDM4 Psmd2 26S proteasome non-	2	3.4%	5												
IPI00130344	SWISS-PROT:Q9Z1Q5 Clic1 Chloride intracellular cha	2	12.4%	5												
IPI00133284	SWISS-PROT:Q9D172 D10Jhu81e;LOC100046684	2	9.4%	5												
IPI00137735	SWISS-PROT:P62852 Rps25 40S ribosomal protein	2	16.8%	5												
IPI00227808	SWISS-PROT:Q4VAA2-1 Cdv3 Isoform 1 of Protein	2	12.8%	5												
IPI00310880	TREMBL:Q3TWW8 Sfrs6 Osteoclast-like cell cDNA, F	2	5.0%	5												
IPI00480357	SWISS-PROT:Q9D0E1-2 Hnrpm Isoform 2 of Heterog	3	4.6%	5												
IPI00623951	SWISS-PROT:Q64522 Hist2h2ab Histone H2A type	2	40.0%	5												
IPI00755495	REFSEQ:XP_985520 LOC382492 similar to ribosom	2	20.8%	5												
IPI00828932	TREMBL:Q3THU7 Clta clathrin, light polypeptide (Lc	2	13.8%	5												
IPI00118676	SWISS-PROT:P60843 Eif4a1 Eukaryotic initiation fac	3	7.9%	4												
IPI00129577	SWISS-PROT:Q9Z0X1 Aifm1 Apoptosis-inducing fact	3	5.9%	4												
IPI00132942	SWISS-PROT:O35685 Nudc Nuclear migration protei	3	9.6%	4												
IPI00133801	SWISS-PROT:Q9D1J3 1110005A23Rik;EG625193 N	2	13.3%	4												
IPI00318841	SWISS-PROT:Q9D8N0 Eef1g Elongation factor 1-gar	2	5.0%	4												
IPI00322312	SWISS-PROT:Q99PT1 Arhgdia Rho GDP-dissociation	3	20.6%	4												
IPI00322749	SWISS-PROT:P62315 Snrpd1 Small nuclear ribonucle	2	27.7%	4												
IPI00469260	SWISS-PROT:O08810 Eftud2 116 kDa U5 small nucl	2	2.9%	4												
IPI00753915	REFSEQ:XP_981653 LOC674706 similar to Zinc fing	3	5.0%	4												
IPI00830743	TREMBL:Q5U448 Sfrs5 splicing factor, arginine/seri	2	10.0%	4												
IPI00890076	TREMBL:B1AX52 Maoa monoamine oxidase A	3	6.5%	4												
IPI00108774	SWISS-PROT:P54728 Rad23b UV excision repair pro	2	9.9%	3												
IPI00109221	SWISS-PROT:Q9EP69 Sacm1l Phosphatidylinositide p	2	3.4%	3												
IPI00120245	SWISS-PROT:P43406 Itgav Integrin alpha-V precurso	2	2.5%	3												
IPI00129466	SWISS-PROT:P83917 Cbx1;LOC100047028 Chromo	2	14.6%	3												
IPI00135231	SWISS-PROT:O88844 Idh1 0 day neonate lung cDNA	2	8.8%	3												
IPI00284444	SWISS-PROT:Q6A068 Cdc5l Cell division cycle 5-rela	2	2.7%	3												
IPI00315187	SWISS-PROT:Q9CQ22 2400001E08Rik UPF0404 pro	2	15.5%	3												
IPI00319965	SWISS-PROT:Q99JI4 Psmd6 26S proteasome non-A	2	5.7%	3												
IPI00320016	SWISS-PROT:Q99K48-1 Nono Isoform 1 of Non-POU	2	4.9%	3												
IPI00321499	SWISS-PROT:P59017 Bcl2l13 Bcl-2-like 13 protein	2	8.3%	3												
IPI00321734	SWISS-PROT:Q9CPU0 Glo1 Lactoylglutathione lyase	2	15.8%	3												
IPI00322209	SWISS-PROT:P11679 Krt8 Keratin, type II cytoskele	2	2.9%	3												
IPI00331146	SWISS-PROT:Q9DBP5 Cmpk1 UMP-CMP kinase	2	9.7%	3												
IPI00403996	SWISS-PROT:Q9Z1X4-2 Ilf3 Isoform 2 of Interleukin	2	4.5%	3												
IPI00555113	SWISS-PROT:P35980 Rpl18 60S ribosomal protein L	2	11.7%	3												
IPI00555140	SWISS-PROT:Q9D0F9 Pgm2;Pgm1 Phosphoglucomut	2	5.2%	3												
IPI00648723	VEGA:OTTMUSP00000011616 Stmn1 12 kDa prote	3	29.4%	3												
IPI00653404	TREMBL:Q3TLQ0 Mtap2 microtubule-associated pro	2	5.0%	3												
IPI00654422	TREMBL:Q3UR88 G3bp1 9 days embryo whole body	2	7.3%	3												
IPI00655088	TREMBL:Q3KQH9 Pcnp Pcnp protein	2	21.6%	3												
IPI00660619	SWISS-PROT:Q6P2L6-4 Whsc1l1 Isoform 4 of Histor	2	1.6%	3												
IPI00667117	SWISS-PROT:P31786 Dbi Acyl-CoA-binding protein	2	39.1%	3												
IPI00754976	ENSEMBL:ENSMUSP00000093719 LOC100039571	2	14.1%	3												
IPI00875864	SWISS-PROT:Q8BP92 Rcn2 Reticulocalbin-2 precurse	2	10.6%	3												
IPI00108125	SWISS-PROT:P63242 Eif5a Eukaryotic translation in	2	22.7%	2												
IPI00112963	SWISS-PROT:P26231 Ctnna1 Catenin alpha-1	2	3.2%	2												
IPI00116254	SWISS-PROT:O08807 Prdx4 Peroxiredoxin-4	2	8.4%	2												
IPI00121534	SWISS-PROT:P00920 Car2 Carbonic anhydrase 2	2	12.3%	2												
IPI00128154	SWISS-PROT:P06797 Ctsl Cathepsin L1 precursor	2	9.0%	2												
IPI00132539	SWISS-PROT:Q9CQH7 Btf3l4 Transcription factor BT	2	30.4%	2												
IPI00323819	SWISS-PROT:P60867 Rps20 40S ribosomal protein	2	19.3%	2												
IPI00329942	SWISS-PROT:P40336-2 Vps26a Isoform 2 of Vacuo	2	8.4%	2												
IPI00331528	SWISS-PROT:Q9QUH0 Glrx Glutaredoxin-1	2	37.4%	2												
IPI00473748	SWISS-PROT:P27546-3 Mtap4 Isoform 3 of Microtul	2	2.9%	2												
IPI00649136	TREMBL:B1ARA5 Rpl26 Ribosomal protein L26	2	16.1%	2												
IPI00753793	SWISS-PROT:P16546-2 Spna2 Isoform 2 of Spectrin	2	1.3%	2												
IPI00755329	SWISS-PROT:Q9CY50 Ssr1 Translocon-associated pr	2	7.7%	2												
IPI00828741	TREMBL:A2AU63 Raly HnRNP-associated with lethal	2	11.2%	2												
IPI00831107	ENSEMBL:ENSMUSP00000106047 Asah1 24 kDa pr	2	16.2%	2												
IPI00857092	TREMBL:A2VDF7 Slc4a4 Slc4a4 protein	2	3.1%	2												
IPI00875567	ENSEMBL:ENSMUSP00000098997 Flna filamin, alph	2	1.2%	2												

Chapter IV:

Characterization of Temporal Changes in HMG-B Family Gene and Protein Expression In Embryonic NSCs Isolated During Embryonic Neural Development

The data presented in Chapter III demonstrate that HMGB-1 and HMGB-2 mRNA and protein were expressed in proliferating neurospheres, findings strongly consistent with previous transcriptional profiling studies which have identified HMG-Bs in progenitor cells *in vitro* (Fortunel et al., 2003) and in the SVZ in vivo (Lim et al., 2006). No study has examined the dynamics of HMG-B mRNA and protein expression in neural stem and progenitor cells, an essential study which would address whether expression of HMG-Bs are tightly regulated in progenitor cells, especially during critical cellular processes such as proliferation and differentiation. The recent study which identified HMGA2 as a regulator of NSC maintenance demonstrated that HMGA2 mRNA and protein were differentially expressed in the forebrain lateral wall during embryonic neural development and the SVZ of aging mice (Nishino et al., 2008), a critical result that led to the subsequent finding that HMGA2 is a regulator of NSC maintenance and exerts its effects in a specific temporal pattern. HMGA2 accomplishes this by altering $p16^{Ink4a}$ expression *in vivo* and promoting NSC self-renewal in young but not aged mice. A study of the differential expression of

HMG-Bs in proliferating and differentiating NSCs would provide insight into the role of HMG-Bs in NSCs and whether they play a possible regulatory role in NSC maintenance and neurogenesis. Therefore, the purpose of this study was to characterize the expression of HMG-B family members in proliferating and differentiating NSCs and further characterize whether these changes in individual HMG-B expression in proliferating and differentiating NSCs were altered during different neural development time points known for dynamics changes in progenitor proliferation and differentiation.

HMGB mRNA and protein expression was studied by isolating NestinGFP neurospheres from the forebrain of NestinGFP transgenic mice at different time points during embryonic neural development. NestinGFP transgenic mice were generated previously and described elsewhere (Mignone et al., 2004). qRT-PCR and quantitative western blots were employed to study changes in HMGB mRNA and protein expression in proliferating and differentiating NSCs isolated during different time points during CNS development. Specifically, NestinGFP+ neurospheres were isolated between E12 and E17, a highly dynamic time period in neural development associated with NSC proliferation in the medial and lateral ganglionic eminences (MGE and LGE) and NSC differentiation in the form of striatal and cortical neurogenesis. In this manner changes in HMG-B mRNA and protein expression in proliferating and differentiating NSCs were characterized, as well as changes that were temporally specified, e.g. changed according to developmental time.

Methods

Neurosphere Formation Assay

Mouse NSCs were isolated from the forebrain of NestinGFP mice at day E12, E14.5, E15.5, and E17.5, and were prepared as described previously (NSC Isolation, Methods, Chapter III), except that each embryonic brain was cut in the ventral-dorsal plane immediately caudal to the telencephalon to ensure the separation of the telencephalon from the developing mid/hindbrain and spinal cord (to ensure the regional specificity of developing forebrain CNS tissue used to generate NSCs). To ascertain that embryos were of the correct developmental age, the developmental characteristics of each embryo were verified using the Theiler Atlas of Mouse Development (Theiler, 1989).

Gradient PCR, qRT-PCR Quantitative Western Blot Analysis

RNA was isolated, quantified, treated with DNAse, reverse transcribed, and treated with RNAse using methods previously described (RT-PCR Analysis, General Methods, Chapter II). cDNA was used to conduct quantitative real time RT-PCR (qRT-PCR) using the SYBRGreen PCR kit (Qiagen) with gene specific primers for HMGB1, B2, B3, and B4 to determine optimal primer annealing temperatures. HMG-B primers and β-Actin primer sequences were previously described (Chapter II). qRT-PCR reactions were run and read in a 7300 Real Time PCR System (Applied Biosystems). Cycling conditions for HMGB1 were as follows: 95ºC for 15 min, 94ºC for 15 sec (melting), 53.2ºC for 30 sec (annealing), 72ºC for 30 sec (extension), repeat for 40 cycles, 4º hold until end. Annealing

temperatures were modified to 58.1º for HMGB2 and HMGB3, and to 50.3º for HMGB4. Fold change in gene expression was calculated using the comparative CT method (Schmittgen and Livak, 2008). All qRT-PCR reactions were run in quadruplicate (4 technical replicates per sample). At least three different biological samples of NSCs at each time point in development were used for each experiment (n=3 experiments), including proliferation and differentiation experiments.

For quantitative westerns, proliferating and differentiating NSCs were lysed and protein determination was done by DC assay, loaded into 12 or 15% Tris Glycine SDS-PAGE gels as previously described (Western Blot Analysis, Chapter II). Membranes were incubated overnight at 4ºC with primary antibodies Rabbit anti-HMGB1 (Abcam, 1:1000), Mouse anti-HMGB2 (Abcam, 1:200), Rabbit anti-HMGB3 (Epitomics, 1:2000), and Rabbit anti-HMGB4 (Abcam, 1:250). All membranes were incubated with mouse anti-alpha Tubulin (Sigma, 1:2000) as loading control. Scanning and visualization of membranes was performed as previously described (Chapter II).

Results

Neurospheres isolated from the forebrain of NestinGFP mice were positive for GFP fluorescence (Figure7 A-C), demonstrating the expression of GFP under the control of this neural stem cell promoter. HMGB mRNA levels are temporally specified in proliferating NestinGFP+ neurospheres isolated at various time points during neural development. HMGB1 and B2 mRNA levels are 5.9 fold and

11.7 fold higher, respectively, in proliferating progenitor cells at E12 than at E15.5 (Figures 7D, E), following an expression pattern similar to that of HMGA2 mRNA levels between E14.5 and P0 (Nishino et al., 2008). HMGB3 mRNA levels are 9.6 fold and 21.3 fold higher in proliferating E12 and E14.5 neurospheres, respectively, than proliferating E15.5 neurospheres (Figure 7F). HMGB4 mRNA levels are also changed in proliferating neurospheres, but the magnitude of this change was negligible (Figure 7G), suggesting that HMGB4 mRNA is not tightly controlled in proliferating neurospheres, as are HMGB1, 2 and 3. These results reveal time-dependant changes in HMGB1, 2, and 3 mRNA levels, but not B4, in proliferating progenitor cells during different time points in embryonic neural development.

To investigate the HMGB mRNA levels in differentiating NSCs, NestinGFP+ neurospheres were cultured from E12, E14.5 and E15.5 forebrains, differentiated on laminin and poly-D-lysine, and analyzed by qRT-PCR. Changes in HMGB mRNA expression in differentiating neurospheres were calculated relative to proliferating neurospheres at each developmental timepoint. Our data revealed that HMGB1 and b2 mRNA levels decrease in differentiating NSCs at all investigated time points during CNS development; E12, E14.5 and E15.5 (Figure 7). Irrespective at which developmental point the NSCs were isolated there was an approximate 5 fold decrease in HMGB1 mRNA levels, and an approximate 10 fold drop in HMGB2 mRNA levels, in differentiating NSCs (Figures 7H, I). HMGB3 mRNA levels decreased 10 fold in differentiating E12 NSCs, did not change significantly in differentiating E14.5 NSCs and decreased two-fold in

differentiating E15.5 NSCs (Figure 7J). Finally, HMGB4 mRNA levels were unchanged in differentiating NSCs at E12 and E14.5, but decreased in differentiating E15.5 NSCs (Figure 7K). These results indicate that differentiating NSCs have differential HMGB mRNAs levels,, but only HMGB3 and HMGB4 demonstrated time–dependant changes in mRNA levels in differentiating NSCs isolated during different time points in neural development. Alternatively, HMGB1 and HMGB2 mRNA levels were lower in differentiating NSCs at all time points examined during neural development.

To assess HMGB protein levels in proliferating and differentiating NSCs, quantitative western blots were performed. HMGB1 and HMGB2 protein levels remained constant in proliferating NSCs isolated from E12 to E17.5 (Figures 8A,B). Low HMGB3 protein levels were detected in proliferating E12 NSCs, sharply increased at E14.5, and remained stable in proliferating NSCs between E14.5 and E17.5 (Figure 8C), consistent with previously described qRT-PCR data (Figure 7F). HMGB4 protein levels were not detectable in E12 NSCs, but were present and stable between E14.5-E17.5 in proliferating NSCs (Figure 8D). Western blots analysis of differentiating E12 NSCs indicated that HMGB1 and HMGB2 protein levels after 48 hours of differentiation were 54.4% and 51.3%, respectively, compared to proliferating E12 NSCs (Figures 8E, F), consistent with qRT-PCR data (Figure 7H, I).

Figure 7: A-C) Isolation of forebrain NestinGFP neurospheres and expression of GFP in NestinGFP neurospheres. D-G) qRT-PCR analysis of HMGB1, 2, 3, and 4 gene expression in proliferating E12.5, E14.5, and E15.5 forebrain neurospheres. H-K) qRT-PCR analysis of HMGB1, 2, 3, and 4 gene expression in differentiating E12.5, E14.5 and E15.5 forebrain neurospheres. N=3 biological samples per time point. Values are Mean+/- SEM. * = p<0.05 and ** = p<0.005

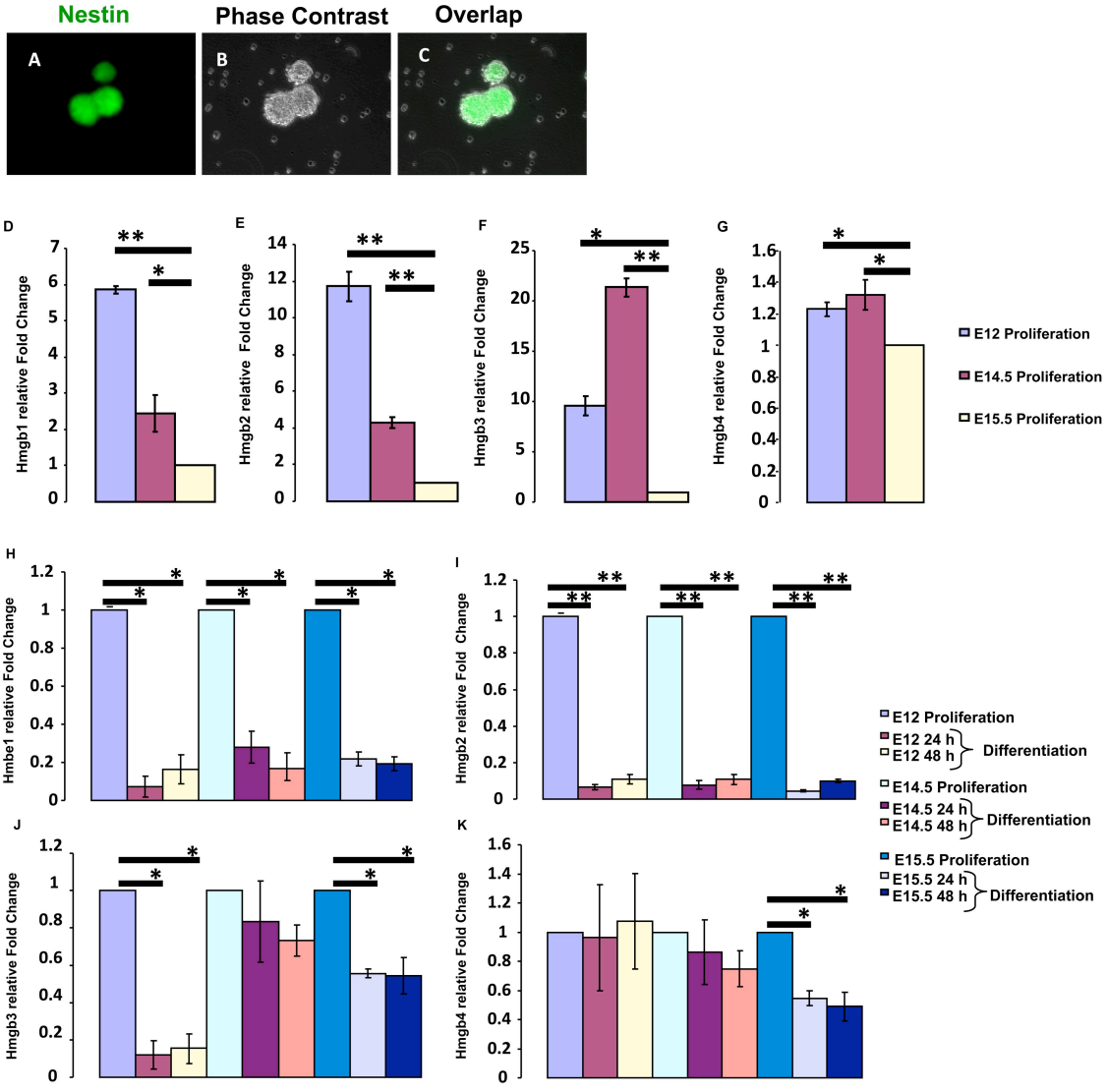

Figure 8: A-D) HMGB1, 2, 3, and 4 protein expression in proliferating E12, E14.5, E15.5 and E17.5 forebrain neurospheres. E-F) HMGB1 and HMGB2 protein expression in differentiating E12 forebrain neurospheres.

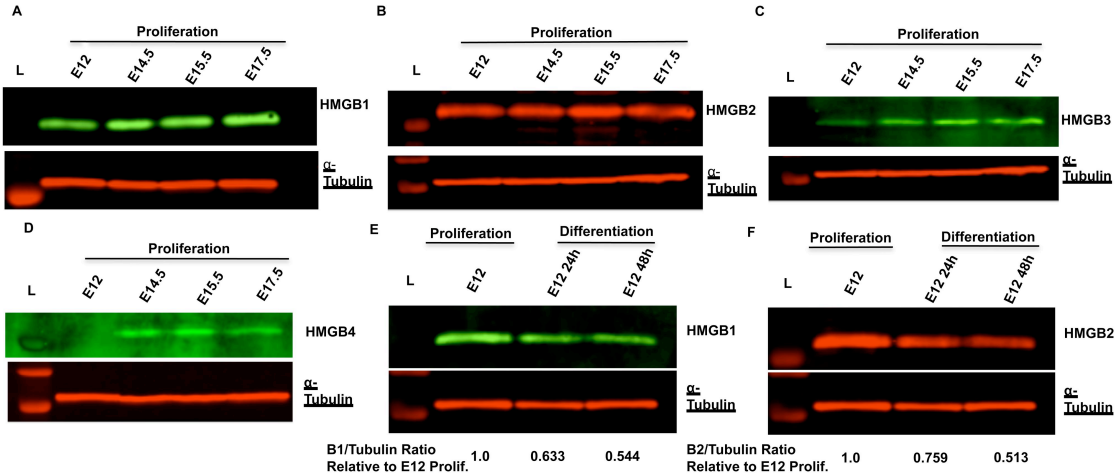

Chapter V:

Altered Subventricular Zone Neural Stem and Progenitor Cell Composition, Aberrant Olfactory Bulb Neurogenesis, and Ventriculomegaly in Young Adult Mice Lacking Chromatin Protein HMGB2

HMG-B mRNA and protein expression are temporally regulated in proliferating and differentiating neural progenitor cells. These dynamic changes in embryonic NSCs are robust, with decreases in HMGB1 and HMGB2 mRNA and protein levels in differentiating progenitors compared to proliferating neural progenitors (Fig 7, Fig 8). Among the largest magnitude changes in HMGB mRNA and protein levels in progenitor cells is HMGB2. HMGB2 mRNA levels decrease 12 fold in proliferating progenitor cells between E12 and E15.5 during neural development (Fig 7, page 42), and HMGB2 mRNA levels decrease almost 10 fold in differentiating neural progenitor cells compared to proliferating progenitor cells (Fig 7, page 42). These changes in HMGB2 levels suggests the possibility that HMGB2 is regulated in proliferating and differentiating progenitor cells because it may play a role in regulating these processes in neural progenitor cells. To address these possibilities, I studied the proliferation and differentiation of NSCs in HMGB2 knock out (HMGB2-/-) mice, a knock out mouse characterized and described previously (Ronfani et al., 2001).

The expression of HMGB2 mRNA in the SVZ of young adult mice has been verified using northern blot analysis (Lim et al., 2006). We first confirmed the presence of HMGB2 at the protein level in neural progenitor cells *in vivo* using HMGB2 immunofluorescence and NestinGFP transgenic mice to detect HMGB2 protein expression in NestinGFP+ neural progenitor cells in the SVZ of young adult mice. These NestinGFP+ progenitor cells proliferate and give rise to neuroblasts which migrate to the OB and differentiate into neurons (Doetsch et al., 1997; Doetsch et al., 1999). Consequently, we examined the proliferation of SVZ cells in WT (HMGB2+/+) and HMGB2-/- mice to determine whether changes in proliferation in the SVZ occurred in the absence of HMGB2 expression. We evaluated the composition of NSCs, NPCs, and neuroblasts in the SVZ of young adult HMGB2-/- mice to determine changes in progenitor cell number that may be explained by this SVZ hyperproliferation. Additionally, we studied the differences in the expression of different CDKIs, known regulators of NSCs and NPCs, in the SVZ in young adult HMGB2-/- mice. Finally, we examined differences in olfactory bulb neurogenesis in young adult HMGB2-/- mice. Our results indicate that mice lacking chromatin protein HMGB2 have a complex neural stem cell phenotype involving *in vivo* changes in expression of different neural stem cell markers, differences in expression of CDKIs in the SVZ, changes in OB granule cell layer neurogenesis, as well as gross abnormalities in neuro-anatomy, including several instances of massive ventriculomegaly.

Methods

In Vivo Proliferation and Differentiation Assays

To assess *in vivo* proliferation 2.5 month old WT and HMGB2-/- mice were intraperitoneal injection (IP) injected with 150 mg/kg BrdU (Sigma) every 12 hours for 2.5 days (5 injections total) and euthanized 12 hours after final injection. Mice were deeply anesthetized using IP injection of 2.5% Avertin solution and transcardially perfused with PBS followed by 4% paraformaldehyde/PBS. Mice brains were dissected out and kept in 4%PFA/PBS at 4°C. Brains were sectioned along the midline and floating 50 μmeters thick sagittal sections were generated by vibratome. All brain sections were collected in series. To assess *in vivo* differentiation, 2 month old WT and HMGB2-/- mice were injected by intraperitoneal injection (IP) with 150 mg/kg BrdU (Sigma) every 12 hours for 2 days (4 injections total) and euthanized 14 days after final injection, at 2.5 months. Perfusion and sectioning was performed as described above.

Immunofluorescence and Confocal Imaging

For proliferation immunofluorescence (IF) staining, one set of serial sections from each mouse were transferred to a new six well plate, washed with PBS, and antigen retrieval for BrdU staining and blocking with goat serum was preformed as previously described (General Methods, Chapter II). Sections were stained with rat anti-BrdU antibody (Serotec, 1:300) and Rabbit anti-Ki67 (Abcam, 1:200) in 0.3%BSA/0.2%TritonX/PBS solution over night at 4°C. For differentiation (IF)

staining, serial sections were transferred to a new six well plate, washed with PBS, and BrdU antigen retrieval was performed as described above. Sections were blocked and then stained with rat anti-BrdU and mouse anti-NeuN (Millipore, 1:1000) in 0.3%BSA/0.2%TritonX/PBS solution over night at 4°C. For progenitor marker (IF) staining serial sections were transferred, washed in PBS, blocked and then stained with mouse anti-GFAP (Dako, 1:500) or rabbit anti-doublecortin (DCX)(Millipore, 1:400) in 0.3%BSA/0.2%TritonX/PBS solution over night at 4°C. For cell cycle marker (IF) staining, serial sections were transferred and washed with PBS and stained with either rabbit anti-$p16^{Ink4a}$ (Santa Cruz, M-156, 1:100), mouse anti-$p21^{Cip1/Waf1}$ (Santa Cruz, 1:100), rabbit anti-p53 (Santa Cruz, 1:100), or rabbit anti-$p27^{Kip1}$ (NeoMarkers, 1:100) in 0.3%BSA/ 0.2%TritonX/ PBS solution over night at 4°C. All sections were washed extensively with PBS and stained with highly cross absorbed secondary antibodies used for dual staining, including highly cross absorbed anti-rat rhodamine red X (Jackson 1:500), anti-mouse FITC (1:200), anti-mouse Cy3 (1:500), anti-Rabbit Cy5 (1:500), and/or anti-rabbit Alexa 488 (Invitrogen, 1:2000). All secondary antibody incubations were performed in 0.3%BSA/ 0.2%TritonX/ PBS solution at room temperature for 1 hour. All sections were washed extensively with PBS following secondary antibody staining, were mounted on Superfrost plus micro slides (VWR), covered with Fluormount G mounting media (Southern Biotech) and covered with a cover glass (Fisher).

A Zeiss LSM 510 confocal microscope system with an Axiovert 200M inverted microscope was used to generate high magnification (100x) Z-stack images of

the entire thickness of sagittal brain sections containing the anterior SVZ (aSVZ), the proximal rostral migratory stream, and the granule cell layer and glomerular layers of the olfactory bulb (differentiation) of WT and HMGB2-/- mice. All brain sections were matched. To determine the number of total proliferating progenitors (BrdU+, Ki67+, and BrdU+/Ki67+ cells) in the aSVZ, 10 total fields of view comprising the aSVZ were imaged using Z-stacks and the cells were quantified using the LSM Image Browser Software (Zeiss). Only proliferating SVZ cells located in the cell dense region approximating the ventricle were quantified, and cells >100μmeters from the ependymal layer were excluded so as not to quantify cells in the striatum. Composite images of aSVZ in WT and HMGB2-/- mice were created by layering each high magnification field of view. To quantify BrdU+, NeuN+ and BrdU+/NeuN+ new born neurons in the OB GCL and GL, Z-stacks were generated from 3 random fields of view in each OB layer and analyzed using LSM software. For progenitor staining, GFAP, NestinGFP and doublecortin expression was stained examined in serial sections and images generated from both lateral and medial brain sections. Expression of $p16^{Ink4a}$, $p21^{Cip1/Waf1}$, p53, and $p27^{Kip1}$ were stained and examined in serial sections and images generated from medial sagittal brain sections.

Statistics

All comparisons were conducted using two-tailed unpaired t tests, and statistical significance cut off for all comparisons was $p \leq 0.05$.

Results

In Vivo HMGB2 Expression in Nestin GFP+ SVZ Progenitors Cells

HMGB2 protein expression in the SVZ of young adult mice was examined by staining brain sections of HMGB2+/+ NestinGFP mice for HMGB2 protein, and further assessing HMGB2 protein expression within Nestin+ SVZ progenitor cells. The results revealed that HMGB2 protein was expressed in the SVZ in young mice (Figure 9A-I), and that it was present in both NestinGFP+ SVZ progenitors cells and NestinGFP^{Neg} cells that were exiting the SVZ, including several cells that appeared to be entering the RMS (Figure 9A-I). The staining was punctate with a nuclear and perinuclear distribution. We note here that despite the expression of HMGB2 in several Nestin+ SVZ progenitor cells, not all Nestin+ SVZ cells expressed HMGB2; in several instances the cells that were brightest in HMGB2 expression were solitary Nestin+ progenitor cells in the SVZ, suggesting that a subpopulation of Nestin+ progenitor cells in the SVZ strongly express HMGB2 protein.

Young adult HMGB2-/- mice exhibited ventriculomegaly and hyperproliferation in the anterior SVZ compared to age matched WT mice

NestinGFP+ SVZ progenitor cells proliferate and give rise to neuroblasts which migrate to the OB and differentiate into neurons (Doetsch et al., 1997; Doetsch et al., 1999). We examined whether changes in HMGB2 expression altered proliferation in the SVZ in regions where the presence of HMGB2 protein

was confirmed. Upon initial examination of several brains from young HMGB2-/- mice, it was observed that 50% of HMGB2-/- mice (7 out of 14 mice) displayed enlarged ventricles at 2.5 months of age, while only 10% of WT mice (1 out of 10) exhibited any detectable enlargement of the ventricles by that age (Figure 10A,B). To assess whether proliferation was affected in the SVZ in young HMGB2-/- mice, we injected 2.5 month HMGB2-/- and WT mice with the nucleoside analog BrdU (150μg/mg) and then stained serial brain sections for BrdU (S phase marker) and the pan cell-cycle proliferation marker Ki67. We enumerated BrdU+, Ki67+, and BrdU+/Ki67+ cells in the anterior SVZ (aSVZ) and found that the BrdU+, Ki67+ and BrdU+/Ki67+ cell numbers and cell densities were elevated in the aSVZ of 2.5 month old HMGB2-/- mice relative to WT mice of the same age (Figure 11). HMGB2-/- mice reached a mean cell density of $4x10^5$ BrdU+/Ki67+ cells per mm^3 in the aSVZ at 2.5 months, which is almost 100% higher than the WT mice [which have a mean cell density of $2x10^5$ BrdU+/Ki67+ cells per mm^3 in the aSVZ at 2.5 months (Mean+/-SEM, n=4 WT and n=5 B2-/- null, $p<0.005$)].

NestinGFP+HMGB2-/- mice have increased numbers of Nestin+GFAP+ NSCs and Doublecortin+ (DCX) Neuroblasts compared to WT Mice.

To further determine the nature of the hyperproliferating cells in the SVZ of young adult HMGB2-/- mice, HMGB2+/- transgenic mice (Ronfani et al., 2001) were crossed with NestinGFP+ transgenic mice (Mignone et al., 2004) to generate compound NestinGFP+HMGB2+/+ and NestinGFP+HMGB2-/- mice.

This allowed us to study NestinGFP NSCs and NPCs in the SVZ of young mice in the presence or absence of HMGB2. We observed that a subset of NestinGFP+HMGB2-/- also exhibited ventriculomegaly, consistent with our previous observations. Additionally, NestinGFP+HMGB+/+ appeared neuro-anatomically intact, similar to HMGB2+/+ (WT) mice, further suggesting that the continued appearance of ventriculomegaly in subsets of HMGB2-/- mice would be specific to the loss of HMGB2.

Using compound NestinGFP+/HMGB2 transgenic mice, we stained for NSC cell marker GFAP, which was expressed in SVZ NSCs (type B cells)(Doetsch et al., 1997; Doetsch et al., 1999). We first examined lateral sagittal brain sections from WT and HMGB2-/- mice. In NestinGFP+HMGB2+/+ mice, GFAP expression was clearly present in the SVZ and colocalized with NestinGFP+ processes of NSCs in the SVZ (Figure 12A). In the NestinGFP+HMGB2-/- there was a dramatic increase in GFAP+ expression and GFAP+ processes in the SVZ; these GFAP+ processes appeared to arise from NestinGFP+ cell bodies in the SVZ (Figure 12B). Orthogonal views of the SVZ in NestinGFP+WT (Figure 12C,E) and NestinGFP+HMGB2-/- (Figure 12D,F) mice and quantification of Nestin+GFAP+ NSC and Nestin+GFAP- NPC cell populations in the SVZ of these two mice indicated that HMGB2-/- mice had higher numbers of Nestin+GFAP+ NSCs and lower numbers of Nestin+GFAP- NPCs than age matched WT mice (Figure 12G). Full resolution 3D reconstruction of the SVZ in WT and HMGB2-/- mice at this age appeared consistent with this observation, showing increased Nestin+GFAP+ SVZ NSCs (Figure 13). Furthermore, GFAP

staining of brain sections form NestinGFP+HMGB2-/- mouse without ventriculomegaly appeared to contain greater GFAP staining in the SVZ compared to age-matched WT mice (Figure 14), seemingly indicating that increased appearance of GFAP expression in SVZ NSCs persisted in the absence of ventriculomegaly in the HMGB2-/- mice, although the degree of this increase in GFAP staining in these HMGB2-/- mice without ventriculomegaly was smaller, and not as pronounced as the large increase in GFAP staining noted in HMGB2-/- mice with ventriculomegaly.

In more medial brain sections there were additional changes in progenitor composition in the SVZ. In medial sagittal sections from NestinGFP+HMGB2-/- the increase in GFAP expression persisted compared to WT mice (Figure 15A,B). Orthogonal views of SVZ near the RMS outlet (Figure 15C,D) and in the more ventral SVZ (Figure 15E,F) indicated that the Nestin+GFAP+ NSC population is higher in the HMGB2-/- mouse and that Nestin+GFAP- NPC population was lower in HMGB2-/- mouse, with quantification of SVZ NSCs and NPCs confirming this observation (Figure 15G), consistent with observations made in lateral brain sections mentioned previously (Figure 12).

Furthermore, analysis of the distribution of total NestinGFP+ alone (without regard to GFAP expression) within the SVZ indicated that HMGB2-/- medial sagittal sections appeared to contain fewer numbers of NestinGFP+ cells in the SVZ, both near the outlet to the RMS and more distally along the ventral axis (Figure 15D,F). Quantification of the NestinGFP- cell population in the SVZ of HMGB2-/- mice indicated higher numbers of this cell population compared to WT

mice (Figures 15G). Full resolution 3D reconstruction of the SVZ confirmed these findings, that there was more GFAP+ expression in HMGB2-/- mice, and greater numbers of Nestin+GFAP+ NSCs compared to WT mice, but paradoxically, this cellular change in SVZ progenitor composition was also associated with increased numbers of NestinGFP- cells in the SVZ of HMGB2-/- mice compared to WT mice (Figure 15G, Figure 16).

We asked whether this population of NestinGFP- cells in the SVZ of HMGB2-/- mice were more advanced progenitor cells, and specifically if they were neuroblasts. We assessed the expression of the neuroblasts using the marker doublecortin (DCX), a transcription factor that labels SVZ neuroblasts (Hack et al., 2005). In lateral sagittal sections, DCX+ neuroblasts were present in SVZ and the outlet to the RMS in both WT and HMGB2-/- mice, but the lateral HMGB2-/- brain sections contained larger clusters of these DCX+ SVZ neuroblasts compared to WT mice (Fig. 17). In more medial sagittal brain sections, the SVZ of HMGB2-/- mice contained larger numbers of DCX+ neuroblasts compared to WT brain sections (Figure 18). HMGB2-/- SVZ contained large elongated cords of DCX+ SVZ cells in medial sagittal sections. These DCX+ cords were greatly enlarged in HMGB2-/- mice compared to WT mice (Fig. 18). Measurement of the length of these DCX+ SVZ cells within the SVZ (from lateral ventricle to striatum) indicated the length of DCX+ cords within the WT SVZ was approximately 50μmeters, and in HMGB2-/- mice it was approximately 100μm. Additionally, the number of DCX+ cells per high power field (hpf) in the SVZ was elevated in HMGB2-/- mice compared to WT mice, with

almost 120 cells/hpf in WT SVZ and 180 cells/hpf in HMGB2-/- SVZ (Figure 18C). These changes in DCX+ neuroblasts demonstrated that the changes in SVZ progenitor composition in HMGB2-/- mice were not exclusive to NSCs and NPCs, and included changes in SVZ neuroblast cell number.

In light of these *in vivo* findings in HMGB2-/- mice, we asked whether changes in known regulators of NSC proliferation and self-renewal were altered in HMGB2-/- mice. As previously described, NSC proliferation and self-renewal are high in embryonic and young mice due to HMGA2 mediated repression of $p16^{Ink4a}$ (Nishino et al., 2008). This led us to ask whether changes in HMGB2-/- SVZ NSC and NPC cell number were mechanistically related to changes in $p16^{Ink4a}$ *in vivo*. We evaluated $p16^{Ink4a}$ protein levels using immunofluorescence, in previously described compound NestinGFP+HMGB2-/- and WT mice. The expression of $p16^{Ink4a}$ in the glomerular layer of the olfactory bulb was confirmed, which constituted a positive control for $p16^{Ink4a}$ expression (Figure 19A). Our results indicated that there was no increase in $p16^{Ink4a}$ protein levels in NestinGFP+ SVZ cells in HMGB2-/- mice at 10 weeks compared to age-matched WT mice (Figure 19B,C). We also examined the protein levels of other CDKIs which have been previously described as negative regulators of NSC and NPC proliferation and self-renewal, including $p21^{Cip1/Waf1}$, $p27^{Kip1}$ and upstream regulator of these to CDKIs, p53 (Doetsch et al., 2002b; Kippin et al., 2005; Meletis et al., 2006). $p21^{Cip1/Waf1}$ was detected in SVZ progenitor cells that were leaving the SVZ and entering the RMS in 10 week old NestinGFP+WT mice (Figure 20C), but in age-matched NestinGFP+HMGB2-/- mice $p21^{Cip1/Waf1}$ protein

levels at the entrance to the RMS was reduced (Figure 20D). Additionally, we were able to detect p53 expression in the Nestin+HMGB2+/+ SVZ cells, confirming the *in vivo* findings of p53 expression in the SVZ in young adult mice (Meletis et al., 2006). The number of p53+NestinGFP+ SVZ progenitor cells were low in WT 10 week old mice, and NestinGFP+HMGB2-/- age-matched mice exhibited an increase in p53+NestinGFP+ cells compared to WT mice (Figure 20). Finally, we examined the expression of CDKI $p27^{Kip1}$ in the SVZ of WT and NestinGFP+HMGB2-/- 10 week old mice. We detected a large decrease in $p27^{Kip1}$ protein levels in NestinGFP+ SVZ progenitors cells in NestinGFP+ HMGB2-/- mice at 10 weeks of age compared to WT mice (Figure 21). Together, these results revealed the increased protein levels of p53 in NestinGFP+ SVZ progenitor cells in HMGB2-/- mice, and decreased protein levels of two CDKIs, $p21^{Cip1/Waf1}$ and $p27^{Kip1}$ in the SVZ of HMGB2-/- mice, suggesting that abnormal NSC and NPC cell number in the SVZ could be mechanistically related to changes in expression of these proteins in young HMGB2-/- mice.

Young HMGB2 knock out mice exhibited aberrant increases in olfactory bulb granule cell layer neurogenesis, but not glomerular layer neurogenesis

Increases in SVZ proliferation and changes in the composition of NSCs, NPCs, and neuroblasts in the SVZ of HMGB2-/- mice coupled with decreases in expression of CDKIs such as $p21^{Cip1/Waf1}$ and $p27^{Kip1}$ in HMGB2-/- mice suggested that HMGB2 plays a role in regulating proper proliferation of SVZ

progenitor cells in vivo; however, what effect HMGB2 has on neural progenitor leaving the SVZ and differentiating during olfactory bulb neurogenesis *in vivo* remains unclear. To examine OB neurogenesis in the young HMGB2-/- mice we explored the differentiation of WT and HMGB2-/- labeled cells *in vivo* as they differentiated into OB neurons. BrdU (150μg/mg) was injected every 12 hours for 2 days in two-month old WT and HMGB2-/- mice. 14 days post injection, BrdU labeled progenitor cells had migrated through the RMS to the OB and differentiated into neurons in the granule cell layer (GCL) and the glomerular layer (GL). Mice were euthanized at 2.5 months. BrdU labeled cells that had recently differentiated into neurons were identified by staining for BrdU and the mature neuronal cell marker NeuN. Our results revealed that there was a 25% increase in BrdU+ cell density in the OB granule cell layer (GCL) of HMGB2-/- mice compared to WT mice of the same age (Fig 22C), but a 4% increase in the total neuronal (NeuN) cell density in the GCL of HMGB2-/- mice (Fig 22E). The cell density of BrdU+/NeuN+ in the GCL of the HMGB2-/- mice remained elevated relative to WT mice, with BrdU+/NeuN+ GCL cell density 40% higher in HMGB2-/- mice (Fig 22G). The percentage of new born neurons among all BrdU labeled cells was elevated in the GCL of HMGB2-/- mice, and was approximately 84.3% after 14 days of differentiation relative to WT mice which were only 73.3% differentiated (Fig 22H), indicating some component of accelerated differentiation/maturation of new born GCL neurons in these young HMGB2-/- mice. The percentage of new born neurons expressed among all GCL neurons in the HMGB2-/- mice was 43.38% after 14 days of differentiation compared to

only 31.74% of all neurons in WT 2.5 month old mice (Fig 22 i). These results demonstrated that the proportion of new born GCL neurons among all neurons in HMGB2-/- mice at 2.5 months was much larger than the proportion of new born GCL neurons in WT mice of the same age.

Despite these changes in GCL neurogenesis we were unable to detect changes in GL neurogenesis in HMGB2-/- mice. BrdU+ cell density, NeuN+ cell density or BrdU+/NeuN+ cell density after 14 days of differentiation in the glomerular layer (GL) of the HMGB2-/- olfactory bulb at 2.5 months of age remained largely unchanged compared to age matched WT mice (Fig 23). Additionally, when new born GL neurons were expressed as a percentage of BrdU or percentage of NeuN cells (Fig 23) there were no differences between WT and HMGB2-/- mice at 2.5 months, suggesting normal GL neurogenesis in the HMGB2-/- mice at this age.

Figure 9: HMGB2 immunofluorescence in young adult NestinGFP+ SVZ progenitors cells ventral to the RMS outlet (A-D) and at the RMS (E-H). Orthogonal view (I) of HMGB2 staining in NestinGFP^{Pos} SVZ cell from (H). All scale bars in white equal 20 μm.

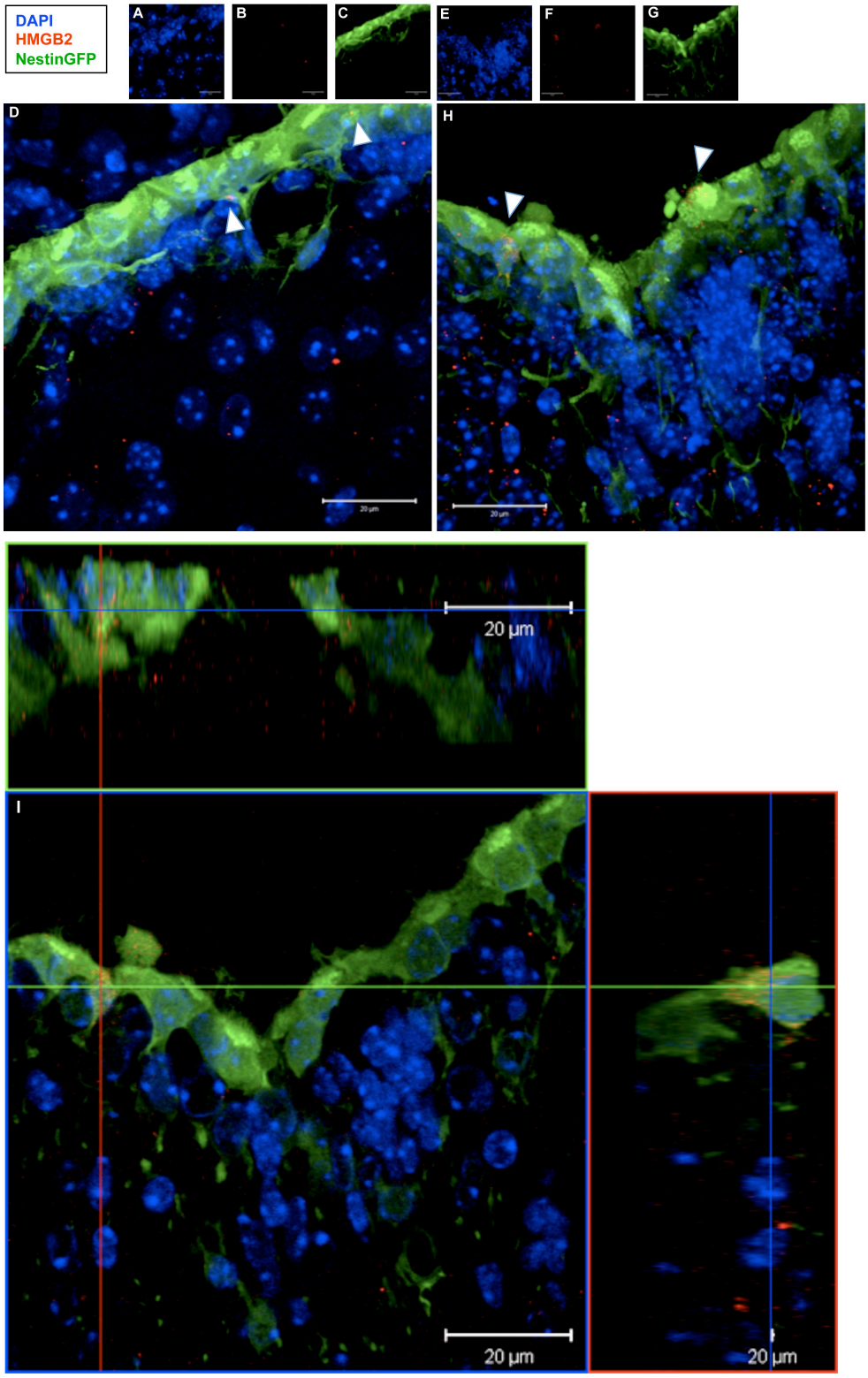

Figure 10: A) Low magnification and B) high magnification pictures of serial sagittal brain sections from WT and HMGB2-/- mice at 10 week stained with DAPI demonstrating increased size of the ventricles in HMGB2-/- mice compared to WT mice. Serial sections in (A) are ordered most lateral (1) to most medial (11).

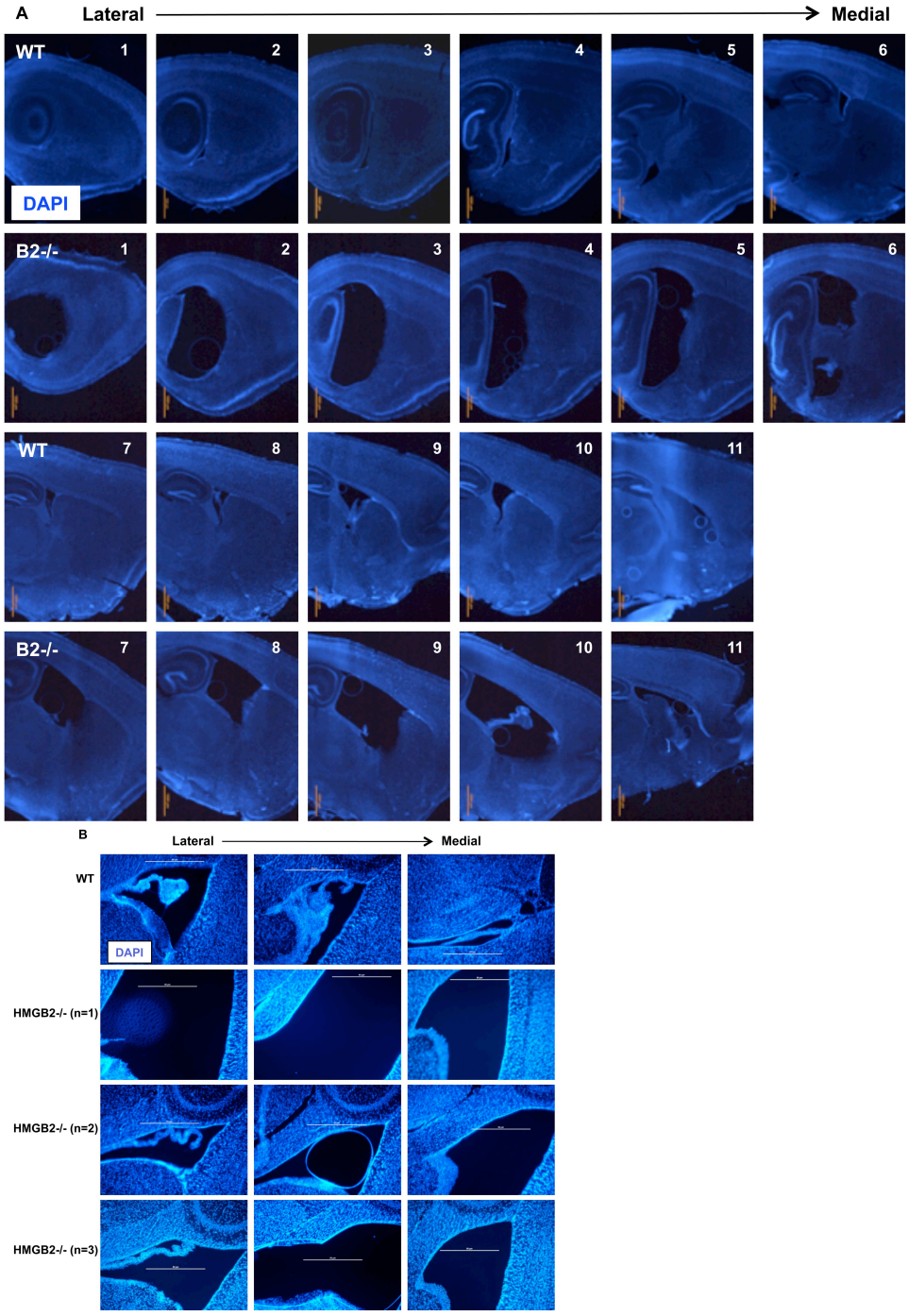

Figure 11: Composite high magnification images of A) WT and B) HMGB2-/- mice at 10 weeks of age injected with BrdU and stained with anti-BrdU (red) and anti-Ki67 (green). Quantification of A) BrdU+ B) Ki67+ and C) BrdU+/Ki67+ SVZ cell densities in 10 week old WT and HMGB2-/- mice. n=4 WT mice and n=5 HMGB2-/- mice. All values are Mean+/-SEM and * = p<0.05 and ** = p<0.005.

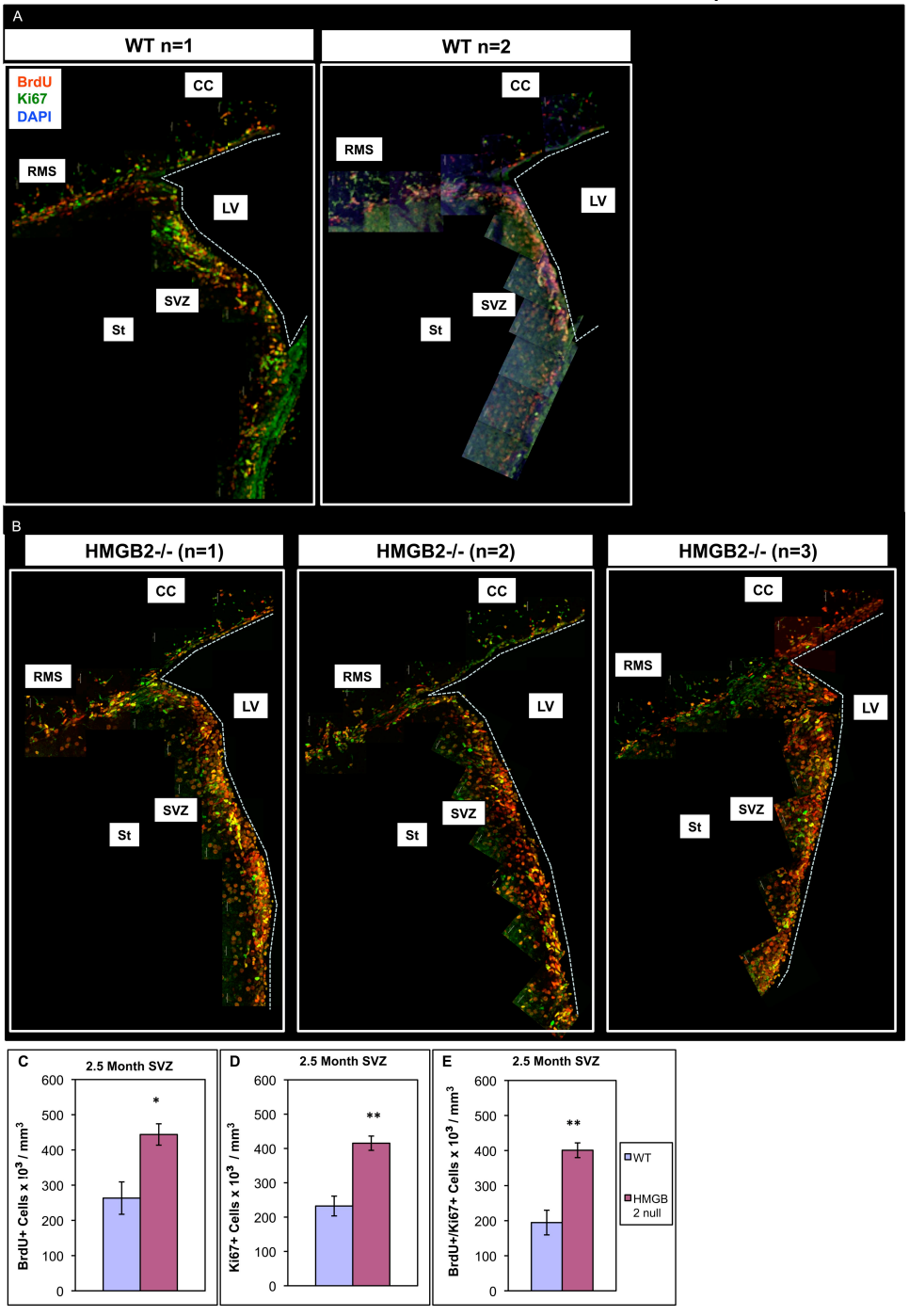

Figure 12: Composite high magnification images of the SVZ in **lateral** sagittal brain sections from a 10 week old (A) NestinGFP+HMGB2+/+ (WT) mouse and a (B) NestinGFP+HMGB2-/- mouse with vetriculomegaly. Sections are stained with anti-GFAP (red). (C,D) Orthogonal view of SVZ near the RMS outlet from (A) and (B). (E,F) Orthogonal view of the ventral SVZ, proximal to the RMS outlet from (A) and (B). G) Quantification of Nestin-, Nestin+, Nestin+GFAP+, and Nestin+GFAP- cell populations in the SVZ of WT (C,E) and HMGB2-/- mice (D,F). Nestin+GFAP+ NSCs are increased and Nestin+GFAP- NPCs are decreased in HMGB2-/- mice compared to age-matched WT mice. Scale bars equal 20μm.

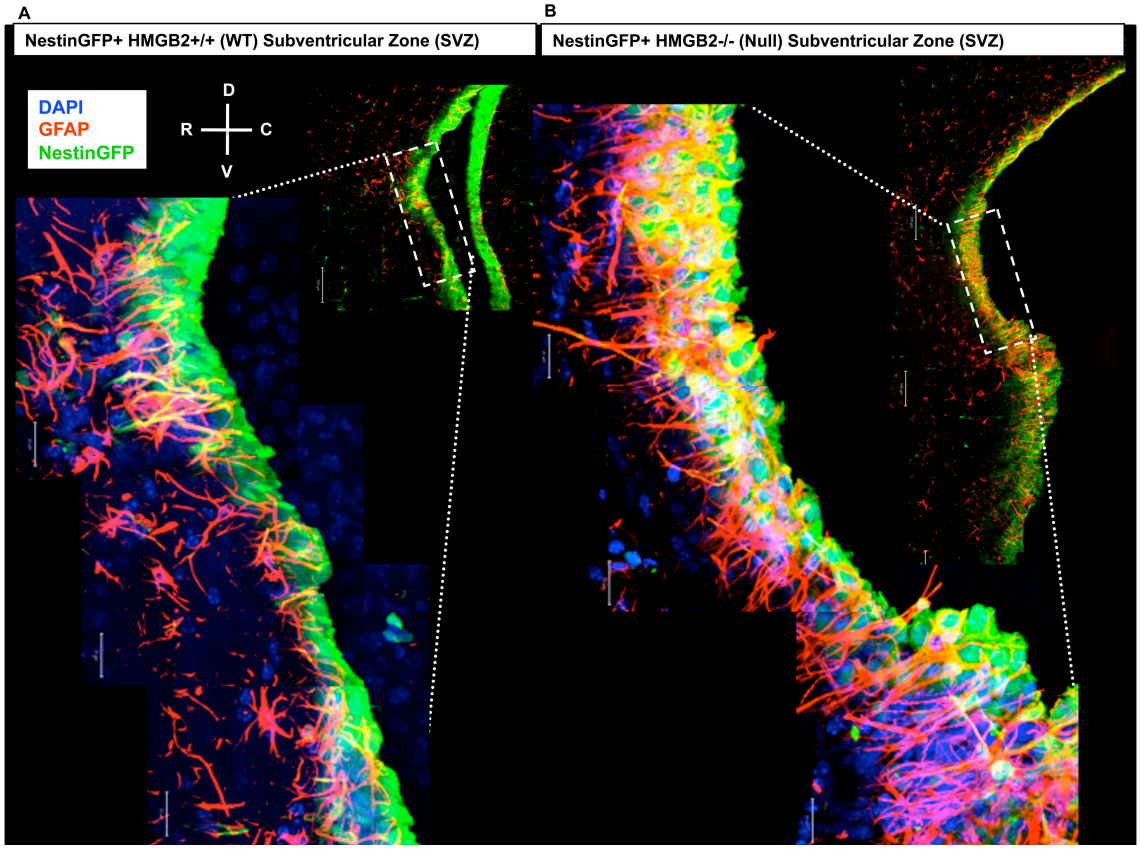

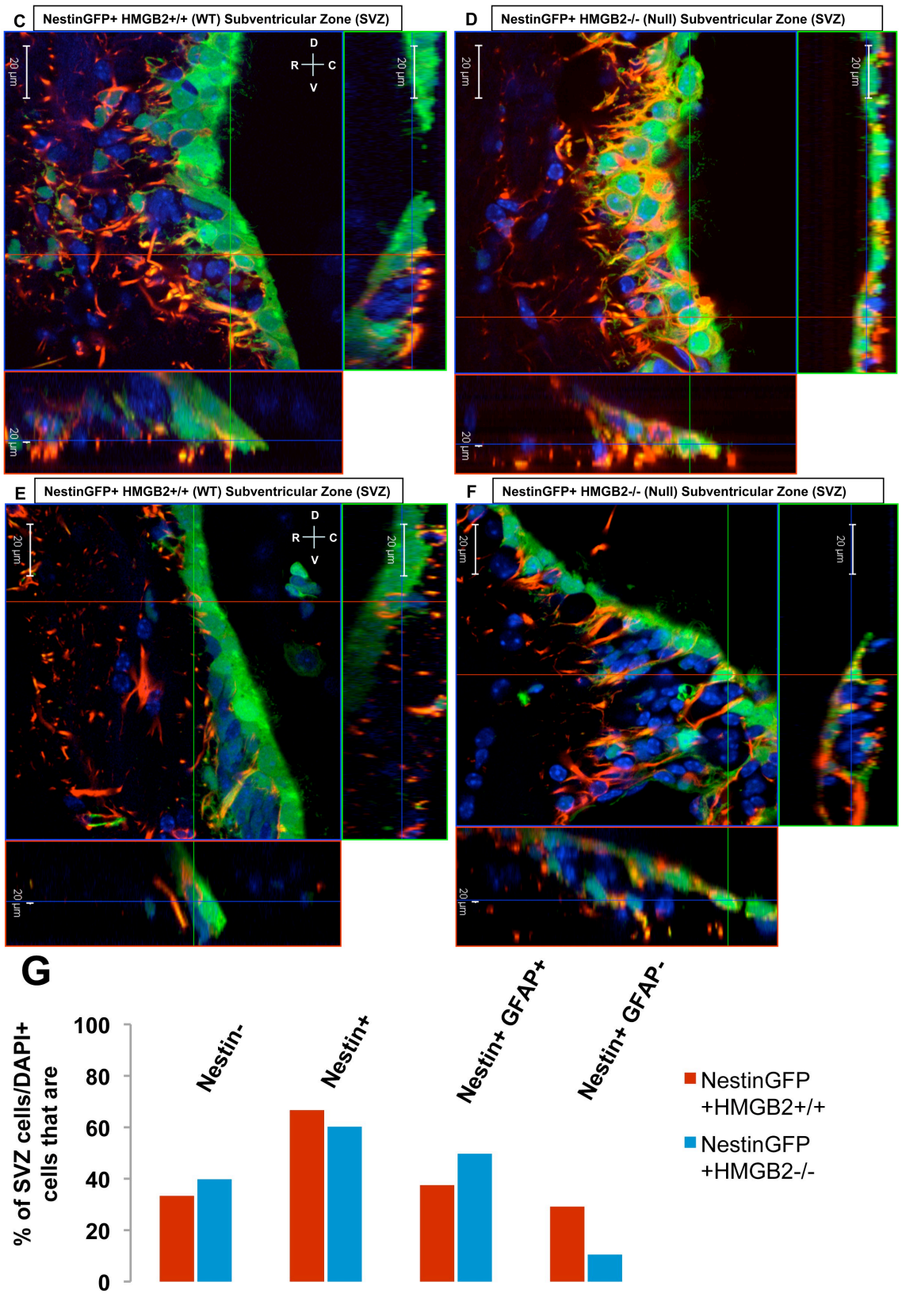
C
NestinGFP+ HMGB2+/+ (WT) Subventricular Zone (SVZ)
D
NestinGFP+ HMGB2-/- (Null) Subventricular Zone (SVZ)
E
NestinGFP+ HMGB2+/+ (WT) Subventricular Zone (SVZ)
F
NestinGFP+ HMGB2-/- (Null) Subventricular Zone (SVZ)
D
R
C
V
20 µm
G
% of SVZ cells/DAPI+ cells that are
100
80
60
40
20
0
Nestin-
Nestin+
Nestin+ GFAP+
Nestin+ GFAP-
NestinGFP +HMGB2+/+
NestinGFP +HMGB2-/-

Figure 13: Full-resolution 3D reconstruction of the SVZ from a **lateral** sagittal brain section (from Figure 12A,B) demonstrating increased expression of NSC marker GFAP in a 10 week old NestinGFP+HMGB2-/- mouse compared to an age-matched WT mouse.

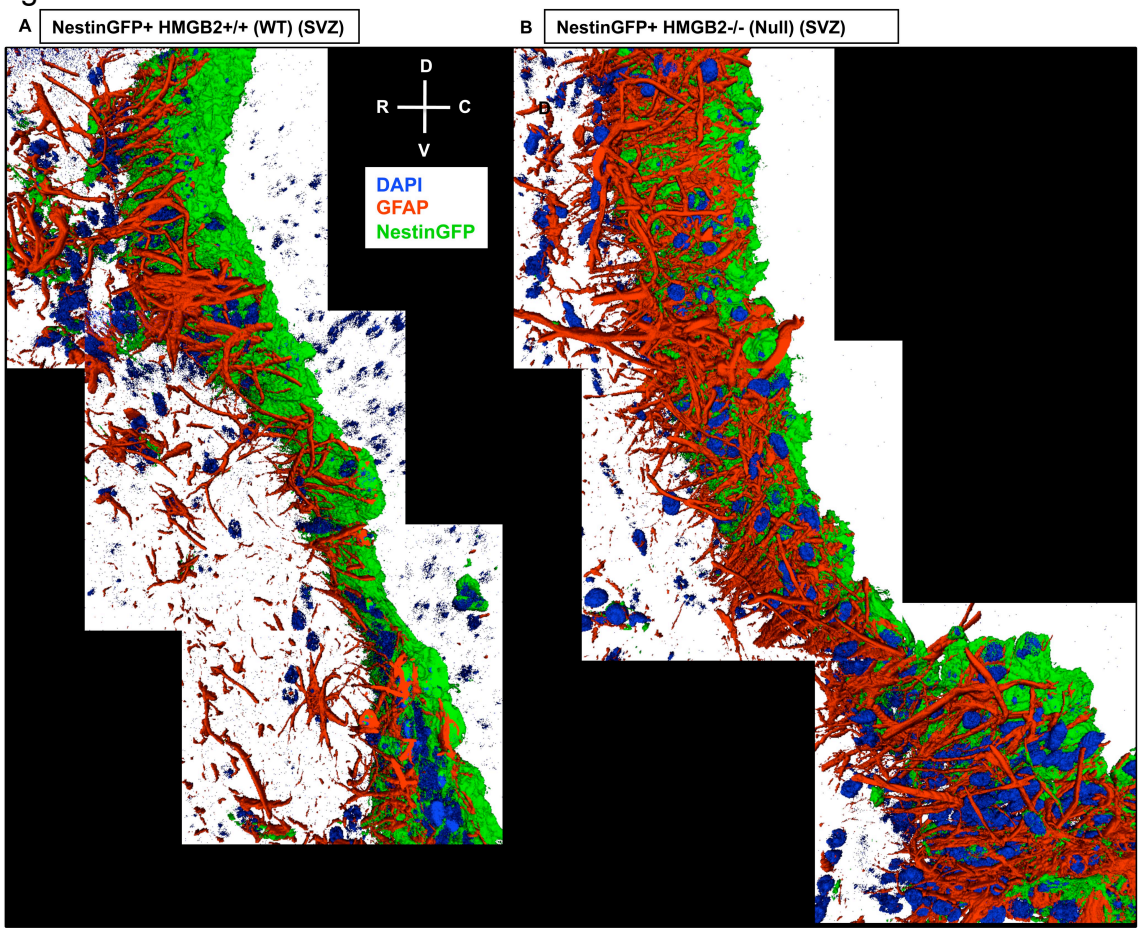

Figure 14: GFAP staining in the SVZ in **lateral** sagittal brain sections from 10 week old (A) NestinGFP+WT and (B) NestinGFP+HMGB2-/- mice (without ventriculomegaly). Scale bars equal 20μm.

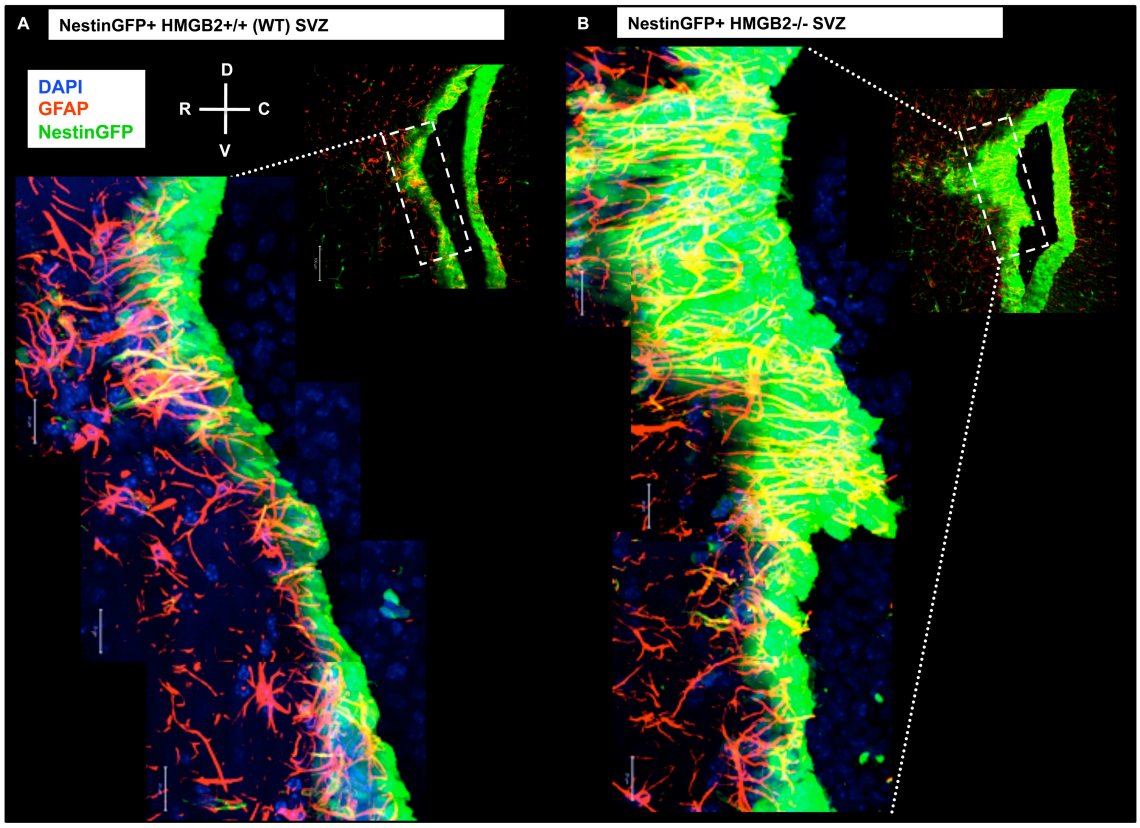

Figure 15: Composite high magnification images of **medial** sagittal brain section from a 10 week old A) NestinGFP+HMGB2+/+ (WT) mouse and B) NestinGFP+HMGB2-/- mouse with vetriculomegaly. Sections are stained with anti-GFAP (red). (C,D) Orthogonal view of SVZ near the RMS outlet from (A) and (B). (E,F) Orthogonal view of the ventral SVZ, proximal to the RMS outlet from (A) and (B). G) Quantification of Nestin-, Nestin+, Nestin+GFAP+, and Nestin+GFAP- cell populations in the SVZ cell of WT (C,E) and HMGB2-/- mice (D,F). Scale bars equal 20μm.

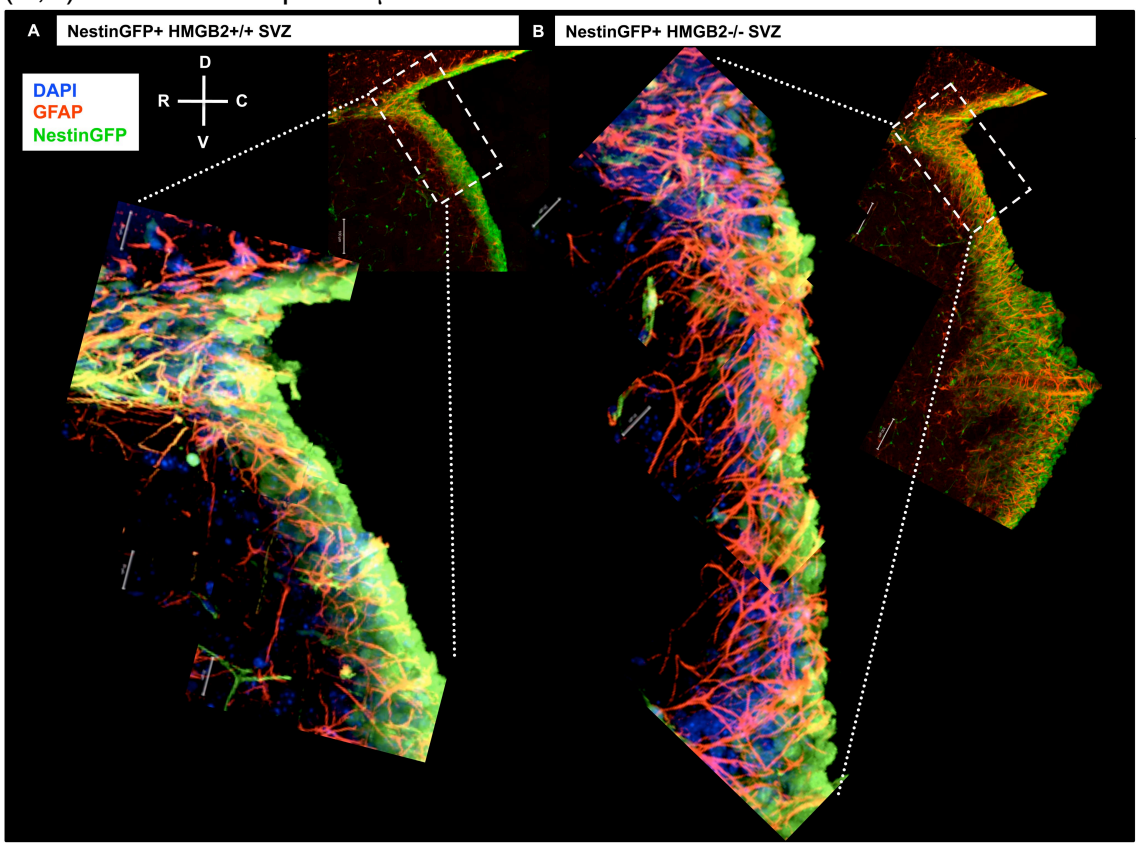

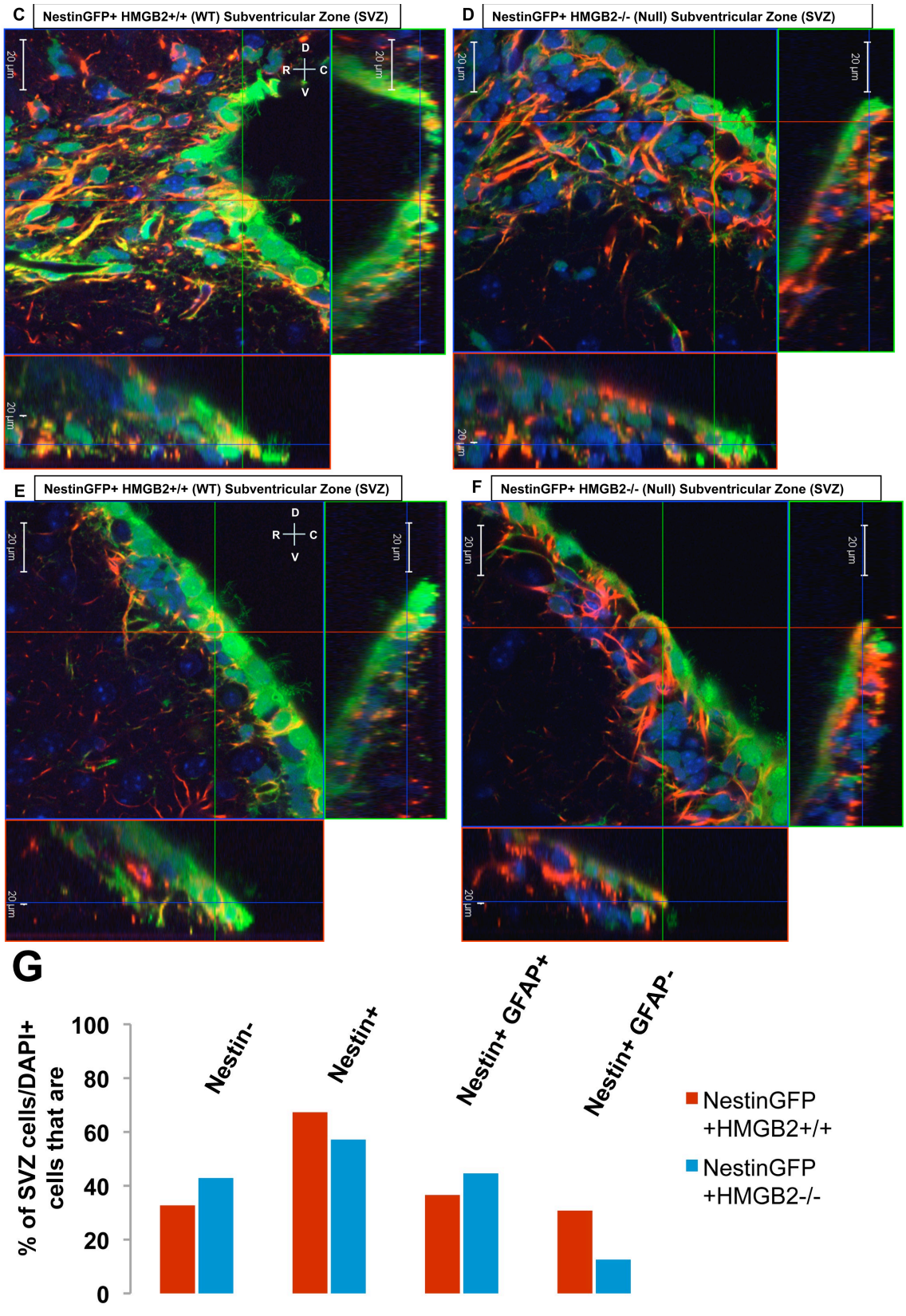
C
NestinGFP+ HMGB2+/+ (WT) Subventricular Zone (SVZ)
D
NestinGFP+ HMGB2-/- (Null) Subventricular Zone (SVZ)
E
NestinGFP+ HMGB2+/+ (WT) Subventricular Zone (SVZ)
F
NestinGFP+ HMGB2-/- (Null) Subventricular Zone (SVZ)
20 µm
D
R
C
V
G
% of SVZ cells/DAPI+ cells that are
100
80
60
40
20
0
Nestin-
Nestin+
Nestin+ GFAP+
Nestin+ GFAP-
NestinGFP +HMGB2+/+
NestinGFP +HMGB2-/-

Figure 16: Full-resolution 3D reconstruction of **medial** sagittal brain section (from Figure 15A,B) indicating increased in Nestin+GFAP+ NSCs in 10 week old NestinGFP+HMGB2-/- mice, but lower total NestinGFP+ cells in HMGB2-/- mice compared to age-matched WT mice.

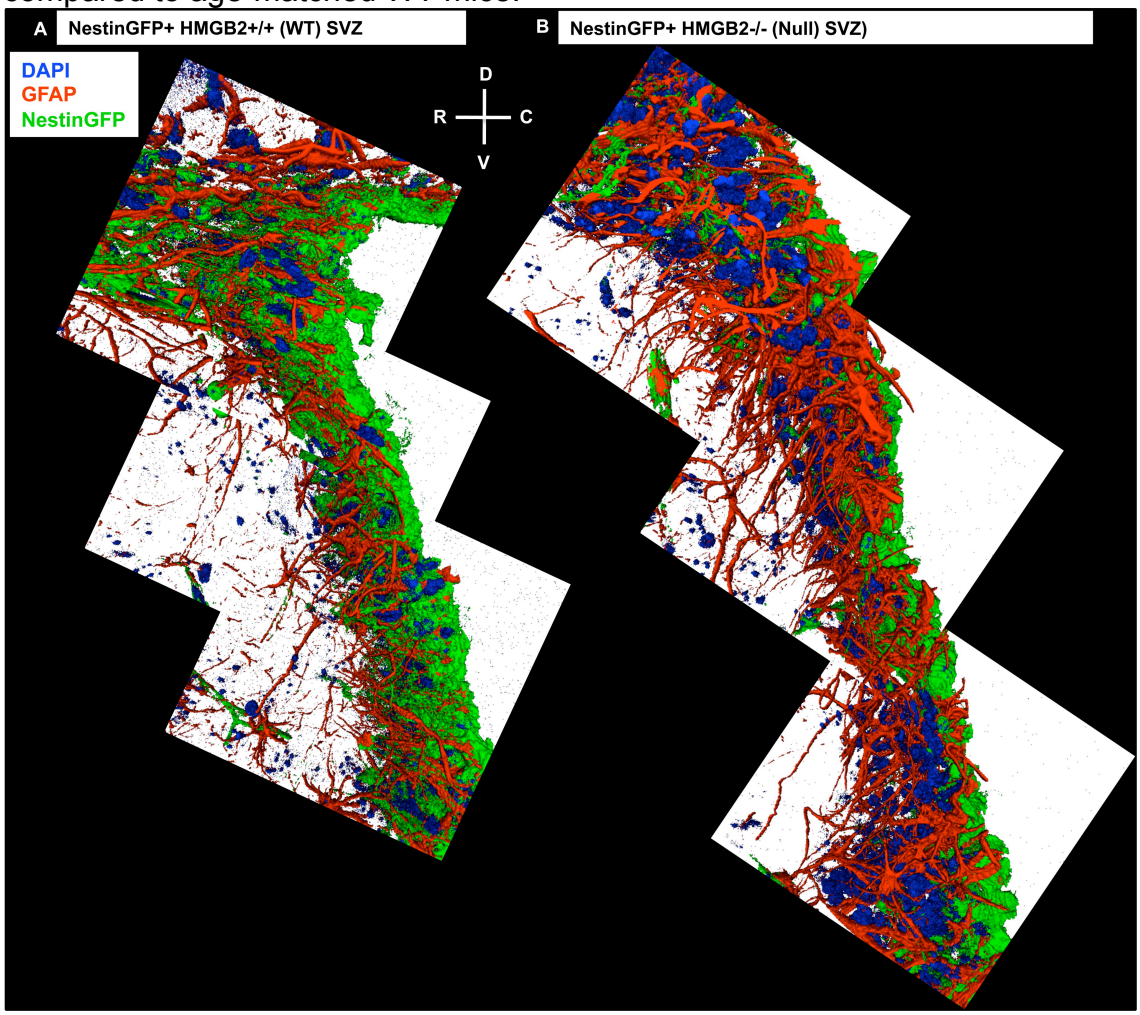

Figure 17: Doublecortin (DCX) staining in **lateral** sagittal brain sections from a 10 week old (A) WT and (B) HMGB2-/- mouse (with ventriculomegaly). Scale bars equal 20μm.

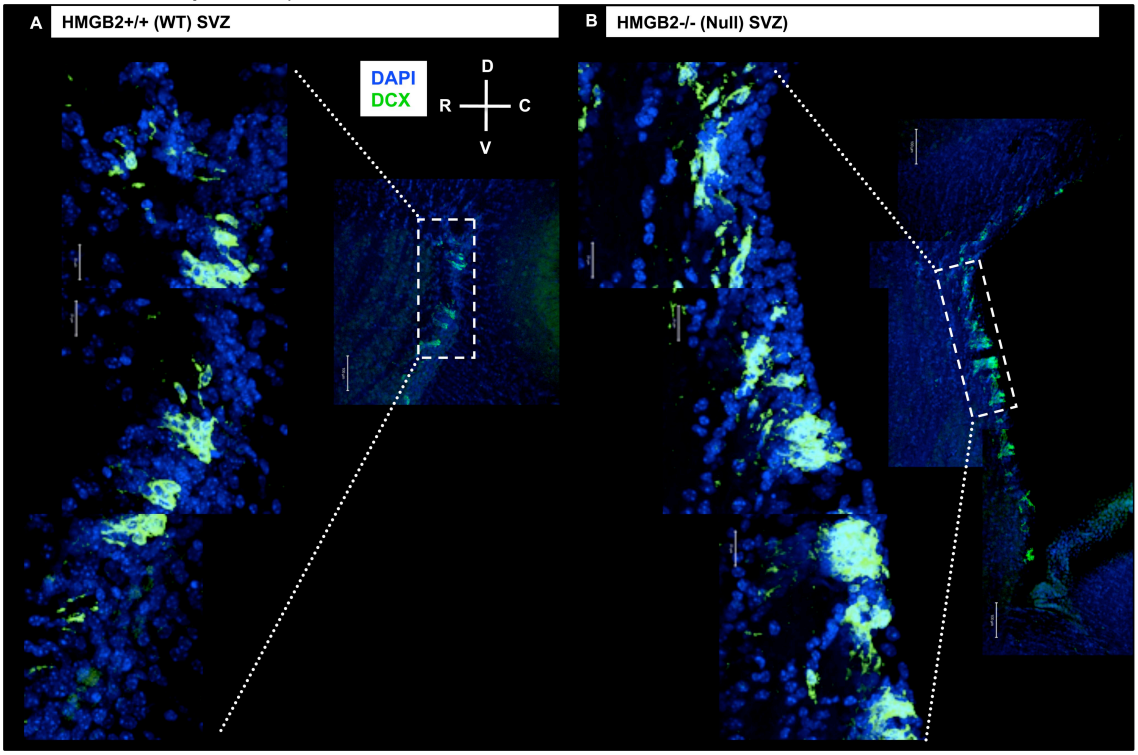

Figure 18: Doublecortin (DCX) staining in **medial** sagittal brain sections from a 10 week old (A) WT and (B) HMGB2-/- mouse (with ventriculomegaly), and (C) quantification of DCX+/hpf in WT and HMGB2-/- SVZ in (A) and (B). Scale bars equal 20μm.

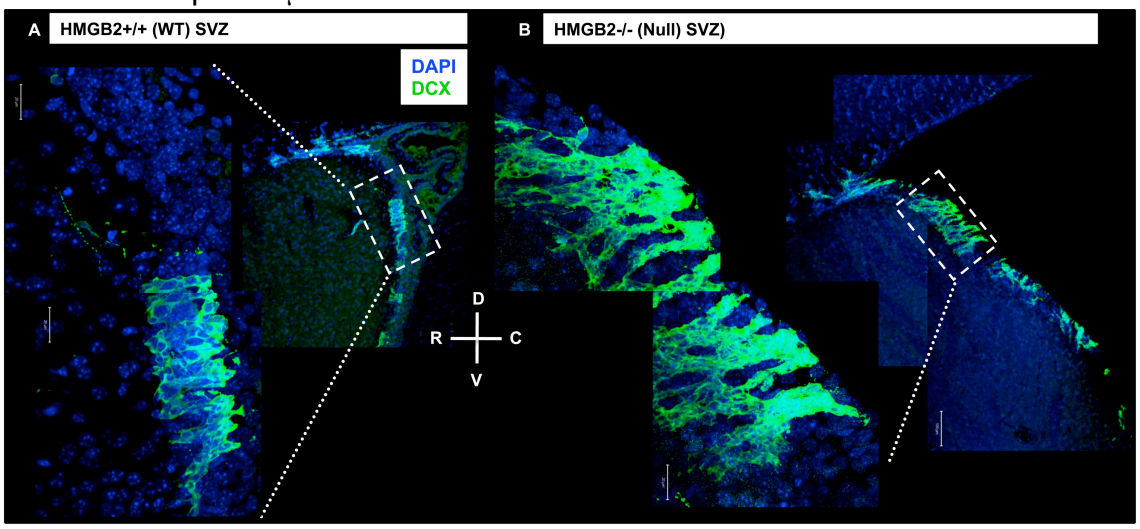

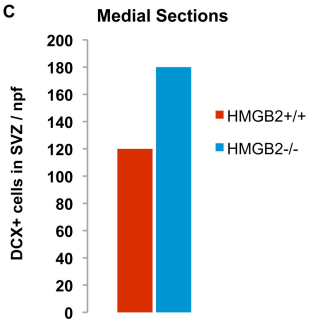

Figure 19: High magnification composite images of p16^{Ink4a} staining in 10 week old (A) NestinGFP+WT olfactory bulb (positive control) (B) NestinGFP+WT SVZ and (C) NestinGFP+HMGB2-/- SVZ. Composite images from (A) and (B) are enlarged in (C) and (D) with NestinGFP channel turned off to visualize p16^{Ink4a} staining in the SVZ of WT and HMGB2-/- mice. White scale bars equal 20 μmeters.

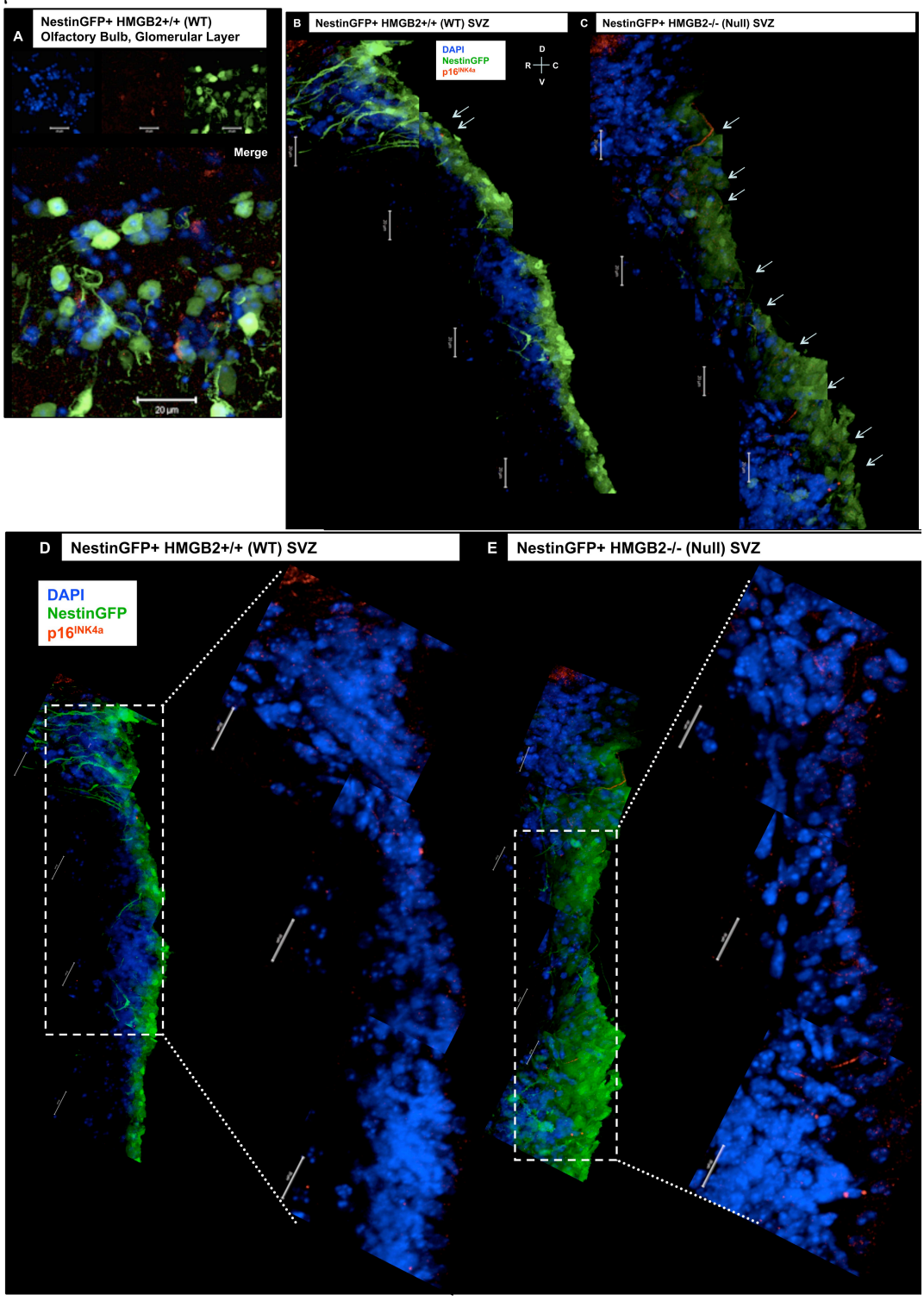

Figure 20: High magnification composite images of p53 and p21$^{Cip1/Waf1}$ staining in 10 week old (A) NestinGFP+WT and (B) HMGB2-/- mice. Composite images of (C) WT and (D) HMGB2-/- SVZ with NestinGFP channel turned off to visualize decreases in p21$^{Cip1/Waf1}$ staining in the SVZ RMS outlet and increases in p53 expression in the SVZ of HMGB2-/- mice. Scale bars equal 20μm.

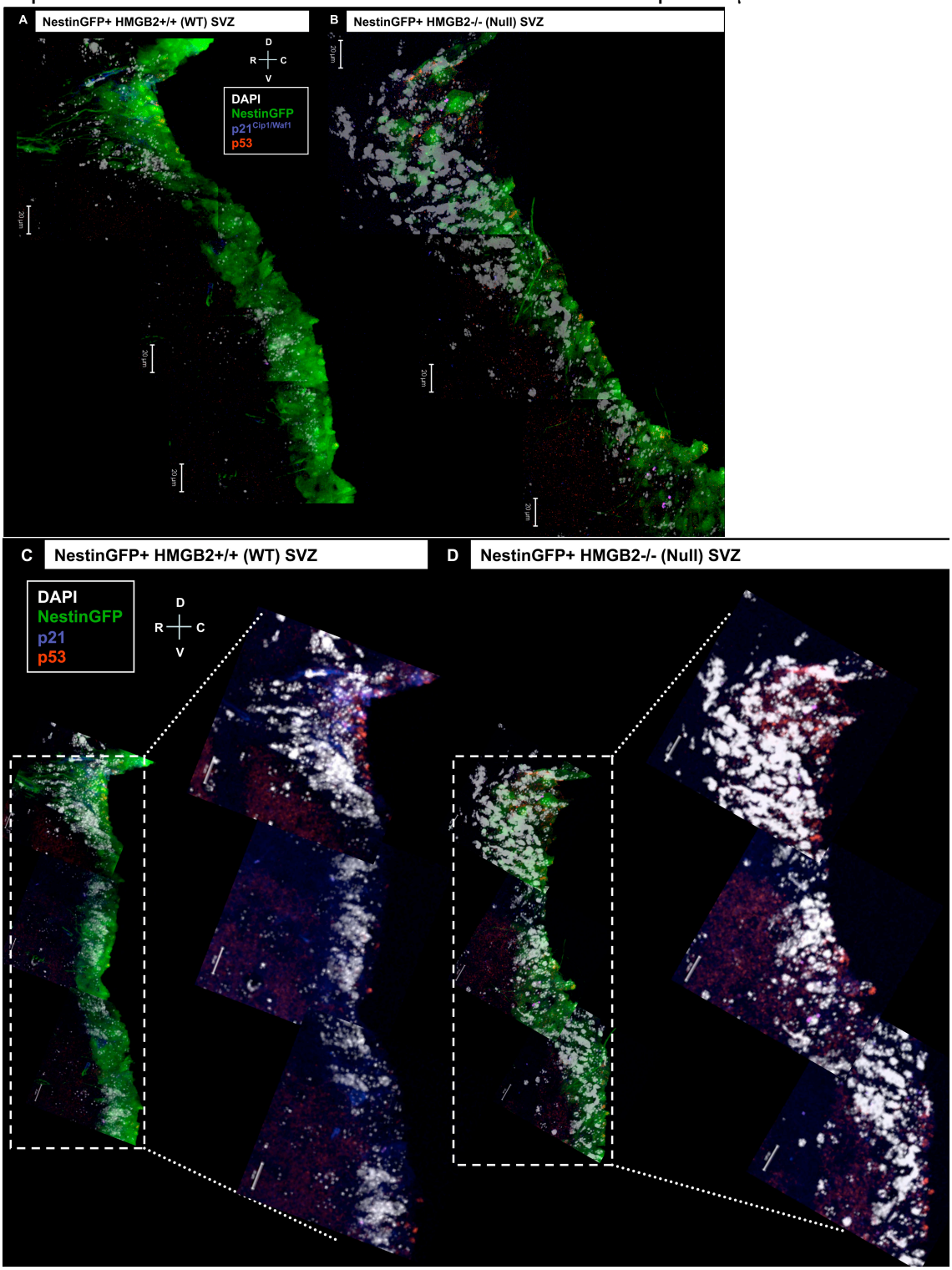

Figure 21: Composite high magnification images of $p27^{Kip1}$ staining in the SVZ of 10 week old (A) NestinGFP+WT and (B) HMGB2-/- mice, including staining at the SVZ RMS outlet in (C) WT and (D) HMGB2-/- mice. Scale bars equal 20μm.

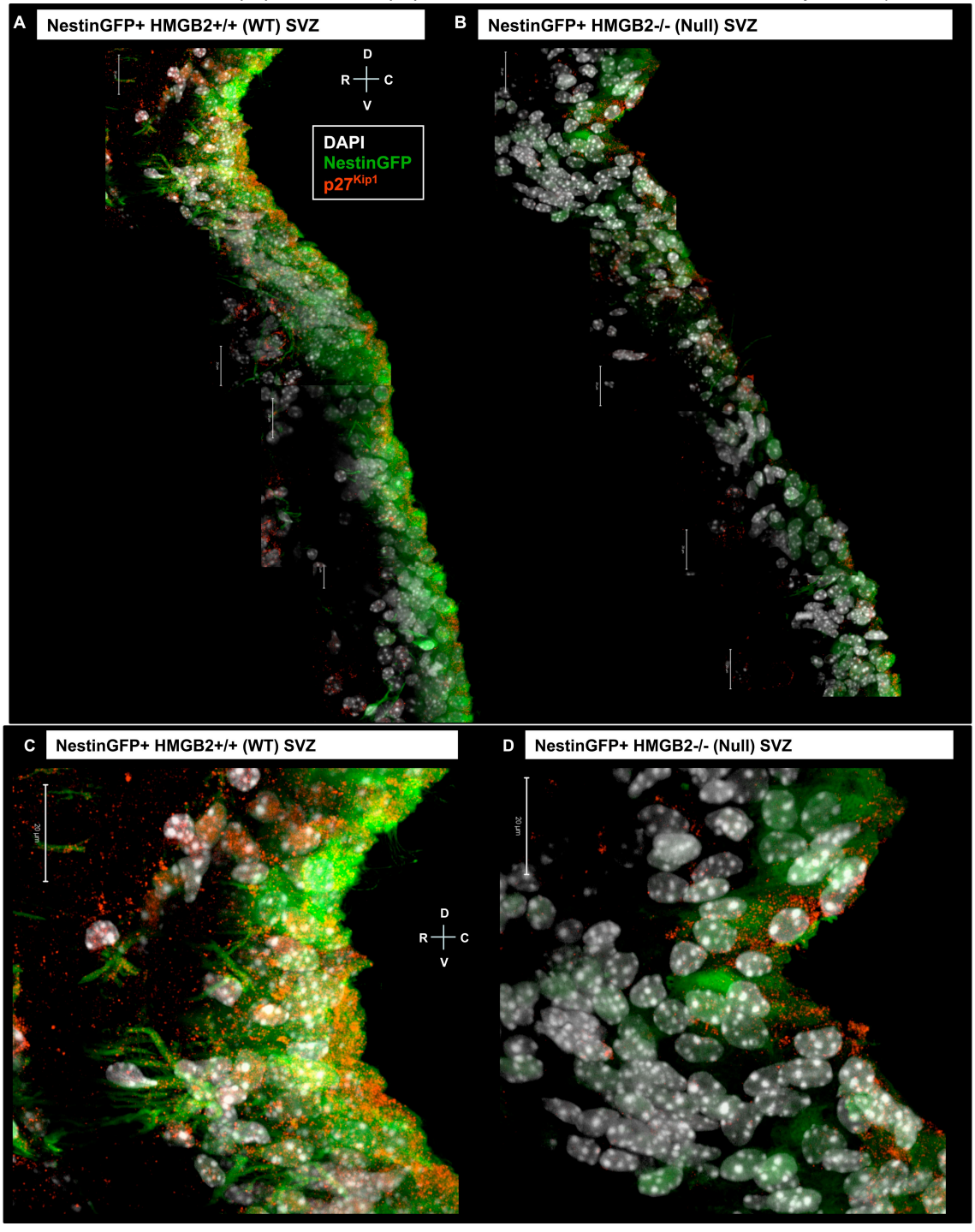

Figure 22: BrdU and NeuN staining in 10 week old (A) WT and (B) HMGB2-/- mice injected 14 days prior with BrdU and (B-I) quantification of BrdU+, NeuN+, and BrdU+NeuN+ cells in the olfactory bulb granule cell layer (GCL). All values are Mean+/- SEM. n= 2-3 mice per genotype. Scale bar equals 20 μmeters.

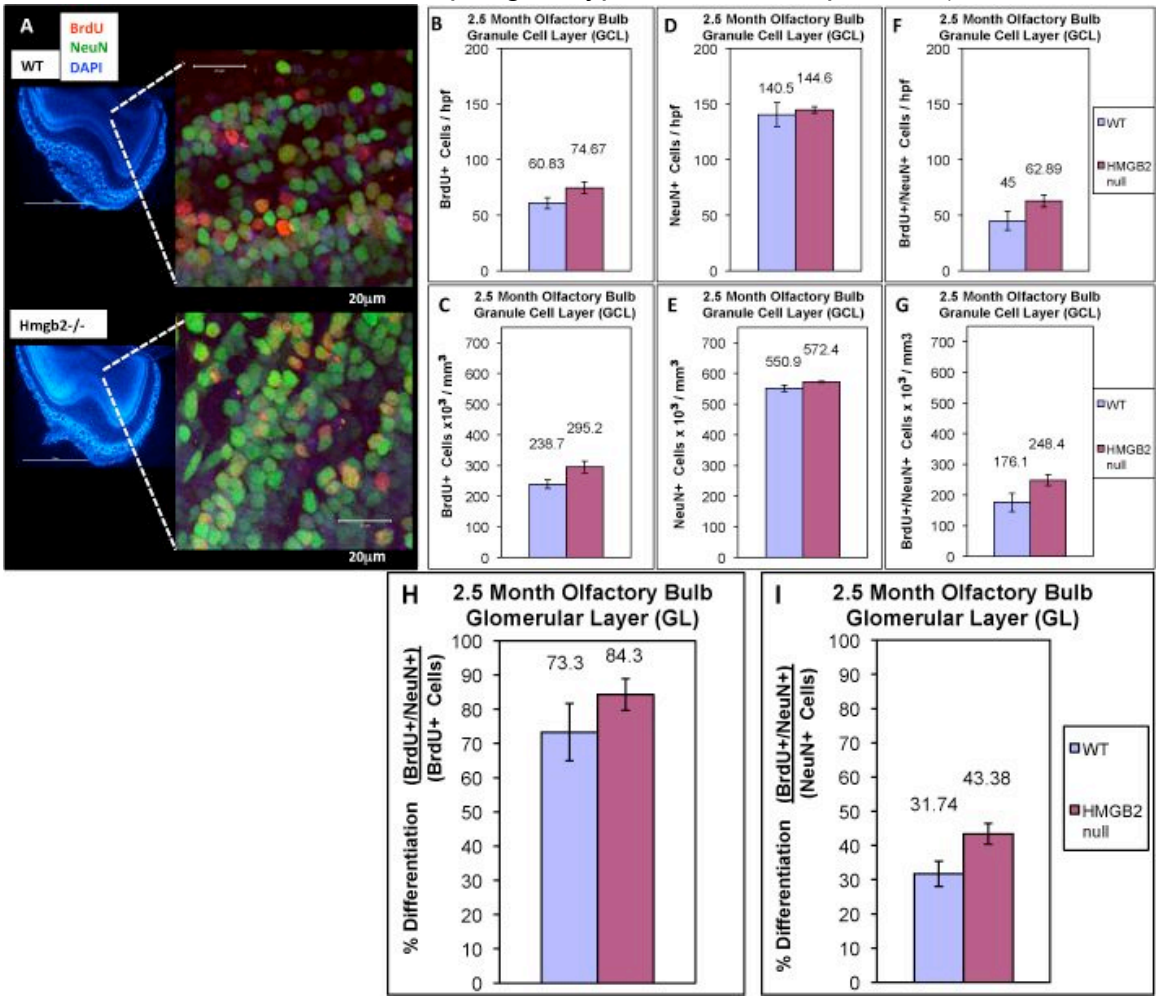

Figure 23: BrdU and NeuN staining in 10 week old (A) WT and (B) HMGB2-/- mice injected 14 days prior with BrdU and (B-I) quantification of BrdU+, NeuN+, and BrdU+NeuN+ cells in the olfactory bulb glomerular layer (GL). All values are Mean+/- SEM. n= 2-3 mice per genotype. Scale bar equals 20 μmeters.

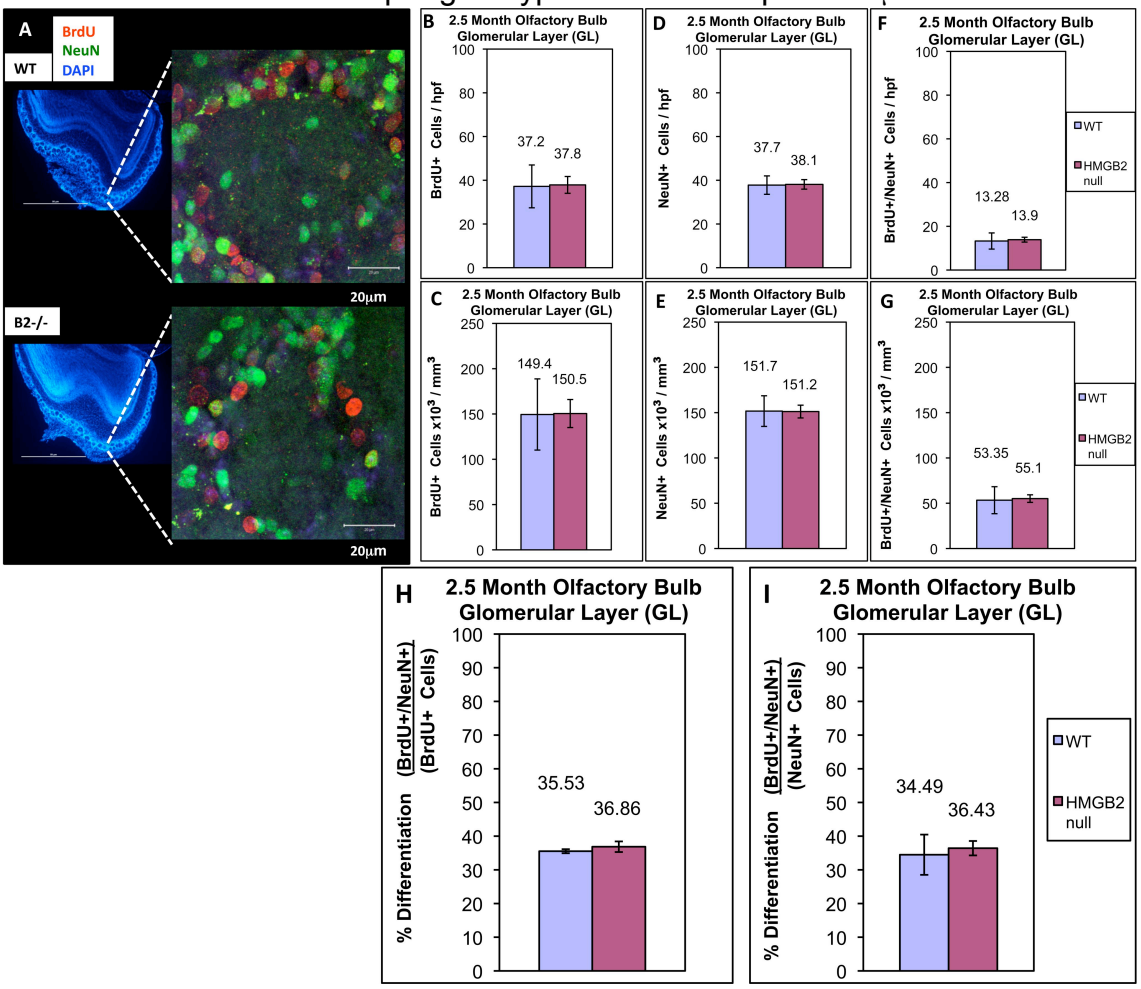

Chapter VI:

Loss of Global p73 Expression Impairs Proliferation of Nestin+ Neural Stem and Progenitor Cells in the Dentate Gyrus of Young Adult Mice

Previous work has demonstrated that adult dentate NSCs have astrocyte like properties, express intermediate filaments nestin and GFAP, and have a distinct radial glial morphology (Seri et al., 2001; Seri et al., 2004). In contrast, early dentate neural progenitors continue to express nestin but lose radial glial morphology and lose the expression of GFAP. These findings were confirmed by other groups, which also demonstrated that the Nestin+GFAP+ positive cells have passive non-inactivating membrane currents consistent with astrocytes (Filippov et al., 2003). Subsequent work demonstrated that dentate Nestin+GFAP+ positive NSCs are district from Nestin+/GFAP- progenitors which possess delayed and inward-rectify currents which can inactivate (Wang et al., 2005). Finally, dentate nestin positive NSCs with radial glial morphology are distinct from nestin positive progenitors which have lost their radial glial morphology and express early markers of neuroblast, such as PSA-NCAM. These Nestin+/PSA-NCAM+ late neural progenitors have a distinctly high input resistance that distinguishes them from both neural stem cells and immature granule neurons (Fukuda et al., 2003). The findings demonstrate that dentate NSCs are a distinct population of cells that possess a unique and distinguishable

radial glial morphology, that express markers of mature astrocytes (GFAP), and that have a unique electrophysiological profile which distinguishes them from early and late nestin positive neural progenitor cells.

Neurogenesis in the DG occurs when NSCs in the subgranular zone (SGZ) proliferate and give rise to progenitor cells which migrate and differentiate into the new granule neurons in the granule cell layer of the DG (Eriksson et al., 1998; Kornack and Rakic, 1999; Seri et al., 2001; Seri et al., 2004). These newborn granule neurons are functional, and possess functional synaptic inputs, action potentials, and other properties of functional granule neurons (van Praag et al., 2002). Although dentate neurogenesis is involved in memory formation (Shors et al., 2001; Jessberger et al., 2009) and plays a role in mood disorders (Santarelli et al., 2003), the precise role of dentate neurogenesis in the CNS is not fully understood.

Yang and colleagues have previously generated and described a global p73 knockout mouse (Yang et al., 2000). p73 is a member of the p53/p63/p73 family of tumor suppressor proteins. One family member, p53, previously described, regulates NSC proliferation and self-renewal in the SVZ of young mice (Meletis et al., 2006), while a second member, p63, regulates proper stem cell maintenance in skin (Blanpain and Fuchs, 2007; Yi et al., 2008). p73-/- mice appear to suffer from a wide number of chronic bacterial infections, but exhibit no increase in spontaneous tumor formation. The neural phenotype of the p73-/- mice is striking; congenital hydrocephalus and dramatically abnormal hippocampal neuroanatomy. The CA1 and CA2 regions of the hippocampus have multiple

wave-like gyrations, with the abnormal hippocampal neuroanatomy more pronounced in the caudal segments along the rostral-caudal axis (Yang et al., 2000). The dentate gyrus has a hypertrophied appearance, with an extended suprapyramidal blade, and a missing infrapyramidal blade.

One potential mechanistic explanation for the hippocampal dysgenesis in the p73-/- mice is a defect in post-natal NSC proliferation and maintenance. As previously described, hippocampal neurogenesis continues during post-natal development and adulthood and plays an integral role in the birth of newborn functional granule neurons in the dentate gyrus. Recent work has demonstrated that the loss of genes that control sonic hedgehog (Shh) signaling, such as Kif3a and Smoothened (Smo), cause a failure in post-natal neurogenesis and the development of a hypotrophic dentate gyrus (Han et al., 2008). The Smo null post-natal neurogenesis defect and hypotrophic dentate gyrus is caused by the failure of GFAP+ radial glial NSCs to develop in the dentate gyrus after embryonic development (Han et al., 2008). Both Kif3a and Smo null mice lack GFAP+ dentate NSCs and both have impaired progenitor proliferation as assessed by BrdU incorporation and staining of proliferation markers Mash1 and PSA-NCAM, thus providing a connection between dentate NSC formation/proliferation with proper development of postnatal dentate neuroanatomy. The Kif3a and Smo null mice share similarities with /phenocopy the neural phenotype of p73-/- mice, which led us to hypothesize that p73 plays a role in proper dentate NSC/progenitor proliferation and maintenance. Consequently, we studied neural progenitor proliferation in WT and p73-/- null

mice to further clarify whether loss of global p73 expression impairs NSC and/or neural progenitor cell proliferation in the context of p73-/- hippocampal dysgenesis.

We used NestinGFP transgenic mice created previously and described elsewhere (Mignone et al., 2004) to study dentate progenitor proliferation within a variable p73 (WT and null) genetic background. We have generated compound NestinGFP/p73 transgenic mice and used them to study and quantify dentate NSC and NPC proliferation in these different p73 genetic backgrounds.

Methods

Compound NestinGFP+p73+/+ and NestinGFP+p73-/- transgenic mice were generated and separated into two groups according to genotype. Mice were housed under standard conditions with free access to food and water and standard 12-hour light cycles. Six-week-old mice were injected with BrdU (150μm/mg) by intraperitoneal injection every 2 hours for 8 hour (4 injections) and sacrificed 24 hours after the final BrdU injection. For sacrifice, mice were deeply anesthetized and transcardially perfused as previously described. Mice brains were dissected out and kept in 4%PFA/PBS at 4 degrees. 50μm sagittal brain sections were collected in series, and stored in 1%PFA/PBS at 4°C until staining.

Immunofluorescence

For immunofluorescence (IF) staining, one set of serial sections from each mouse were transferred to a new six well plate, washed with PBS, and antigen retrieval for BrdU staining was preformed as previously described (General Methods, Chapter II). Sections were stained with Rat anti-BrdU antibody (Serotec, 1:300) in 10% goat serum/0.3% BSA/0.2% Triton X/PBS solution over night at 4°C. For duel staining, rat anti-BrdU and rabbit anti-GFAP (Millipore, 1:1000) were used in 10% goat serum/0.3%BSA/0.2%TritonX/PBS solution. All sections were incubated in primary antibody staining solution overnight at 4°C, washed extensively with 1x PBS, and stained with species-specific secondary antibody solution including anti-Rat Rhodamine Red X (Jackson) and anti-Rabbit Cy5 (Jackson, 1:500) in 0.3%BSA/0.2%TritonX/1xPBS solution. All secondary antibody staining were done as previously described (General Methods, Chapter II). To assess changes in progenitor survival, TUNEL staining (Roche) of brain sections was preformed as directed according to manufacturer protocol. WT brain sections were permeabilized with 0.2%tritonX/PBS and treated for 15 minutes with DNase (Invitrogen), washed with PBS, and used as a positive control for TUNEL detection. Withholding TUNEL secondary antibody staining (withholding fluorophore) was used as a TUNEL negative staining control. All TUNEL stains were followed as directed by manufacturer protocol.

Imaging and Quantification

11 serial brain sections were examined per mouse. A Zeiss LSM 510 confocal microscope system was used to generate Z-stack images of the entire thickness of all sagittal brain sections from both the p73+/+NestinGFP+ and p73-

/-NestinGFP+ groups. To determine the number of total proliferating progenitors in the WT and p73-/- mice, the total number of BrdU+/Nestin+ cells in the dentate subgranular zone (SGZ) from each mouse was quantified using the LSM Image Browser Software (Zeiss). To determine the number of total proliferating neural stem cells (NSCs) and total proliferating NPCs in WT and p73-/- mice the total number of BrdU+/Nestin+/GFAP+ (NSCs) cells and total BrdU+/Nestin+/GFAP- (NPCs) cells in the SGZ were quantified using the LSM software. Nestin+ cells located outside the SGZ, such as the hilus or in the granule cell layer (GCL) were not included in our quantification.

Results

Nestin+/p73-/- mice are phenotypically similar to p73-/- mice; p73-/- Nestin+ Progenitors Appear to have an aberrant morphology and appear to be fewer in number than Nestin+ SGZ WT Progenitors.

Yang and colleagues have previously described the hippocampal dysgenesis in p73-/- mice as a hypertrophied DG with extended suprapyramidal blade and missing infrapyramidal blade. Here, the same phenotype was observed in NestinGFP+/p73-/- mice. Similar wave-like gyrations in the CA1, CA2, and CA3 of the hippocampus were observed in NestinGFP+p73-/- mice, and an extended superpyramidal blade. In addition to these previous observations, there are additional differences in the SGZ of NestinGFP+p73-/- mice compared to WT mice, including changes in progenitor morphology and cell number that have not been previously noted, and are apparent using these compound transgenic

NestinGFP+p73-/- mice. The SGZ of the upper blade appeared to contain fewer nestin+ progenitors than the upper blade of the WT mouse (Figure 24), and the lower p73 blade appeared to have an SGZ but the SGZ was greatly truncated, and contained a very small number of nestin+ progenitors compared to WT mice (Figure 24). Additionally, no granule cell layer (GCL) was apparent above this profoundly truncated lower blade SGZ.

The NestinGFP+p73-/- mice had both Nestin+ neural stem cells that elaborated long processes and reached the molecular layer, and nestin progenitors that did not (Figure 24), demonstrating that p73-/- mice retained the ability to produce adult dentate neural stem and progenitor cells in the young adult hippocampus. Despite the presence of these cells, the NestinGFP+p73-/- progenitors appeared distinct from WT progenitors because there were fewer absolute numbers of cells with neural stem cell morphology, e.g. Nestin+ cells with large somas that elaborated long processes that reached the molecular layer. The appearance of fewer adult dentate stem and progenitor cells in p73-/- mice suggested a possible impairment of p73-/- neural stem/progenitor cells in vivo.

Loss of Global p73 Expression Impairs Proliferation of Dentate Progenitor cells; Proliferation of both NSCs and NPCs in p73-/- mice are impaired compared to WT mice.

To study changes in dentate neural stem and progenitor proliferation in p73-/- mice, we injected BrdU (150mg/kg, 4 injections) into 6 week old Nestin/p73-/-

and Nestin/p73+/+ mice to label proliferating nestin+ dentate progenitor cells. The number of BrdU+/Nestin+ cells in the dentate in 6-week-old p73-/- mice decreased by 61% compared to age-matched WT mice (Figures 25). The mean number of BrdU+/Nestin+ cells in the DG per mouse was 1720+/-119 cells (WT) and 666+/-97.5 cells in p73-/- mice ($n \geq 3$, $p=0.0024$)(Figure25). We subdivided the dentate nestin+ progenitor population into neural stem and neural progenitor cells by staining for GFAP in addition to BrdU so that we could quantify the number of proliferating neural stem cells (BrdU+/Nestin+/GFAP+) and proliferating neural progenitor cells (BrdU+/Nestin+/GFAP-) in the WT and p73-/- 6-week-old mice. We found that the number of proliferating dentate NSCs decreased by 75% in p73-/- 6-week-old mice (Figure 26). The mean number of BrdU+/Nestin+/GFAP+ proliferating NSCs dropped from 386+/-51.1 cells (WT) to 92+/-7.2 cells in p73-/- DG ($n \geq 3$, $p=0.0047$)(Figure 26). We also found that the number of proliferating DG neural progenitor cells decreased by 57% in p73-/- 6 week-old mice compared to WT mice (Figure 26). The mean number of BrdU+/Nestin+/GFAP- proliferating progenitor cells decreased from 1334+/-95.4 cells (WT) to 574+/-104.2 cells in p73-/- mice ($n \geq 3$, $p=0.0058$)(Figure 26). TUNEL staining and cleaved-caspase 3 visualization in NestinGFPp73+/+ and NestinGFPp73-/- mice demonstrated no increase in Tunel+NestinGFP+ cells or cleaved-caspase 3+NestinGFP+ cells in the DG of p73-/- mice compared to age-matched WT mice (Figure 27), indicating that the changes in proliferating NSCs and NPCs in the DG of 6 week old p73-/- mice were not accompanied with changes in DG progenitor survival.

Figure 24: 6 week old SGZ in p73-/- and WT mice.

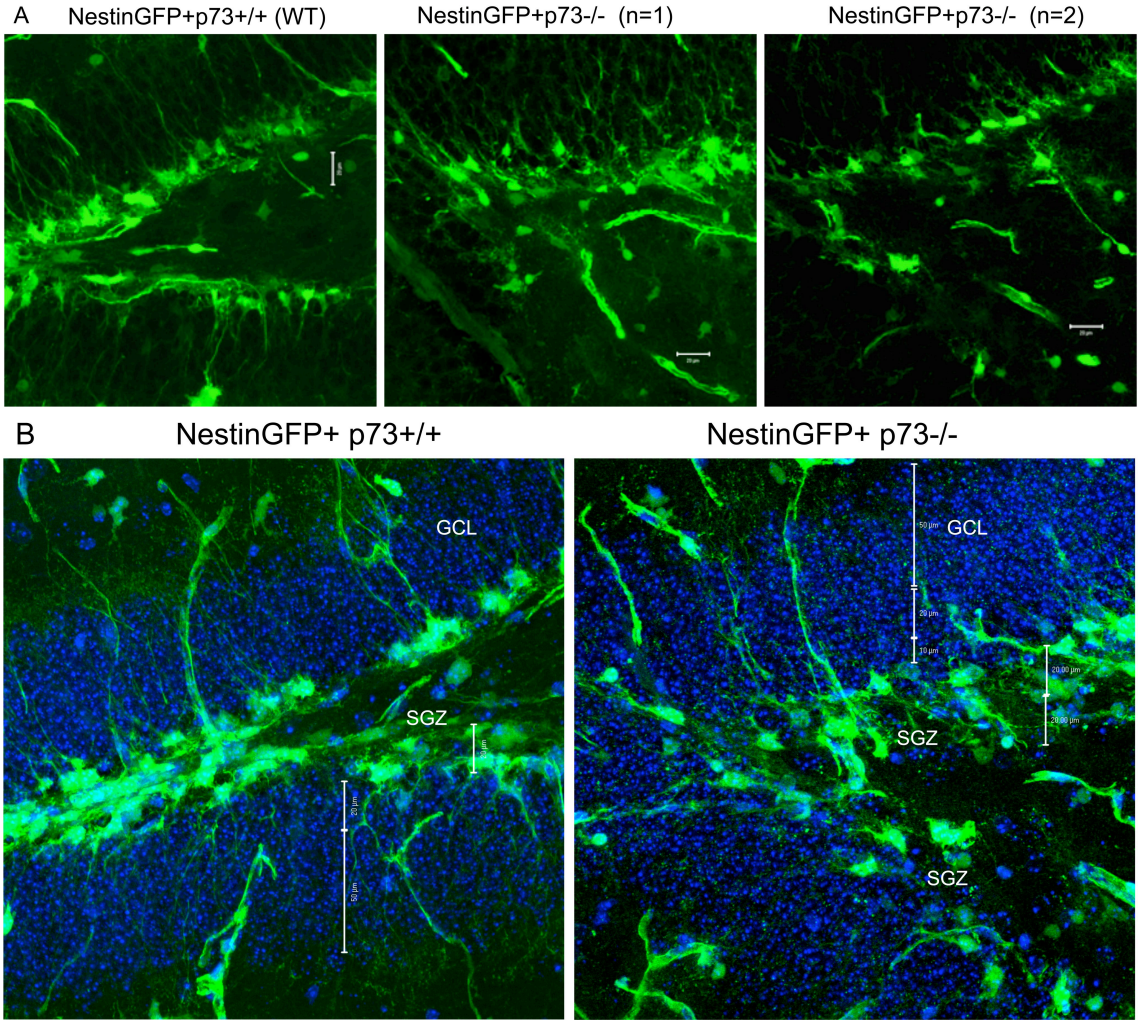

Figure 25: BrdU staining in 6 week old (A) NestinGFP+WT and (B) p73-/- mice previously injected with BrdU and (C) quantification of proliferating BrdU+NestinGFP+ DG progenitor cells in WT and p73-/- mice.

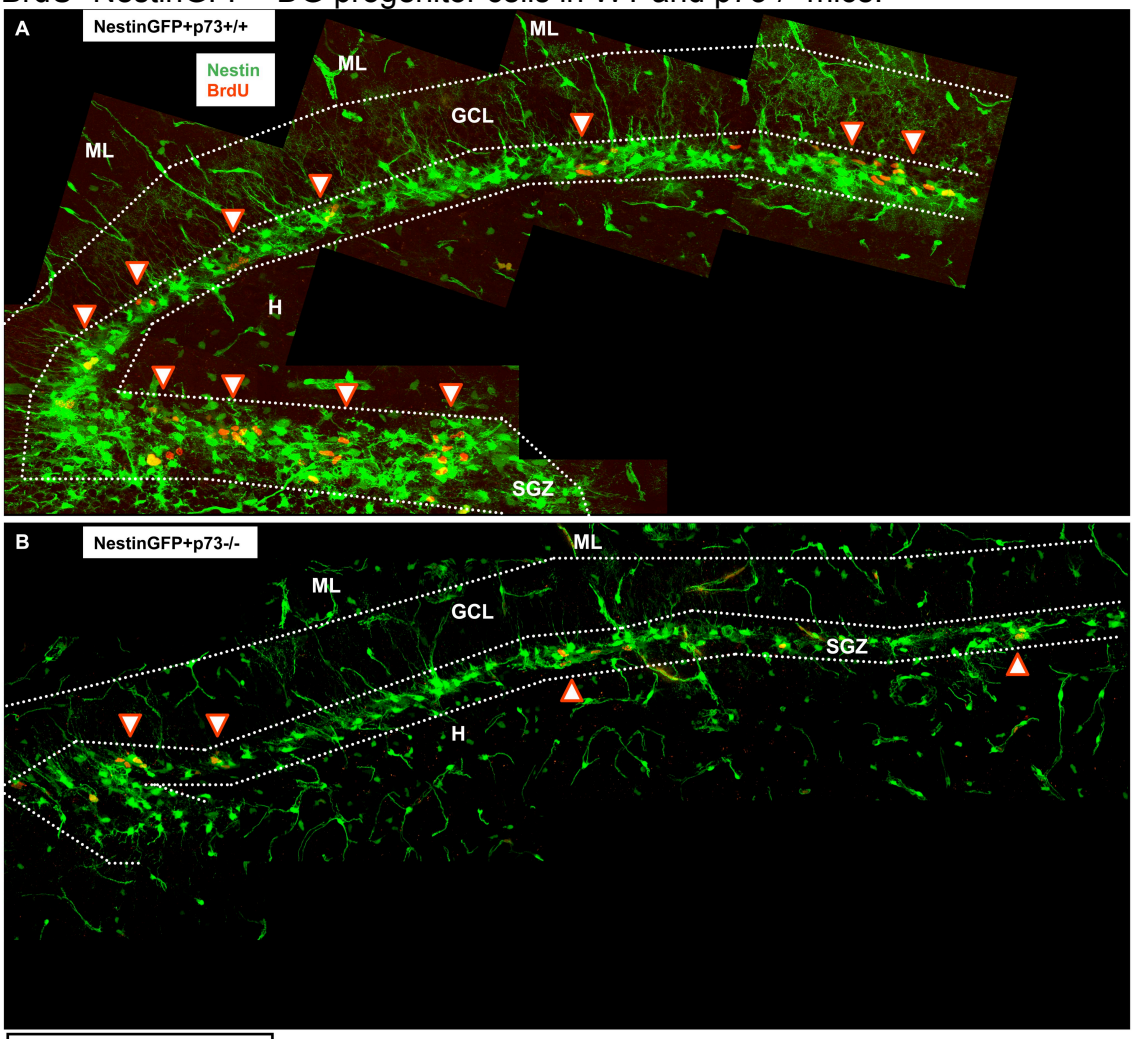

Figure 26: BrdU and GFAP staining in 6 week old (A) NestinGFP+WT and (B) p73-/- mice, and quantification of proliferating (C) BrdU+NestinGFP+GFAP+ NSCs and (D) BrdU+NestinGFP+GFAP- NPCs in the DG of WT and p73-/- mice. Scale bars equal 20μm.

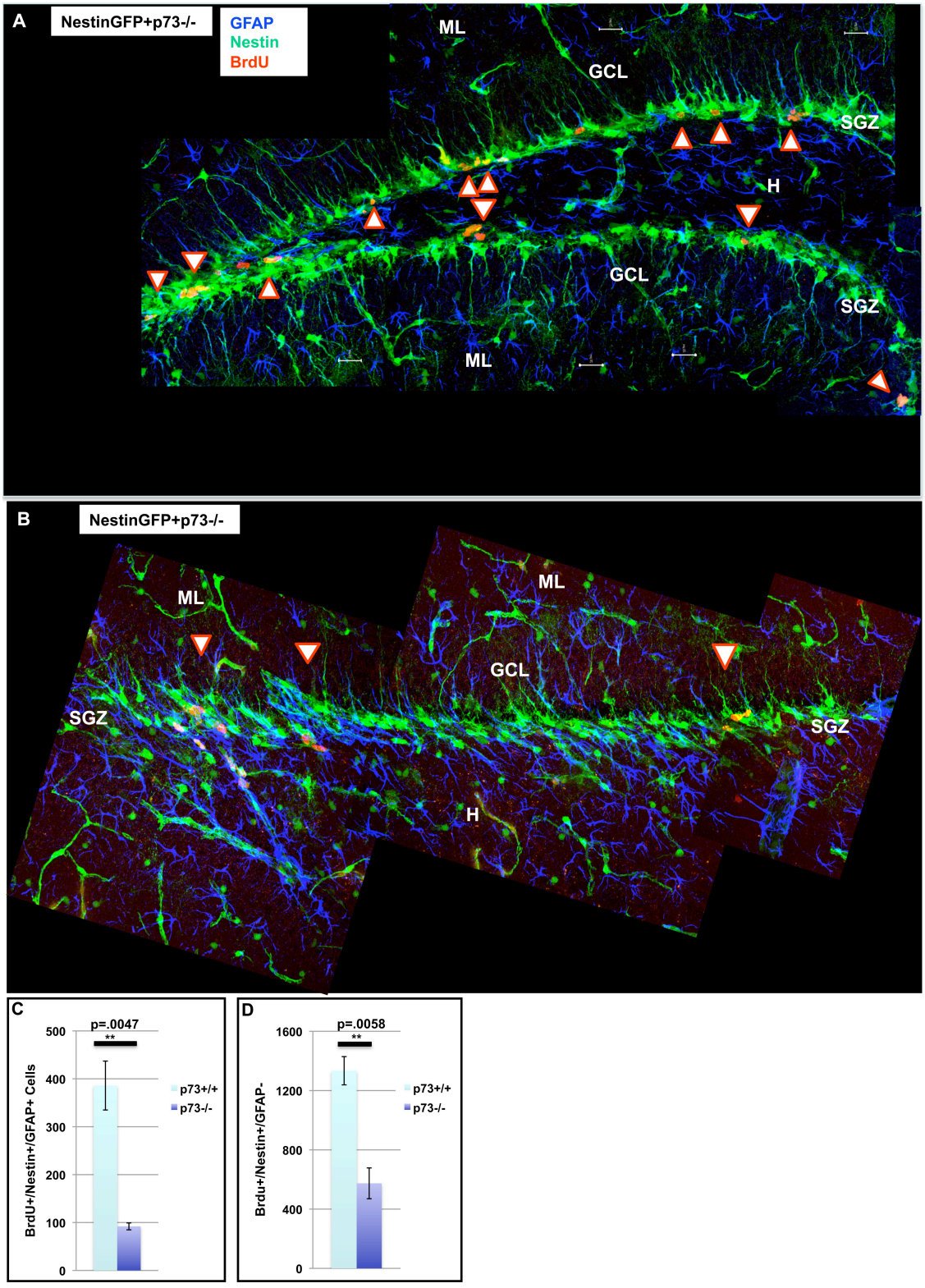

Figure 27: (A) TUNEL and (B) cleaved caspase 3 staining in 6 week old NestinGFP+WT and p73-/- mice.

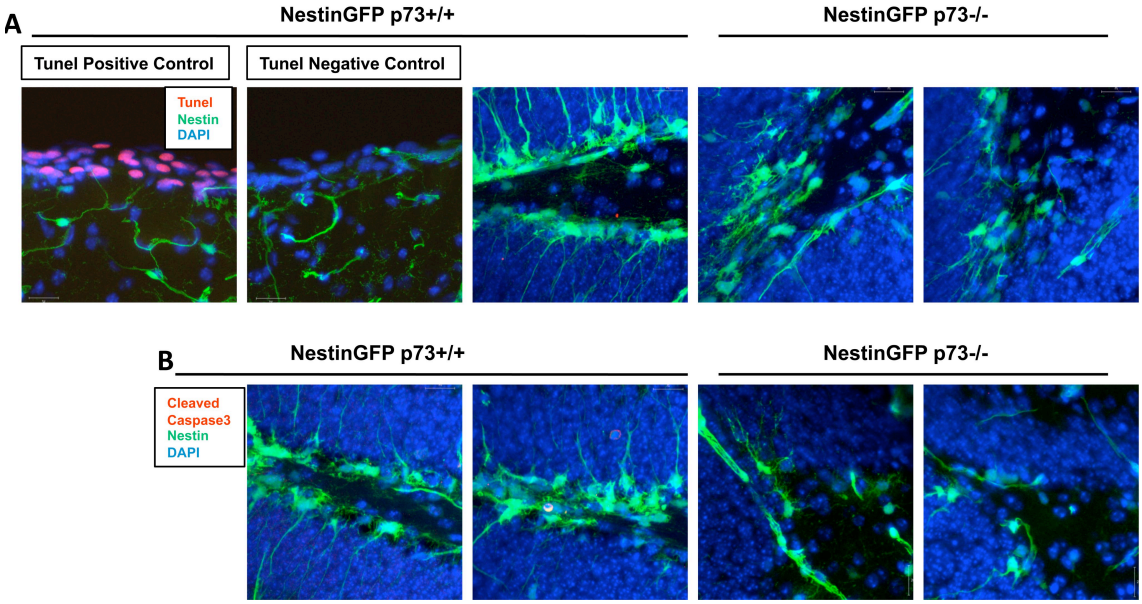

Chapter VII:

General Discussion of HMGB2 and Adult Neurogenesis

Previous studies have demonstrated an association between HMG-B chromatin proteins and NSCs *in vitro* and *in vivo* (Ramalho-Santos et al., 2002; Fortunel et al., 2003; Karsten et al., 2003; Gurok et al., 2004; Lim et al., 2006), but a full description of HMG-B gene and protein expression in progenitors cells and their functional role regulating NSC/NPC cell processes has not been explored or reported in the scientific literature. The purpose of this project was to: 1) characterize the expression of HMG-B family members in NSCs, 2) test the hypothesis that HMGB2 regulates proper maintenance of adult SVZ NSCs and NPCs, and 3) test the hypothesis that changes in HMGB2-dependant progenitor maintenance in vivo is mechanistically related to changes in expression of different CDKIs in the adult SVZ progenitor cells.

An initial study was conducted to examine the proteome of neural progenitor cells and identify proteins whose role in progenitor function remained unexamined. Quantitative shotgun proteomics analysis of proliferating E12.5 neurospheres was performed and led to the identification of 384 proteins expressed in proliferating progenitors, including several proteins not previously reported. These uncharacterized proteins included nuclear matrix protein matrin3, chromatin structural proteins HMGB1 and HMGB2, myristoylated

alanine-rich C kinase substrate (Marcks), a protein kinase C substrate involved in regulating actin filament crosslinking(Blackshear, 1993) that plays a role in embryonic radial glial proliferation and positioning during mouse cortical development (Weimer et al., 2009) was also prominently expressed in NSCs. Marcks-like protein (MLP), also a substrate for protein kinase C, was identified as well. Mutations in MARCKS and MLP have been associated with neural tube defects (Stumpo et al., 1998). Chromobox1 (Cbx1), the mammalian homolog of Drosophila heterochromatin protein HP1-β, that regulates NSC proliferation and plays a role in mouse cortical development (Aucott et al., 2008), was also identified, as was Chromobox3 (Cbx3)(mammalian HP1-γ). The analysis identified numerous arginine-serine rich RNA splicing factors (Sfrs1, Sfrs3, Sfrs4, Sfrs7, Sfrs9, and Sfrs10) and RNA binding proteins including fused-in-sarcoma (Fus) and Tar43-DNA-binding protein (Tardbp), suggesting a prominent role for RNA function and metabolism in NSCs.

We focused on the chromatin structural proteins of the HMG-B family and confirmed that all HMGB mRNAs and proteins were present in proliferating NSCs. Subsequent attempt to characterize the expression of HMG-B family members in these progenitors revealed that HMGB1, 2, and 3 mRNA and protein expression are dynamic and change substantially in proliferating and differentiating NSCs. The HMGB1 and B2 gene expression patterns resembled the expression pattern of HMGA2 in NSCs (Nishino et al., 2008). HMGA2 expression is higher in the NSC proliferative compartment of the embryonic telencephalon (ventricle zone) than in the differentiated compartment (cortex),

similar to our findings that B1 and B2 expression was enriched in proliferating progenitor cells, and both mRNA and protein expression decreased in differentiating progenitors. This result suggests the possibility that HMGB1 and B2 are functioning in a manner analogous to HMGA2 in progenitor cells, potentially regulating progenitor proliferation in a manner similar to HMGA2, mediated in part by changes in $p16^{Ink4a}$ expression.

These findings, in conjunction with previous data demonstrating strong expression of HMGB2 in the SVZ, led to the hypothesis that HMGB2 expression is enriched in proliferating NSCs and NPCs because it plays a role in regulating proper maintenance of SVZ NSCs and NPCs. To test this hypothesis, WT and HMGB2-/- mice were used to conduct *in vivo* proliferation assays to test progenitor proliferation in the SVZ *in vivo*, which demonstrated that young 10 week old HMGB2-/- mice have higher numbers of proliferating cells in the SVZ than age-matched WT mice. In conjunction with these findings it was noted that subsets of HMGB2-/- mice at 10 weeks of age have ventriculomegaly, a phenotype rarely observed in age-matched WT mice.

To help define the cell identity of these hyperproliferating SVZ cells, HMGB2 transgenic mice were crossed with NestinGFP transgenic mice to generate compound NestinGFPHMGB2 WT and HMGB2-/- mice to study differences in SVZ progenitor cell number in these variable HMGB2 genetic backgrounds. Using these compound transgenic mice, there is a strong increase in the expression of GFAP in the SVZ of HMGB2-/- mice, indicating that expression of this NSC marker increases in HMGB2-/- mice. In lateral brain sections, HMGB2-

/- mice had higher numbers of NestinGFP+GFAP+ NSCs in the SVZ, but lower numbers of NestinGFP+GFAP- NPCs compared to WT mice. HMGB2-/- mice also contained higher numbers of type A DCX+ neuroblasts in the SVZ compared to WT mice.

It remained mechanistically unclear why HMGB2-/- nice have aberrant SVZ hyperproliferation and an increase expression of NSC and neuroblast markers in the SVZ. A comparison of young HMGB2-/- mice with HMGA2-/- mice to gain further mechanistic insight into the HMGB2-/- SVZ phenotype indicates that young HMGA2-/- mice have fewer proliferating (BrdU+) SVZ progenitor cells than WT mice due to the loss of HMGA2 mediated repression of $p19^{Arf}$ and $p16^{Ink4a}$ expression, a phenotype rescued in vivo by the compound loss of $p19^{Arf}$ and $p16^{Ink4a}$ (Nishino et al., 2008). In contrast, young HMGB2-/- mice have greater numbers of proliferating (BrdU+, Ki67+) cells in the SVZ than WT mice, the opposite SVZ phenotype of HMGA2-/- mice. Additionally, loss of $p16^{Ink4a}$ alone does not lead to an increase in the number of BrdU+ proliferating SVZ progenitors in young adult mice (Molofsky et al., 2006). Therefore, the SVZ phenotype of young HMGB2-/- mice does not phenocopy HMGA2-/- or $p16^{Ink4a-/-}$ mice. To examine whether there were differences in $p16^{Ink4a}$ expression in the HMGB2-/- SVZ in vivo, WT and HMGB2-/- sections were stained for $p16^{Ink4a}$. Changes in $p16^{Ink4a}$ expression in the SVZ of 10 week old HMGB2-/- mice were not detected, suggesting an alternative mechanistic explanation besides $p16^{Ink4a}$ were responsible for the HMGB2-/- neural phenotype.

These results suggested a distinct molecular pathway for HMGB2 in regulating NSC proliferation and progenitor cell number in vivo. Alternative regulatory pathways that may explain the HMGB2-/- SVZ phenotype include changes in expression in the CIP/KIP family of cyclin dependant kinase inhibitors (CDKIs) and/or changes in p53 family expression. Loss of the CIP/KIP family member $p21^{Cip1}$ causes hyperproliferation in the SVZ in young adult mice (Kippin et al., 2005). Loss of CIP/KIP family member $p27^{Kip1}$ causes an increase in BrdU+ proliferating cells in the SVZ of 9 week old mice (Doetsch et al., 2002b). Loss of tumor suppressor protein p53 leads to an increase in SVZ proliferation in young p53-/- mice (Meletis et al., 2006). These knockout mice demonstrate NSC phenotypes that resemble components of the SVZ phenotype observed in young HMGB2-/- mice, suggesting a possible role for HMGB2 in $p21^{Cip1}$/ $p27^{Kip1}$/p53 mediated NSC/progenitor proliferation. $p21^{Cip1}$ and $p27^{Kip1}$ are gene targets of p53, and previous work has shown that HMGB1 and HMGB2 regulate transcription of target genes of members of the p53 family, including gene targets of p53 and p73(Stros et al., 2002). It remained unclear whether HMGB1 and B2 mediate p53 gene target expression in SVZ NSCs and/or NPCs; such a molecular dynamic would provide one possible mechanistic explanation for why young HMGB2-/- phenocopy $p21^{Cip1}$, $p27^{Kip1}$, and p53 knockout mice: young HMGB2-/- SVZ hyperproliferation may be due to aberrant gene expression of p53 target genes, including $p21^{Cip1}$ and $p27^{Kip1}$; alternatively (potentially) the hyperproliferation may be due to aberrant upstream p53 gene expression itself that affects the downstream elements $p21^{Cip1}$ and $p27^{Kip1}$. To examine whether

there were differences in $p21^{Cip1}$, $p27^{Kip1}$, and p53 expression in the HMGB2-/- SVZ in vivo, WT and HMGB2-/- sections were analyzed for changes in SVZ protein levels of the different factors. Changes in $p21^{Cip1}$, $p27^{Kip1}$, and p53 protein levels in the SVZ of 10 week old HMGB2-/- mice were detected; protein levels of $p21^{Cip1}$ and $p27^{Kip1}$ CDKIs in the SVZ were lower in HMGB2-/- mice compared to WT control, and p53 protein levels appears higher in the SVZ of HMGB2-/- mice than age-matched WT controls. These data suggest that altered proliferation of neural progenitor cells in the SVZ of HMGB2-/- is due to dysregulation of HMGB2 mediated expression of CDKIs, including $p21^{Cip1/Waf1}$ and $p27^{Kip1}$.

These results can be integrated and explained using different models of SVZ stem and progenitor proliferation. In model A the loss of HMGB2 protein expression leads to the loss of proper gene expression of p53 target genes, causing a decrease in $p21^{Cip/Waf1}$ and $p27^{Kip1}$ protein expression, which leads to hyperproliferation and self-renewal (asymmetric cell division) of type B NSCs. This increase in proliferation and asymmetric cell divisions of type B NSCs would lead to higher numbers of type B NSCs and type C NPCs. Unfortunately this model is too simplistic for our data and does not address why HMGB2-/- mice have lower numbers of type C NPCs, and higher numbers of DCX+ neuroblasts in the SVZ. In model B, the loss of HMGB2 protein expression leads to loss of proper gene expression of p53 target genes, causing a decrease in $p21^{Cip/Waf1}$ and $p27^{Kip1}$ protein levels, which leads to hyperproliferation and self-renewal (asymmetric cell division) of type B NSCs and a hyperproliferation and

symmetrical cell division of type C NPCs into type A neuroblasts. This second model would lead to the increase in NSC cell number, a decrease in type C NPC cell number and an increase in type A neuroblasts, a possibility that reproduces the cell distribution of stem and progenitor cells in the SVZ of HMGB2-/- mice. The third model that may explain the HMGB2-/- neural phenotype may be that type B NSCs and give rise to DCX+ neuroblasts directly, bypassing type C NPCs. In this model, increase in the division of type B NSCs directly into type A neuroblasts would reproduce the cell distribution noted in the HMGB2-/- SVZ of increased NSCs, lower NPCs, and higher neuroblasts.

Finally, these data on changes in $p21^{Cip1/Waf1}$, $p27^{Kip1}$ and p53 expression in HMGB2-/- mice can be integrated with previous data on HMGA2 mediated $p16^{Ink4a}$ expression to propose a new comprehensive model of NSC proliferation in young adult mice. In this proposed new model (Fig 28), HMGA2 promotes the proliferation of NSCs by reducing levels of $p16^{Ink4a}$ as previously described (Nishino et al., 2008), while HMGB2 represses the proliferation of SVZ NSCs by promoting the proper expression of $p21^{Cip1/Waf1}$ and $p27^{Kip1}$ (Fig 28).

In conclusion, HMGB chromatin structural proteins are differentially expressed in proliferating and differentiating embryonic NSCs. Loss of HMGB2 in young mice is associated with altered SVZ stem and progenitor cell number in vivo, including SVZ hyperproliferation, increased numbers of SVZ NSCs and neuroblasts, increased numbers of new born neurons in the olfactory bulb granule cell layer, and ventriculomegaly in a subset of HMGB2-/- mice,

demonstrating a novel role for HMGB2 in proper proliferation of SVZ neural progenitor cells, and GCL olfactory bulb neurogenesis, in young adult mice.

Figure 28: Proposed integrated model/mechanism of HMGBa2/HMGB2/CDKI expression in NSC proliferation in young adult mice.

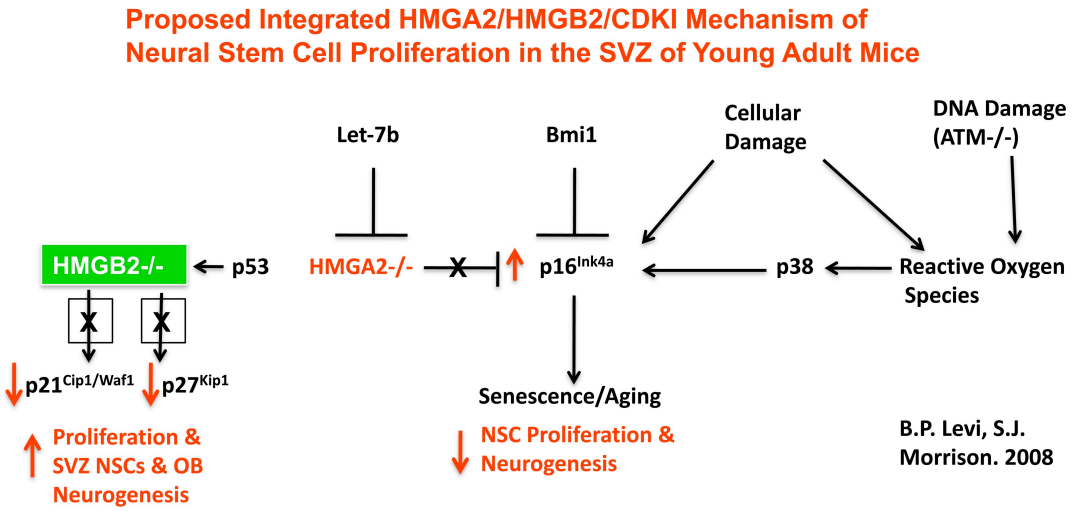

Chapter VIII:

Future Directions

Future studies on HMGB2-/- mice should focus on additional experiments that would further elucidate the mechanism by which neural stem and progenitor cell proliferation and olfactory bulb neurogenesis are altered by the loss of HMGB2. Future studies on HMGB2-/- mice should focus on introducing the expression of different CDKIs, such as $p21^{Cip1/Waf1}$ and $p27^{Kip1}$, in SVZ neural progenitor cells to determine whether proper expression of these CDKIs downstream of HMGB2 in HMGB2-/- neural progenitor cells can cause NSC /NPC /neuroblast cell numbers in the SVZ to revert back to WT levels. For example, HMGB2-/- SVZ neural progenitor cells can be infected with control virus or experimental virus expressing $p21^{Cip1/Waf1}$ or $p27^{Kip1}$ under the control of a nestin promoter and analyzed by immunofluorescence and confocal imaging. Quantification of NSC /NPC /neuroblast cell numbers in the SVZ of HMGB2-/- mice would allow for the determination of whether expression of these CDKIs allow HMGB2-/- NSCs /NPCs /neuroblast cell numbers to revert back to WT levels. Alternatively, the re-introduction of HMGB2 expression in the SVZ of HMGB2-/- mice can be done by infecting SVZ cells with a virus expressing HMGB2, and NSC/NPC/neuroblasts cell number can be examined in a similar manner. Additionally, re-introducing expression of HMGB2 *in vivo* using a viral approach has the benefit of being able

to analyze CDKI expression in the SVZ. For example, HMGB2-/- mice infected with control and experimental virus expressing HMGB2 can be analyzed by western blot analysis as well as tissue immunofluorescence to determine whether $p21^{Cip1/Waf1}$ and $p27^{Kip1}$ protein expression is augmented as a result of re-introducing HMGB2 expression in the SVZ. These experiments will play an integral role in providing definitive proof that HMGB2 regulates $p21^{Cip1/Waf1}$ and $p27^{Kip1}$ in SVZ neural progenitor in vivo.

More recent work on HMGB2 has demonstrated that HMGB2 also plays a role in regulating cell survival in vivo. The loss of HMGB2 causes premature osteoarthritis, which is due to the accelerated loss of articular cartilage in HMGB2-/- mice (Taniguchi et al., 2009). A subsequent study demonstrated that HMGB2 plays a role in the Wnt/Beta-Catenin signaling pathway, that HMGB2 increases Lef-1 binding to its target sites and "potentiates the transcriptional activation of the Lef-1-beta-catenin complex"(Taniguchi et al., 2009). This interplay between HMGB2 and the Wnt/beta-catenin signaling pathway leads to the suppression of apoptosis of chondrocytes in the articular cartilage. The survival of chondrocytes promotes the proper maintenance of the articular cartilage over time (during aging). HMGB2-/- mice do not have HMGB2 protein to facilitate proper interaction with the Lef-1-beta-catenin complex and therefore have increases apoptosis of chondrocytes in the articular cartilage. Impaired survival of chondrocytes leads to the premature loss of articular cartilage in aging mice and the subsequent formation of premature osteoarthritis (Taniguchi et al., 2009). These results are striking and very pertinent to neurogenesis because the

Wnt/beta-catenin signaling pathway is a known regulator of NSC proliferation and self-renewal in vivo (Qu et al.; Lie et al., 2005; Kuwabara et al., 2009). Future studies should examine whether changes in Wnt/beta-catenin signaling occurs in the SVZ in HMGB2-/- mice compared to WT mice, whether these changes in Wnt/beta-catenin signaling are the molecular basis for changes in the proliferation (and possibly the survival of) NSCs, NPCs, and neuroblasts in the SVZ in young and aged HMGB2-/- mice.

This project has focused on the role of HMGB2 in regulating proliferation of SVZ progenitor cells, but little is known about the regulation of HMG-B gene expression and protein synthesis. Our data demonstrated a decrease in HMGB1 and B2 mRNA levels in proliferating NSCs between E12 and E15.5, while HMGB1 and B2 protein expression remained stable during the same time, presumably due to the long half lives that the HMGB proteins are reported to have (~65 hours). An alternative mechanistic explanation may exist which could explain these findings; that HMGB1 and B2 expression in proliferating NSCs, like HMGA2, are negatively regulated by microRNA(s). We briefly explored this hypothesis using web-based analytical tools. Using MicroCosym Targets Version 5 and miRBase (Enright Lab, European Bioinformatics Lab), analytical tools that search for microRNA binding sites in target mRNAs (Griffiths-Jones et al., 2006; Griffiths-Jones et al., 2008) we found putative microRNA binding sites in HMGB1 and HMGB3 mRNA, and 45 different miRNA binding sites in HMGB2 (data not shown). Among them were several binding sites for members of the Let-7 family of microRNAs, including Let-7a,f,g and Let7-b, a known negative regulator of

HMGA2 expression in NSCs (Nishino et al., 2008). It remains unclear what, if any, role microRNAs have in the regulation of HMGB1 or B2 expression in proliferating NSCs, and whether a second microRNA-HMG axis involving microRNAs and HMG-Bs exists in proliferating NSCs. Future experiments to examine whether Let-7 microRNAs negatively regulate HMGB2 in NSCs would help provide a clearer molecular mechanism for HMGB2 mediated NSC/NPC proliferation and self-renewal.

Finally, this project has focused most exclusively on the role of HMGB2 in proper SVZ progenitor proliferation and maintenance, and did not specifically address whether a function role for HMGB1, HMGB3, and HMGB4 proteins exists in adult SVZ NSCs and NPCs during proliferation and OB neurogenesis. HMGB1-/- mice were created and previously described and appear to die shortly after birth due to hypoglycemia (Calogero et al., 1999). HMGB3-/- mice were created and previously described, and appear to have a defect in proper maintenance of hematopoietic stem cells (HSCs)(Nemeth et al., 2003). Loss of HMGB3 disrupts the proper proliferation and differentiation of myeloid and lymphoid progenitor cells (Nemeth et al., 2005; Nemeth et al., 2006). Despite these findings in HMGB3-/- HSCs, and previous reports demonstrating that NSCs also express HMGB3 (Fortunel et al., 2003), no study has been conducted on the role of HMGB3 in proper NSC and neural progenitors *in vivo*. Future work should also focus on the role of HMGB3 in proper NSC proliferation, and to determine whether loss of HMGB3 also causes disruptions in the balance of proliferation vs. differentiation in neural progenitor cells (in a similar manner in

which this occurs in the hematopoietic compartment). Crossing NestinGFP transgenic mice and HMGB3-/- transgenic mice to create compound transgenic mice would allow for the examination of NestinGFP progenitor cells in the variable HMGB3 WT and null genetic background, and provide further data on the role of HMGB3 in proper neural stem and progenitor cell proliferation and differentiation in vivo.

References

Alberts B (2008) Molecular biology of the cell, 5th Edition. New York: Garland Science.

Alexson TO, Hitoshi S, Coles BL, Bernstein A, van der Kooy D (2006) Notch signaling is required to maintain all neural stem cell populations--irrespective of spatial or temporal niche. Dev Neurosci 28:34-48.

Altman J (1969) Autoradiographic and histological studies of postnatal neurogenesis. IV. Cell proliferation and migration in the anterior forebrain, with special reference to persisting neurogenesis in the olfactory bulb. J Comp Neurol 137:433-457.

Altman J, Das GD (1965a) Autoradiographic and histological evidence of postnatal hippocampal neurogenesis in rats. J Comp Neurol 124:319-335.

Altman J, Das GD (1965b) Post-natal origin of microneurones in the rat brain. Nature 207:953-956.

Altman J, Das GD (1966) Autoradiographic and histological studies of postnatal neurogenesis. I. A longitudinal investigation of the kinetics, migration and transformation of cells incorporating tritiated thymidine in neonate rats, with special reference to postnatal neurogenesis in some brain regions. J Comp Neurol 126:337-389.

Aucott R, Bullwinkel J, Yu Y, Shi W, Billur M, Brown JP, Menzel U, Kioussis D, Wang G, Reisert I, Weimer J, Pandita RK, Sharma GG, Pandita TK, Fundele R, Singh PB (2008) HP1-beta is required for development of the cerebral neocortex and neuromuscular junctions. J Cell Biol 183:597-606.

Bianchi ME, Agresti A (2005) HMG proteins: dynamic players in gene regulation and differentiation. Curr Opin Genet Dev 15:496-506.

Blackshear PJ (1993) The MARCKS family of cellular protein kinase C substrates. J Biol Chem 268:1501-1504.

Blanpain C, Fuchs E (2007) p63: revving up epithelial stem-cell potential. Nat Cell Biol 9:731-733.

Bustin M (1999) Regulation of DNA-dependent activities by the functional motifs of the high-mobility-group chromosomal proteins. Mol Cell Biol 19:5237-5246.

Bustin M (2001) Revised nomenclature for high mobility group (HMG) chromosomal proteins. Trends Biochem Sci 26:152-153.

Calogero S, Grassi F, Aguzzi A, Voigtlander T, Ferrier P, Ferrari S, Bianchi ME (1999) The lack of chromosomal protein Hmg1 does not disrupt cell growth but causes lethal hypoglycaemia in newborn mice. Nat Genet 22:276-280.

Caviness VS, Jr. (1973) Time of neuron origin in the hippocampus and dentate gyrus of normal and reeler mutant mice: an autoradiographic analysis. J Comp Neurol 151:113-120.

Chen EI, Cociorva D, Norris JL, Yates JR, 3rd (2007) Optimization of mass spectrometry-compatible surfactants for shotgun proteomics. J Proteome Res 6:2529-2538.

Curtis MA, Kam M, Nannmark U, Anderson MF, Axell MZ, Wikkelso C, Holtas S, van Roon-Mom WM, Bjork-Eriksson T, Nordborg C, Frisen J, Dragunow M, Faull RL, Eriksson PS (2007) Human neuroblasts migrate to the olfactory bulb via a lateral ventricular extension. Science 315:1243-1249.
Doetsch F, Garcia-Verdugo JM, Alvarez-Buylla A (1997) Cellular composition and three-dimensional organization of the subventricular germinal zone in the adult mammalian brain. J Neurosci 17:5046-5061.
Doetsch F, Caille I, Lim DA, Garcia-Verdugo JM, Alvarez-Buylla A (1999) Subventricular zone astrocytes are neural stem cells in the adult mammalian brain. Cell 97:703-716.
Doetsch F, Petreanu L, Caille I, Garcia-Verdugo JM, Alvarez-Buylla A (2002a) EGF converts transit-amplifying neurogenic precursors in the adult brain into multipotent stem cells. Neuron 36:1021-1034.
Doetsch F, Verdugo JM, Caille I, Alvarez-Buylla A, Chao MV, Casaccia-Bonnefil P (2002b) Lack of the cell-cycle inhibitor p27Kip1 results in selective increase of transit-amplifying cells for adult neurogenesis. J Neurosci 22:2255-2264.
Enwere E, Shingo T, Gregg C, Fujikawa H, Ohta S, Weiss S (2004) Aging results in reduced epidermal growth factor receptor signaling, diminished olfactory neurogenesis, and deficits in fine olfactory discrimination. J Neurosci 24:8354-8365.
Eriksson PS, Perfilieva E, Bjork-Eriksson T, Alborn AM, Nordborg C, Peterson DA, Gage FH (1998) Neurogenesis in the adult human hippocampus. Nat Med 4:1313-1317.
Filippov V, Kronenberg G, Pivneva T, Reuter K, Steiner B, Wang LP, Yamaguchi M, Kettenmann H, Kempermann G (2003) Subpopulation of nestin-expressing progenitor cells in the adult murine hippocampus shows electrophysiological and morphological characteristics of astrocytes. Mol Cell Neurosci 23:373-382.
Fortunel NO, Otu HH, Ng HH, Chen J, Mu X, Chevassut T, Li X, Joseph M, Bailey C, Hatzfeld JA, Hatzfeld A, Usta F, Vega VB, Long PM, Libermann TA, Lim B (2003) Comment on " 'Stemness': transcriptional profiling of embryonic and adult stem cells" and "a stem cell molecular signature". Science 302:393; author reply 393.
Fukuda S, Kato F, Tozuka Y, Yamaguchi M, Miyamoto Y, Hisatsune T (2003) Two distinct subpopulations of nestin-positive cells in adult mouse dentate gyrus. J Neurosci 23:9357-9366.
Gage FH (2000) Mammalian neural stem cells. Science 287:1433-1438.
Griffiths-Jones S, Saini HK, van Dongen S, Enright AJ (2008) miRBase: tools for microRNA genomics. Nucleic Acids Res 36:D154-158.
Griffiths-Jones S, Grocock RJ, van Dongen S, Bateman A, Enright AJ (2006) miRBase: microRNA sequences, targets and gene nomenclature. Nucleic Acids Res 34:D140-144.
Gritti A, Frolichsthal-Schoeller P, Galli R, Parati EA, Cova L, Pagano SF, Bjornson CR, Vescovi AL (1999) Epidermal and fibroblast growth factors behave as mitogenic regulators for a single multipotent stem cell-like

population from the subventricular region of the adult mouse forebrain. J Neurosci 19:3287-3297.
Gurok U, Steinhoff C, Lipkowitz B, Ropers HH, Scharff C, Nuber UA (2004) Gene expression changes in the course of neural progenitor cell differentiation. J Neurosci 24:5982-6002.
Hack MA, Saghatelyan A, de Chevigny A, Pfeifer A, Ashery-Padan R, Lledo PM, Gotz M (2005) Neuronal fate determinants of adult olfactory bulb neurogenesis. Nat Neurosci 8:865-872.
Han YG, Spassky N, Romaguera-Ros M, Garcia-Verdugo JM, Aguilar A, Schneider-Maunoury S, Alvarez-Buylla A (2008) Hedgehog signaling and primary cilia are required for the formation of adult neural stem cells. Nat Neurosci 11:277-284.
Hitoshi S, Alexson T, Tropepe V, Donoviel D, Elia AJ, Nye JS, Conlon RA, Mak TW, Bernstein A, van der Kooy D (2002) Notch pathway molecules are essential for the maintenance, but not the generation, of mammalian neural stem cells. Genes Dev 16:846-858.
Hock R, Furusawa T, Ueda T, Bustin M (2007) HMG chromosomal proteins in development and disease. Trends Cell Biol 17:72-79.
Jacobs JJ, Kieboom K, Marino S, DePinho RA, van Lohuizen M (1999) The oncogene and Polycomb-group gene bmi-1 regulates cell proliferation and senescence through the ink4a locus. Nature 397:164-168.
Jessberger S, Clark RE, Broadbent NJ, Clemenson GD, Jr., Consiglio A, Lie DC, Squire LR, Gage FH (2009) Dentate gyrus-specific knockdown of adult neurogenesis impairs spatial and object recognition memory in adult rats. Learn Mem 16:147-154.
Karsten SL, Kudo LC, Jackson R, Sabatti C, Kornblum HI, Geschwind DH (2003) Global analysis of gene expression in neural progenitors reveals specific cell-cycle, signaling, and metabolic networks. Dev Biol 261:165-182.
Kippin TE, Martens DJ, van der Kooy D (2005) p21 loss compromises the relative quiescence of forebrain stem cell proliferation leading to exhaustion of their proliferation capacity. Genes Dev 19:756-767.
Kirschenbaum B, Doetsch F, Lois C, Alvarez-Buylla A (1999) Adult subventricular zone neuronal precursors continue to proliferate and migrate in the absence of the olfactory bulb. J Neurosci 19:2171-2180.
Kornack DR, Rakic P (1999) Continuation of neurogenesis in the hippocampus of the adult macaque monkey. Proc Natl Acad Sci U S A 96:5768-5773.
Kriegstein A, Alvarez-Buylla A (2009) The glial nature of embryonic and adult neural stem cells. Annu Rev Neurosci 32:149-184.
Kuwabara T, Hsieh J, Muotri A, Yeo G, Warashina M, Lie DC, Moore L, Nakashima K, Asashima M, Gage FH (2009) Wnt-mediated activation of NeuroD1 and retro-elements during adult neurogenesis. Nat Neurosci 12:1097-1105.
Lee YS, Dutta A (2007) The tumor suppressor microRNA let-7 represses the HMGA2 oncogene. Genes Dev 21:1025-1030.
Levi BP, Morrison SJ (2008) Stem cells use distinct self-renewal programs at different ages. Cold Spring Harb Symp Quant Biol 73:539-553.

Liao L, McClatchy DB, Yates JR (2009) Shotgun proteomics in neuroscience. Neuron 63:12-26.
Lie DC, Colamarino SA, Song HJ, Desire L, Mira H, Consiglio A, Lein ES, Jessberger S, Lansford H, Dearie AR, Gage FH (2005) Wnt signalling regulates adult hippocampal neurogenesis. Nature 437:1370-1375.
Lim DA, Tramontin AD, Trevejo JM, Herrera DG, Garcia-Verdugo JM, Alvarez-Buylla A (2000) Noggin antagonizes BMP signaling to create a niche for adult neurogenesis. Neuron 28:713-726.
Lim DA, Suarez-Farinas M, Naef F, Hacker CR, Menn B, Takebayashi H, Magnasco M, Patil N, Alvarez-Buylla A (2006) In vivo transcriptional profile analysis reveals RNA splicing and chromatin remodeling as prominent processes for adult neurogenesis. Mol Cell Neurosci 31:131-148.
Lois C, Alvarez-Buylla A (1994) Long-distance neuronal migration in the adult mammalian brain. Science 264:1145-1148.
Lois C, Garcia-Verdugo JM, Alvarez-Buylla A (1996) Chain migration of neuronal precursors. Science 271:978-981.
Love JJ, Li X, Case DA, Giese K, Grosschedl R, Wright PE (1995) Structural basis for DNA bending by the architectural transcription factor LEF-1. Nature 376:791-795.
Lowe SW, Sherr CJ (2003) Tumor suppression by Ink4a-Arf: progress and puzzles. Curr Opin Genet Dev 13:77-83.
Maslov AY, Barone TA, Plunkett RJ, Pruitt SC (2004) Neural stem cell detection, characterization, and age-related changes in the subventricular zone of mice. J Neurosci 24:1726-1733.
Meletis K, Wirta V, Hede SM, Nister M, Lundeberg J, Frisen J (2006) p53 suppresses the self-renewal of adult neural stem cells. Development 133:363-369.
Mignone JL, Kukekov V, Chiang AS, Steindler D, Enikolopov G (2004) Neural stem and progenitor cells in nestin-GFP transgenic mice. J Comp Neurol 469:311-324.
Ming GL, Song H (2005) Adult neurogenesis in the mammalian central nervous system. Annu Rev Neurosci 28:223-250.
Mizutani K, Yoon K, Dang L, Tokunaga A, Gaiano N (2007) Differential Notch signalling distinguishes neural stem cells from intermediate progenitors. Nature 449:351-355.
Molofsky AV, He S, Bydon M, Morrison SJ, Pardal R (2005) Bmi-1 promotes neural stem cell self-renewal and neural development but not mouse growth and survival by repressing the p16Ink4a and p19Arf senescence pathways. Genes Dev 19:1432-1437.
Molofsky AV, Pardal R, Iwashita T, Park IK, Clarke MF, Morrison SJ (2003) Bmi-1 dependence distinguishes neural stem cell self-renewal from progenitor proliferation. Nature 425:962-967.
Molofsky AV, Slutsky SG, Joseph NM, He S, Pardal R, Krishnamurthy J, Sharpless NE, Morrison SJ (2006) Increasing p16INK4a expression decreases forebrain progenitors and neurogenesis during ageing. Nature 443:448-452.

Nemeth MJ, Kirby MR, Bodine DM (2006) HMGB3 regulates the balance between hematopoietic stem cell self-renewal and differentiation. Proc Natl Acad Sci U S A 103:13783-13788.
Nemeth MJ, Cline AP, Anderson SM, Garrett-Beal LJ, Bodine DM (2005) HMGB3 deficiency deregulates proliferation and differentiation of common lymphoid and myeloid progenitors. Blood 105:627-634.
Nemeth MJ, Curtis DJ, Kirby MR, Garrett-Beal LJ, Seidel NE, Cline AP, Bodine DM (2003) HMGB3: an HMG-box family member expressed in primitive hematopoietic cells that inhibits myeloid and B-cell differentiation. Blood 102:1298-1306.
Nishino J, Kim I, Chada K, Morrison SJ (2008) HMGA2 promotes neural stem cell self-renewal in young but not old mice by reducing p16Ink4a and p19Arf Expression. Cell 135:227-239.
Qu Q, Sun G, Li W, Yang S, Ye P, Zhao C, Yu RT, Gage FH, Evans RM, Shi Y Orphan nuclear receptor TLX activates Wnt/beta-catenin signalling to stimulate neural stem cell proliferation and self-renewal. Nat Cell Biol 12:31-40; sup pp 31-39.
Ramalho-Santos M, Yoon S, Matsuzaki Y, Mulligan RC, Melton DA (2002) "Stemness": transcriptional profiling of embryonic and adult stem cells. Science 298:597-600.
Read CM, Cary PD, Crane-Robinson C, Driscoll PC, Norman DG (1993) Solution structure of a DNA-binding domain from HMG1. Nucleic Acids Res 21:3427-3436.
Reynolds BA, Weiss S (1992) Generation of neurons and astrocytes from isolated cells of the adult mammalian central nervous system. Science 255:1707-1710.
Reynolds BA, Weiss S (1996) Clonal and population analyses demonstrate that an EGF-responsive mammalian embryonic CNS precursor is a stem cell. Dev Biol 175:1-13.
Reynolds BA, Tetzlaff W, Weiss S (1992) A multipotent EGF-responsive striatal embryonic progenitor cell produces neurons and astrocytes. J Neurosci 12:4565-4574.
Ronfani L, Ferraguti M, Croci L, Ovitt CE, Scholer HR, Consalez GG, Bianchi ME (2001) Reduced fertility and spermatogenesis defects in mice lacking chromosomal protein HMGB2. Development 128:1265-1273.
Santarelli L, Saxe M, Gross C, Surget A, Battaglia F, Dulawa S, Weisstaub N, Lee J, Duman R, Arancio O, Belzung C, Hen R (2003) Requirement of hippocampal neurogenesis for the behavioral effects of antidepressants. Science 301:805-809.
Schmittgen TD, Livak KJ (2008) Analyzing real-time PCR data by the comparative C(T) method. Nat Protoc 3:1101-1108.
Seki T, Arai Y (1991) The persistent expression of a highly polysialylated NCAM in the dentate gyrus of the adult rat. Neurosci Res 12:503-513.
Seki T, Arai Y (1993) Distribution and possible roles of the highly polysialylated neural cell adhesion molecule (NCAM-H) in the developing and adult central nervous system. Neurosci Res 17:265-290.

Seri B, Garcia-Verdugo JM, McEwen BS, Alvarez-Buylla A (2001) Astrocytes give rise to new neurons in the adult mammalian hippocampus. J Neurosci 21:7153-7160.
Seri B, Garcia-Verdugo JM, Collado-Morente L, McEwen BS, Alvarez-Buylla A (2004) Cell types, lineage, and architecture of the germinal zone in the adult dentate gyrus. J Comp Neurol 478:359-378.
Shors TJ, Miesegaes G, Beylin A, Zhao M, Rydel T, Gould E (2001) Neurogenesis in the adult is involved in the formation of trace memories. Nature 410:372-376.
Stros M, Ozaki T, Bacikova A, Kageyama H, Nakagawara A (2002) HMGB1 and HMGB2 cell-specifically down-regulate the p53- and p73-dependent sequence-specific transactivation from the human Bax gene promoter. J Biol Chem 277:7157-7164.
Stumpo DJ, Eddy RL, Jr., Haley LL, Sait S, Shows TB, Lai WS, Young WS, 3rd, Speer MC, Dehejia A, Polymeropoulos M, Blackshear PJ (1998) Promoter sequence, expression, and fine chromosomal mapping of the human gene (MLP) encoding the MARCKS-like protein: identification of neighboring and linked polymorphic loci for MLP and MACS and use in the evaluation of human neural tube defects. Genomics 49:253-264.
Taniguchi N, Carames B, Kawakami Y, Amendt BA, Komiya S, Lotz M (2009) Chromatin protein HMGB2 regulates articular cartilage surface maintenance via beta-catenin pathway. Proc Natl Acad Sci U S A 106:16817-16822.
Tanner S, Shu H, Frank A, Wang LC, Zandi E, Mumby M, Pevzner PA, Bafna V (2005) InsPecT: identification of posttranslationally modified peptides from tandem mass spectra. Anal Chem 77:4626-4639.
Theiler K (1989) The house mouse : atlas of embryonic development. New York: Springer-Verlag.
Thomas JO (2001) HMG1 and 2: architectural DNA-binding proteins. Biochem Soc Trans 29:395-401.
van Praag H, Schinder AF, Christie BR, Toni N, Palmer TD, Gage FH (2002) Functional neurogenesis in the adult hippocampus. Nature 415:1030-1034.
Wang LP, Kempermann G, Kettenmann H (2005) A subpopulation of precursor cells in the mouse dentate gyrus receives synaptic GABAergic input. Mol Cell Neurosci 29:181-189.
Weimer JM, Yokota Y, Stanco A, Stumpo DJ, Blackshear PJ, Anton ES (2009) MARCKS modulates radial progenitor placement, proliferation and organization in the developing cerebral cortex. Development 136:2965-2975.
Weir HM, Kraulis PJ, Hill CS, Raine AR, Laue ED, Thomas JO (1993) Structure of the HMG box motif in the B-domain of HMG1. EMBO J 12:1311-1319.
Werner MH, Huth JR, Gronenborn AM, Clore GM (1995) Molecular basis of human 46X,Y sex reversal revealed from the three-dimensional solution structure of the human SRY-DNA complex. Cell 81:705-714.

Wichterle H, Garcia-Verdugo JM, Alvarez-Buylla A (1997) Direct evidence for homotypic, glia-independent neuronal migration. Neuron 18:779-791.
Yang A, Walker N, Bronson R, Kaghad M, Oosterwegel M, Bonnin J, Vagner C, Bonnet H, Dikkes P, Sharpe A, McKeon F, Caput D (2000) p73-deficient mice have neurological, pheromonal and inflammatory defects but lack spontaneous tumours. Nature 404:99-103.
Yi R, Poy MN, Stoffel M, Fuchs E (2008) A skin microRNA promotes differentiation by repressing 'stemness'. Nature 452:225-229.